Universitetet i Stavanger

FACULTY OF SCIENCE AND TECHNOLOGY

MASTER'S THESIS

Study programme/specialisation: Marine and Offshore Technology	Spring semester, 2019. Open/~~Confidential~~
Author: Oyegbile Afolarinwa David	…… (signature of author)
Programme coordinator: Supervisor(s): Dr. Charlotte Obhrai	
Title of master's thesis: Wind Profile Usage in Wind Farm Installation Campaign Simulations	
Credits (ECTS): 30	
Keywords: Wind Farm; Offshore; Atmospheric Stability; Installation Campaign; Power Production; Wind Energy; Wind Profile; Boundary-Layer Meteorology; FINO data base; Waiting on Weather.	Number of pages: 75 + supplemental material/other: 92 Stavanger, 15th of June 2019 date/year

Stavanger, 15 June 2018

Abstract

Simulation tools are used in the wind industry to analyse and understand installation campaigns for strategic planning purposes. These tools use vertical wind profiles to estimate wind speeds at various heights. Where these wind speeds are limiting criteria for marine operations offshore, the wind profile used is of utmost importance for waiting on weather; one of the major cost and risk drivers in wind projects, especially offshore. This study investigates the impact the wind profile used in these simulation tools can have on the results obtained. 9 years of weather data obtained from the FINO3 platform and the reference height used to extrapolate the wind speed was 30 m. The atmospheric conditions at the site were assessed and also, the accuracy of different wind extrapolation model (A power law wind profile with an exponent of 0.12 and 0.14, the logarithmic wind profile with and without stability correction and the extended wind profile proposed by Gryning) were evaluated. The results showed that for all stability conditions, the extended wind profile performs either as well as the other wind profiles considered in this study for unstable conditions. Except for near neutral unstable conditions where the power law wind profile with an exponent of 0.12 performs better. During stable conditions, it performs significantly better. Analyses were carried out based on the various wind weather windows required for offshore installation campaign defined in this study. It was found that the data from the power law wind profile (both) underestimated the number of available wind weather wind for the various installation operations. Compared to that of the measured data underestimation of up approximately 17% and 23% were obtained for the power law wind profile with an exponent of 0.12 and 0.14 respectively. False wind weather windows were also predicted due to the large underestimations of the wind speed at the hub heights during stable conditions. While when using the data from extended wind profile the number of available windows for installation operations with a wind speed limit less than 14 m/s was overestimated. Overestimation of up to 8% was observed. For the other required wind weather windows (i.e .installation operation with wind speed limit equals or greater than 14 m/s), the number of available wind weather windows appeared to closely match that of the measured data (the accuracy in estimating the number of available wind weather windows range from - 0.5% to 1.22%). Based on these findings, a new approach to wind profile modelling in wind farm installation campaign simulations using the extended wind profile is suggested. The new approach with a compensation factor of 0.25 m/s had an accuracy within ±1% when estimating the number of available weather windows. The impact the wind profile model adopted will have on the accumulated waiting on weather during installation campaign and possible power production is also assessed. The results show that atmospheric stability clearly affects the accumulated waiting on weather during offshore wind farm campaign simulation, and should be considered when simulations involving the installation phase of a wind farm project are involved. A better estimation of the possible power production is also achieved when atmospheric stability is accounted for.

KEYWORDS: Wind Farm; Offshore; Atmospheric Stability; Simulation; Installation Campaign; Power Production; Wind Energy; Wind Profile; Boundary-Layer Meteorology; FINO data base; Waiting on weather.

Acknowledgement

I would like to express my gratitude to my supervisor, Dr. Charlotte Obhrai for her support and guidance throughout the course of this thesis work.

I would also like to thank Ole-Erik Endrerud and Shoreline for granting access to their intelligent simulation tools.

Symbols and Abbreviations

Abbreviations

API	American Petroleum Institute
AWoW	Accumulated waiting on weather
DNV	Det Norske Veritas
GL	Germanischer Lloyd
IEC	International Electrotechnical Committee
ISO	International Standards Organization
OD	Operation duration
RMSE	Root mean square error
ROV	Remotely operated vehicles
SA	Simulated Annealing
WSL	Wind speed limit
WTIV	Wind turbine installation vessel

Symbols

α	Power law exponent
γ_{BD}	Businger Dyer parameter
γ_{FC}	Free convection parameter
ζ	Dimensionless stability parameter
θ_v	Virtual potential temperature
$\varkappa$	Von Karman constant
μ	Dimensionless stability parameter in equation [21]
ν	Velocity scale
ϱ_0	Unperturbed density
ϕ_M	Dimensionless wind gradient
ψ_M	stability dependent function
Γ	Integral of stability correction function
Υ	Closing term in equation [25]
Ω	Last term in equation [25]
A	Resistant function in equation [21]
A_c	Chornock constant
B	Resistant function in equation [21]
f	Coriolis parameter
G	Geostrophic wind speed
g	Acceleration due to gravity
h	Boundary layer height
l	Local length scale
L	Monin-obukhov length

p	Coefficient in equation [29] &[30]
q	Coefficient in equation [29] &[30]
r	Mixing ratio
R	Richardson number
RI	Bulk-Richardson number
T	Temperature
T_z	Mean wind speed in equation [38]
u	Wind speed
u_{hub}	Wind speed at hub height
u_z	Measured wind speed in equation [30]
$u*_0$	Friction velocity
z	Reference height
z_{hub}	hub height

List Of Figures

List Of Tables

1 Introduction

Wind energy, both onshore and offshore, is one of the key technological options for a shift to a decarbonised energy supply. Causing, among other benefits, a reduction in fossil fuel use and greenhouse gas emissions (Ortega-Izquierdo and del Río 2016). The installed wind power capacity offshore is currently increasing by 50% per year and steady growth is foreseen for the coming years, especially in Europe (Consult 2014). Despite the environmental motivations, the economic efficiency of wind power is becoming more and more significant for the further development of the wind power industry (Ma et al. 2015). Hence the wind industry, especially the offshore wind industry, is in a new era where intelligent simulation software tools are being used to model key aspects of wind energy asset management at every stage of the asset lifecycle. Doing so is enabling the industry to effectively scale its activities and also, improving the ability to quickly and more sustainably deploy wind energy around the world.

These intelligent simulation tools make use of wind speed at various heights as one of the inputs to analyse and understand various stages of the asset life cycle (estimate power production and waiting on weather time, especially during installation campaign simulations). Direct measurements of wind speed at sea are extremely costly and therefore only available for a few sites and restricted time periods (Badger et al. 2016). Due to a lack of measurement at these required heights, Near-surface wind measurements are often extrapolated to the necessary heights using wind profile extrapolation models. Where these wind speeds are limiting criteria for marine operations offshore, the wind profile extrapolation model used will be of utmost importance for waiting on weather; one of the major cost and risk drivers in offshore wind projects. It is therefore questioned to what extent the choice of adopted wind profile extrapolation models will affect the outputs of these simulation tools.

In the scope of wind turbine design, there is a growing interest in accurate methodologies to describe far offshore atmospheric conditions. Current standards such as IEC 61400-3 and DNV-OS-J101 for designing offshore wind turbines are based on onshore experience (Obhrai et al. 2012) and show shortcomings in adaptation to the maritime environment.

In contrast to wind flow conditions over land meteorological situation offshore is different mainly due to three important effects (Tambke et al. 2006).

1) The non-linear wind-wave interaction leads to a variable, but small surface roughness.
2) The large heat capacity of the water strongly affects the spatiotemporal characteristics of thermal stratification of the air.
3) Internal boundary layers caused by the land-sea discontinuity modify the structure of the marine atmospheric flow.

The most widely used extrapolation method is the power law model, a model that relies only on the wind speed at a reference height and a shear exponent. The shear exponent governs the amount of wind shear between the reference height and the turbine height

(Petersen et al. 1998). Though incorporating atmospheric stability into wind resource modelling is becoming common (Argyle and Watson 2014), a majority of assessed processes assumed that the atmospheric stability is keeping neutral. The effects of atmospheric stability on wind shear exponent and wind turbine power curve are studied by Sumner and Masson (2006), they proved that the annual power output of a wind farm would be misestimated if the effects of atmospheric stability were ignored. It was also presented by Bratton and Womeldorf (2011) that the wind speed at hub height which is derived from the near-surface measurements is not accurate, because the closer to the surface, the larger the wind shear exponent is. Therefore it is important to grasp wind profile distribution under different atmospheric stabilities, it would help increase the accuracy of wind resource assessment and improve the economic efficiency of wind farm construction. A reliable prediction of the wind resource is even more crucial for offshore sites where the projects depends on the favourable wind conditions of the sites, since the higher energy yield has to compensate for the additional installation and maintenance cost. Majority of available literature works are based on the effects of atmospheric stability on wind profile and the corresponding impact on wind resource assessment in terms of power production, wind turbine fatigue load. Non was found on the effect the wind profile adopted during offshore installation campaign simulation will have on the waiting on weather time; one of the major cost and risk drivers in offshore wind projects.

The goal of this study is twofold. First is to investigate and provide new insights into atmospheric conditions offshore and also, the accuracy of various vertical wind profile models using Meteorological data from Forschungsplattform in Nord-und Ostsee 3 (FINO3) offshore measurement platform. The FINO3 site is located about 80 km west off the coast of the German North Sea island of Sylt. Such information is critical for hub height wind speed climatologies that are based on near-surface wind observations and could provide valuable new findings for wind energy developers, who must often use extrapolation methods when hub height wind speed data are not available. Second is to investigate the impact of these wind profile on offshore wind farm installation campaign simulations results and then provide advice on the appropriate model. In this study, the sensitivity of accumulated waiting on weather during installation campaign simulations is considered as well estimated power production using Shoreline intelligent simulation tools. Section 2 gives a background on wind profiles and on offshore wind farm installation. Section 3 describes in detail the data used in this study and also gives insights into atmospheric conditions offshore. Section 4 describes the analysis and results on wind profile models. Section 5 describes the analysis and results on the accumulated waiting on weather and estimated power production. Finally, Section 7 provides a discussion and section 8 a conclusion.

2. Background

Due to the subject matter of this project, the analysis and presentation of the underlying literature is divided into the area of offshore wind profile and the area of installation of offshore wind farms.

2.1. Offshore wind profile

External wind conditions in the offshore regime are defined in guidelines by Det Norske Veritas (DNV), International Electrotechnical Committee (IEC) and Germanischer Lloyd (GL).

- DNV-OS-J101: Design of Offshore Wind Turbine Structures, September 2011
- DNV-RP-C205: Environmental Conditions & Environmental Loads, October 2010
- DNV-RP-J101: Use of Remote Sensing for Wind Energy Assessments, April 2011
- IEC 61400-1. Wind Turbines – Part 1: Design Requirements, 2005
- IEC 61400-3: Wind Turbines – Part 3: Design Requirements for Offshore Wind Turbines, 2009
- GL Guideline for the Certification of Offshore Wind Turbines, Ed. 2005

The American Petroleum Institute (API 2000) and the International Standards Organization (ISO 2004) have developed standards relevant to offshore technologies. These standards do not specifically address offshore wind turbines; however considerable guidance is given for the design of offshore structures in general, particularly with regard to structural integrity. The API and ISO guidelines are referenced here for completeness but are not discussed in detail.

All the standards state that the wind conditions should preferably be determined from measurements at the site in question. The site conditions should then be correlated with long-term records from local meteorological stations. The IEC standards state that the measurement period should be sufficiently long to obtain reliable parameters but they do not specify a time period. The GL guidelines specify that a minimum measuring period of 6 months is required. However, if seasonal variations contribute significantly to the wind conditions, then the measurement period should account for this. The DNV-RP-C205 recommends that for design the wind climate database should cover a 10-year period or more of continuous data with sufficient time resolution. In the absence of suitable long term measurements, they suggest that the wind velocity climate can be estimated from hindcast wind data and DNV-RP-C205 references the World Meteorological Organisation (WMO 1983) to obtain the minimum requirements to hindcast models and their accuracy. The offshore wind standard DNV-OS-J101 suggests that the 10 min mean value of wind speed should be obtained from several years of data.

The wind speed at 10 m is often used as the reference height in all the standards. When wind speed data are only available for heights other than the reference height then a suitable wind profile must be assumed. The assumed wind profile is used to define the average vertical wind shear across the rotor swept area. The standards recommend different

wind profile models to determine the vertical structure of the Marine Boundary Layer (MBL), a brief description of the wind profile models considered in this study is presented below:

2.1.1. Power law

The wind profile $\overline{U}(z)$ denotes the average wind speed as a function of a reference height z above the ground.

$$\overline{U}(z) = U_{hub}\left[\frac{z}{z_{hub}}\right]^{\alpha} \quad [1]$$

Where U_{hub} is the wind speed at the hub height z_{hub}, and α is the power law exponent. This model assumes neutral stability based on a constant roughness length of 0.002 m to be used over the sea. The power law has no explicit theoretical basis and is just a function known to fit the logarithmic wind profile. This profile is widely used in engineering applications because it is easier to work with a power law than with the logarithmic wind profile. This method does not take account of roughness effects due to waves and thermal effects due to atmospheric stability (Obhrai et al. 2012).

The IEC 64100-3 and GL standards recommend this simple exponential wind profile with the exponent $\alpha = 0.12$ for all wind speeds.

2.1.2. Logarithmic wind speed profile

$$\overline{u}(z) = \left[\frac{u_*}{\varkappa}\right] ln\left[\frac{z}{z_0}\right] \quad [2]$$

Where $\varkappa$ is the von Karman constant, assumed to be 0.4 (Högström 1988), z is the reference height and z_0 is the aerodynamic roughness length calculated using the Charnock's relation (Charnock 1955). The roughness length can be considered as the point where the wind speed becomes zero when extrapolated towards the surface using Monin-Obukhov theory (Stull 1988b). This dependence is expressed by:

$$z_0 = \frac{A_c u_*^2}{g} \quad [3]$$

where g is the acceleration due to gravity and the empirical constant A_c is the Charnock constant.

The DNV-OS-J101 standards suggest logarithmic wind speed profile for neutral atmospheric conditions, as an alternative to the logarithmic profile the DNV-OS-J101 guideline also suggest the power law in equation [1].

2.1.3. Stability corrected logarithmic wind profile

For stability corrections of wind profiles reference is made to DNV-RP-C205 standard. Wind profiles are derived from the logarithmic model presented in Equation [2], modified by a stability correction. The stability-corrected logarithmic wind profile reads:

$$\overline{U}(z) = \frac{u_*}{k}\left[ln\left(\frac{z}{z_0}\right) \pm \psi_M\left(\frac{z}{l}\right)\right] \quad [4]$$

in which ψ_M is a stability-dependent function, which is positive for stable conditions, negative for unstable conditions, and zero for neutral conditions. The stability function ψ_M depends on the height z and the Monin-Obukhov length L. The DNV-RP-C205 guideline references (Stull 1988b) for the relevant expressions between ψ_M and L. They state that the Monin-Obukhov length L can be calculated using the Richardson number R which is a dimensionless parameter whose value determines whether convection is free or forced defined as follows:

$$R = \frac{g\frac{d\varrho_0}{dz}}{\varrho_0\left(\frac{dU}{dz}\right)^2} \quad [5]$$

where g is the acceleration of gravity, ϱ_0 is the unperturbed density, $d\varrho_0/dz$ is the vertical density gradient and dU/dz is the vertical gradient of the horizontal wind speed. When data for the Richardson number R are not available, the DNV-RP-C205 guideline suggests that the Richardson number can be computed from averaged conditions by the method described in Panofsky and Dutton (1984).

2.1.4 The extended wind profile model

In this study, the extended wind profile proposed by Gryning will also be considered. For the sake of clarity, we show the derivation in this section. Also, the parametrization adopted in this study is shown. Unless stated otherwise, the equations and derivations are taken from M. C. Holtslag, Bierbooms, and van Bussel (2017).

Theoretical derivation of the wind shear profile

Based on dimensional analysis, wind shear in terms of the gradient $\partial\overline{U}/\partial z$ depends on a velocity scale ν and a local length scale l as

$$\frac{\partial\overline{U}}{\partial z} = \frac{\nu}{l} \quad [6]$$

Following Monin-Obukhov theory (Monin and Obukhov 1954; Obukhov 1971), one adopts the surface friction velocity u_{*0} as relevant velocity scale, assumed to be constant close to the surface, and the height z as relevant local length scale. Incorporating the definition of the dimensionless wind gradient ϕ_M to account for stability effects (see Businger et al. (1971); Stull (1988a)) one finds

$$\frac{\partial \overline{U}}{\partial z} = \frac{u_{*0}\phi_M}{\varkappa z} \qquad [7]$$

Where $\varkappa$ is the von Karman constant, assumed to be 0.4 (Högström 1988). The principle arguments proposed by Gryning are that in the atmospheric boundary layer the friction velocity decreases linearly with height, and that the local length scale l can be decomposed into a summation of three specific length scales. These three specific length scales correspond to a local surface layer length scale (assumed to be ϕ_M/z, similar as in surface layer scaling), a local middle layer length scale (assumed to be $1/l_{ML}$, which has to be parametrized) and a local upper layer length scale (assumed to equal $1/(h-z)$, where h is the boundary layer height). Incorporating these principle arguments in Equation [6], and taking into account the von Karman constant, results in

$$\frac{\partial \overline{U}}{\partial z} = \frac{u_{*0}}{\varkappa}\left[1 - \frac{z}{h}\right]\left(\frac{\phi_M}{z} + \frac{1}{l_{ML}} + \frac{1}{h-z}\right) \qquad [8]$$

In surface layer scaling it is assumed that the dimensional wind gradient is a universal function of stability in terms of ζ, where ζ is defined as

$$\zeta = \frac{z}{L} = -\frac{z\varkappa g[\overline{w'\theta'_v}]_s}{u_{*0}^3\overline{\theta_v}} \qquad [9]$$

Here L is the Obukhov length, g is the gravitational acceleration, $(\overline{w'\theta'_v})_s$ is the turbulent flux of virtual potential heat at the surface and θ_v is the virtual potential temperature. The dependence of ϕ_M on stability has been studied extensively in literature, and the Kansas experiment is likely the most well-known study (Businger et al. 1971; Haugen, Kaimal, and Bradley 1971), though more recent studies are shown by Akylas and Tombrou (2005); Chenge and Brutsaert (2005). For unstable conditions, one typically considers either the Businger-Dyer formulation (Businger et al. 1971) or the so-called Free-Convection formulation (Paulson 1970), respectively

$$\phi_M = [1 - \gamma_{BD}\zeta]^{-1/4} \qquad [10]$$

$$\phi_M = [1 - \gamma_{FC}\zeta]^{-1/3} \qquad [11]$$

With $\gamma_{BD} = 19.3$ (Högström 1988) and $\gamma_{FC} = 12.87$ (Fairall, Bradley, and Rogers 1996). For stable conditions, one typically considers the Businger-Dyer formulation (Businger et al. 1971) or the formulation of Holtslag (M. C. Holtslag, Bierbooms, and van Bussel 2015), respectively

$$\phi_M = 1 + \beta\zeta \quad [12]$$

$$\phi_M = 1 + \zeta[a + b[exp(-d\zeta)[+ c - d\zeta]]] \quad [13]$$

with $\beta = 6$ (Högström 1988), and the coefficients a, b, c and d are respectively 1, 2/3, 5 and 0.35 (Beljaars and Holtslag 1991). The shown functions of ϕ_M all become one for neutral conditions where $\zeta = 0$. Integration of Equation [7] with respect to height results in the diabatic surface layer profile (the same as the stability corrected logarithmic wind profile in equation [4], the last term in equation [14] is generally neglected since $\psi(\zeta) \gg \psi(\zeta_0)$ (Holtslag et al. 2014)).

$$\overline{U}(z) = \frac{u_*}{\kappa}\left[ln\left(\frac{z}{z_0}\right) - \psi(\zeta) + \psi(\zeta_0)\right] \quad [14]$$

where z_0 is the aerodynamic roughness length, $\zeta_0 = z_0/L$ and ψ is a stability correction function, which originates from (Paulson 1970).

$$-\int_{\zeta_0}^{\zeta} \frac{1-\phi_M}{\zeta} d\zeta = -\psi(\zeta) + \psi(\zeta_0) \quad [15]$$

The choice of adopting specific ϕ_M-functions in this study thus has an impact when deriving the extended wind profile, because of the required integration of Equation [8] (the integration results in multiple terms, not just ψ as obtained for the surface layer wind profile). Following Gryning et al. (2007); the Free-Convection formulation is adopted for unstable conditions, and the Businger-Dyer formulation is adopted for stable conditions, to derive the extended wind shear profile. Since two specific ϕ_M-functions for stable and unstable conditions are selected, also the stability correction functions typically found in surface layer scaling shear profiles are set. For respectively stable and unstable conditions these are

$$\psi(\zeta) = -\beta\zeta \quad [16]$$

$$\psi(\zeta) = \frac{3}{2}In\left(\frac{x^2 + x + 1}{3}\right) - \sqrt{3}arctan\left(\frac{2x+1}{\sqrt{3}}\right) + \frac{\pi}{\sqrt{3}} \quad [17]$$

Where $x = [1 - \gamma_{FC}\zeta]^{-1/3}$. Due to the linearity of Equation [16], one can write for stable conditions

$$\psi(\zeta) = \frac{z}{h}\psi(\zeta_h) \quad [18]$$

where $\zeta_h = h/L$. Both ψ-functions are zero for neutral conditions. Integration of Equation [8] with respect to height, and assuming $z_0/h = 0$, leads to the following extended shear profile for respectively stable and unstable conditions

$$\overline{U}(z) = \frac{u*_0}{\kappa}\left[ln\left(\frac{z}{z_0}\right) + \frac{1}{2}\left[2 - \frac{z}{h}\right]\left[\frac{z}{h}\frac{h}{l_{ML}} - \psi(\zeta)\right]\right] \quad [19]$$

$$\overline{U}(z) = \frac{u*_0}{\kappa}\left[ln\left(\frac{z}{z_0}\right) - \psi(\zeta) + \psi(\zeta_0) + \frac{z}{h}\left[1 - \frac{3}{2}\frac{x_z^2 - x_0^2}{x_z^3 - 1}\right] + \frac{1}{2}\left[2 - \frac{z}{h}\right]\frac{z}{h}\frac{h}{l_{ML}}\right] \quad [20]$$

where the subscripts z and 0 correspond to using respectively z and z_0 in x. Note that one could rewrite the term $z/h\, h/l_{ML}$ in these equations, but this is not done since a parametrization of h/l_{ML} will be derived. Besides, by incorporating Equation [18] in combination with the assumption that $z_0/h = 0$, there is no $\psi(z_0/L)$-term in the shear profile for stable conditions.

Parametrization of h/l_{ML}

For the parametrization of l_{ML} we consider the geostrophic wind speed at the top of the boundary layer. A common expression for the geostrophic wind is obtained for barotrophic, stationary conditions as (Blackadar and Tennekes 1968; Zilitinkevich and Deardorff 1974).

$$G = \frac{u*_0}{\kappa}\sqrt{[In\left(\frac{u*_0}{fz_0}\right) - B(\mu)]^2 + A^2(\mu)} \quad [21]$$

where G is the geostrophic wind speed, f is the Coriolis parameter, A and B are the resistance functions that will be parametrized shortly and μ is the dimensionless stability parameter $u*_0/fL$. It is recognised however that Equation [21] is invalid if the boundary layer height h is not uniquely defined by μ alone, and in practice h also depends on other processes not taken into account in μ, such as entrainment and the vertical wind speed at the top of the boundary layer (Byun 1991; Zilitinkevich and Deardorff 1974). As such, an alternate formulation of Equation [21] is proposed in Zilitinkevich and Deardorff (1974) where the boundary layer height h is a unique variable, which results in (see Equation [15] of Zilitinkevich and Deardorff (1974)).

$$G = \frac{u*_0}{\varkappa}\sqrt{[In\left(\frac{h}{z_0}\right) - B\left(\frac{h}{L}\right)]^2 + A^2\left(\frac{h}{L}\right)} \quad [22]$$

Since the resistance functions now depend on the dimensionless parameter h/L instead of μ, the parametrization of A and B will differ compared to using Equation [21] (Byun 1991). Evaluating Equations [19] and [20] at $z = h$ and combining with Equation [22] yields expressions for h/l_{ML}

$$\frac{h}{l_{ML}} = 2\left[\sqrt{\left[In\left(\frac{h}{z_0}\right) - B\left(\frac{h}{L}\right)\right]^2 + A^2\left(\frac{h}{L}\right)} - In\left(\frac{h}{z_0}\right)\right] + \psi\left(\frac{h}{L}\right) \quad [23]$$

$$\frac{h}{l_{ML}} = 2\left[\sqrt{\left[In\left(\frac{h}{z_0}\right) - B\left(\frac{h}{L}\right)\right]^2 + A^2\left(\frac{h}{L}\right)} - In\left(\frac{h}{z_0}\right) + \psi\left(\frac{h}{L}\right) - \psi\left(\frac{z_0}{L}\right) - \left[1 - \frac{3}{2}\frac{x_h^2 - x_0^2}{x_h^3 - 1}\right]\right] \quad [24]$$

Where the subscript h denotes the usage of h/L instead of z/L in x. For the sake of clarity, the extended wind shear profile is rewritten as

$$\overline{U}(z) = \frac{u*_0}{\varkappa}\left[ln\left(\frac{z}{z_0}\right) + \Upsilon + \Omega\right] \quad [25]$$

where the last term is similar in notation for stable and unstable conditions and given by

$$\Omega = \frac{z}{h}\left[2 - \frac{z}{h}\right]\left[\sqrt{\left[In\left(\frac{h}{z_0}\right) - B\left(\frac{h}{L}\right)\right]^2 + A^2\left(\frac{h}{L}\right)} - In\left(\frac{h}{z_0}\right)\right] \quad [26]$$

and all remaining terms are combined into a closing term. For stable conditions, no terms remain due to the linearity of the stability correction function. We then find for respectively stable and unstable conditions

$$\Upsilon = 0 \quad [27]$$

$$\Upsilon = \frac{z}{h}\left[2 - \frac{z}{h}\right]\left[\psi\left(\frac{h}{L}\right) - \psi\left(\frac{z_0}{L}\right)\right] - \left[\psi\left(\frac{z}{L}\right) - \psi\left(\frac{z_0}{L}\right)\right] + \frac{3}{2}\frac{z}{h}\left[\left[2 - \frac{z}{h}\right]\frac{x_h^2 - x_0^2}{x_h^3 - 1} - \frac{x_z^2 - x_0^2}{x_z^3 - 1}\right] - \frac{z}{h}\left[1 - \frac{z}{h}\right] \quad [28]$$

Combined, this wind shear profile is a function of the same parameters as the surface layer wind shear profile (thus z, z_0, L and $u*_0$), and three extra parameters: the boundary layer height h, and the two resistance functions A and B.

Parametrization of the resistance function A and B

The resistance functions A and B are parametrized following M. C. Holtslag, Bierbooms, and van Bussel (2017).

$$A = \frac{q+1}{q}\frac{\varkappa u_{*0}}{fh} \quad [29]$$

$$B = \frac{p+1}{p} - \psi\left(\frac{z_0}{L}\right) - \frac{\psi(\frac{h}{L})}{p} + \frac{p+1}{p\frac{h}{L}}\left[\Gamma\left(\frac{h}{L}\right) - \Gamma\left(\frac{z_0}{L}\right)\right] \quad [30]$$

where p and q are coefficients that vary between 1 and 3 (with $q = 1$ if the friction velocity decreases linearly with height and $p = 1.5$ for neutral conditions) and Γ is the integral of the stability correction function

$$\Gamma\left(\frac{h}{L}\right) = \int \psi\left(\frac{h}{L}\right) d\frac{h}{L} \quad [31]$$

In the absence of a proper parametrization of p as a function of stability, we assume $p = 1.5$. For stable and unstable conditions Γ equals respectively

$$\Gamma\left(\frac{h}{L}\right) = \frac{1}{2}\frac{h}{L}\psi\left(\frac{h}{L}\right) \quad [32]$$

$$\Gamma\left(\frac{h}{L}\right) = \frac{h}{L}\left[\psi\left(\frac{h}{L}\right) - 1\right] - \frac{3}{2}\frac{x_h^2}{\gamma_{FC}} + \frac{31}{16\gamma_{FC}} \quad [33]$$

Combined this results for stable and unstable conditions respectively in

$$B = \frac{p+1}{p} + \frac{1}{2}\frac{p-1}{p}\psi\left(\frac{h}{L}\right) - \psi\left(\frac{z_0}{L}\right) \quad [34]$$

$$B = \frac{3}{2}\frac{p+1}{P}\frac{x_h^2 - x_0^2}{x_h^3 - 1} + \psi\left(\frac{h}{L}\right) - \psi\left(\frac{z_0}{L}\right) \quad [35]$$

where again it is assumed that $z_0/h = 0$. For neutral conditions, these equations match, since

$$\lim_{L\to\infty}\frac{x_h^2 - x_0^2}{x_h^3 - 1} = \frac{2}{3} \quad [36]$$

We thus find for neutral conditions $B = 1.67$, and A is a function of the dimensionless parameter $u*_0/fh$. With the above parametrization, the extended wind profile is a function of z_0, h, L and $u*_0$.

2.1.4. Current research

The standard logarithmic profile in equation [2] and power law profile in equation [1] given in the design standards both assume homogeneous and neutral wind conditions. Neumann, Emeis, and Illig (2007) compared average wind velocity profiles measured offshore at the FINO1 platform with the vertical wind profile computed using the power law as recommended in the IEC 6400-3 (2009) and GL (2005) guidelines. The predicted power law profile gave poor results particularly at heights above 40m. The standard predicted profile tended to underestimate wind speed under stable conditions. Offshore wind profiles can be governed more by atmospheric stability than by the roughness parameter z_0 (Lange et al. 2004; Motta, Barthelmie, and Vølund 2005) and there is a general consensus in the scientific literature that the inclusion of stability effects into the standard logarithmic profile in equation [4] greatly improves vertical wind profile predictions.

A paper by Obhrai et al. (2012) carried out a review on the current state of the art in offshore wind modelling and identified the gaps between best knowledge and best practice. Also, data from FINO3 were used to estimate the gradient Richardson number (the temperature (at 29 m & 95 m) and wind speed (at 50 m & 90 m) at the two elevations). The conditions were then classified according to stability classes using limits. The results show that very unstable conditions dominate at the FINO3 site (48.6%). The wind profiles were then normalised using the velocity measured at 50m and the mean profile for each of the stability classes was calculated. The observed profiles show a deviation from the standard logarithmic profile for all thermal conditions. There was also consistent bending of the profile above 80 m for all thermal conditions. Their initial analysis of the data at FINO3 also suggests that the average wind speed profile above 80 m deviates from the standard MOST surface layer theory. Eliassen et al. (2012) investigated the impact of stability on the fatigue of an offshore wind turbine using data the same data from FINO3. Their study showed that fatigue loading at the root of the blades increases by 40% when stability is taken into account.

Motta, Barthelmie, and Vølund (2005) used long term data (4 years) from three Danish offshore meteorological masts to investigate the role of the stability on the marine vertical wind profile. The fetches at each of these masts varied from 2 km up to 100 km. They found that by applying the stability corrections to very stable conditions a change in velocity of up to 50% from the original value was obtained. Two of the masts (Vindeby & Rødsand) were close to the coast and there was therefore evidence of a land sea discontinuity under certain wind directions but this was not studied in great detail. The wind climate at Rødsand has been further studied by Lange et al. (2004) who also observed wind profiles which deviated from the standard logarithmic profile. Deviations were observed under conditions of warm air advection over a colder sea surface, even for fetches up to 30 km. They suggest that in coastal waters warm air advection is a frequent occurrence which will have an important

effect on the average wind profile. They do not however suggest any alternative methods to model the vertical wind profile under this type of condition.

Tambke et al. (2004) found that measured wind profiles at Horns Rev and FINO1 showed deviations from the standard logarithmic profiles for all thermal conditions. They dismiss the possibility of land sea discontinuity effects as these observations were seen for long fetches up to 800 km. They instead suggest that the observed deviations were the result of a decrease in the height of the atmospheric boundary layer due to lower turbulence in the offshore marine environment. They conclude that the upper instruments could be in the Ekman layer where surface theory and hence a logarithmic profile is no longer valid. They propose an alternative method to model the vertical wind profile which is based on the inertial coupling between the Ekman layer of the atmosphere and the ocean with constant shear stress in between.

Peña, Gryning, and Hasager (2008) compared atmospheric turbulent flux measurements performed in 2004 with a sonic anemometer to a bulk Richardson number formulation of the atmospheric stability. This was then used to classify the LiDAR/cup wind speed profiles into atmospheric stability classes. The observations were compared to a simplified model for the wind speed profile that accounts for the effect of the boundary-layer height. For unstable and neutral atmospheric conditions the boundary-layer height was neglected, whereas for stable conditions it was comparable to the measuring heights and therefore essential to include. It was interesting to note that, although it was derived from a different physical approach, the simplified wind speed profile conforms to the traditional expressions of the surface layer when the effect of the boundary-layer height is neglected.

Gryning et al. (2007) analysed profiles of meteorological measurements from a 160 m high mast at the National Test Site for wind turbines at Høvsøre (Denmark) and at a 250 m high TV tower at Hamburg (Germany). This showed that the wind profile based on surface-layer theory and Monin-Obukhov scaling was valid up to a height of 50–80 m. At higher levels, deviations from the measurements progressively occurred. An extension to the wind profile in the surface layer was formulated for the entire boundary layer, with emphasis on the lowest 200–300 m and considering only wind speeds above 3 m s−1 at 10 m height. The friction velocity was taken to decrease linearly through the boundary layer. The wind profile length scale was composed of three component length scales. In the surface layer, the first length scale was taken to increase linearly with height with a stability correction following Monin-Obukhov similarity. Above the surface layer the second length scale (L_{MBL}) was independent of height but not of stability, and at the top of the boundary layer, the third length scale was assumed to be negligible. A simple model for the combined length scale that controls the wind profile and its stability dependence was formulated by inverse summation. Based on these assumptions the wind profile for the entire boundary layer was derived. A parameterization of L_{MBL} was formulated using the geostrophic drag law, which relates friction velocity and geostrophic wind. The empirical parameterization of the resistance law functions A and B in the geostrophic drag law is uncertain, making it impractical. Therefore an expression for the length scale, L_{MBL}, for applied use was suggested, based on measurements from the two sites.

M. C. Holtslag, Bierbooms, and van Bussel (2017) extended the diabatic surface layer wind shear model for offshore wind energy purposes to higher altitudes based on Gryning's wind profile and the resistance functions proposed by Byun. The wind profile was in theory applicable up to the boundary layer height, which is parametrized with the

Rossby-Montgomery equation. The coefficient c of the Rossby-Montgomery equation was found to be stability dependent with decreasing values up to 0.04 for stable conditions and increasing values up to 0.17 for unstable conditions. The proposed shear profile was validated with 1 year of offshore observation data, and a significant improvement in accuracy was found compared to traditional surface layer shear profiles or power laws. The influence of adopting this extended shear profile for wind energy was analysed in terms of the kinetic energy flux and blade root fatigue loads experienced by a wind turbine. It was found that, especially for stable conditions, results deviate significantly compared to using the traditional surface layer shear profile. The kinetic energy flux decreases by up to 15%.

2.2. Installation of Offshore Wind Farms

Installation of offshore wind farms is the last step before commissioning of an offshore wind farm, which contributes to approximately 20-30% of development costs or 15-20% of the price of energy (Asgarpour 2016). The basic steps involved in the installation campaign of an offshore wind farm are briefly described in this section.

2.2.1. Delivery of Components

First, the components are delivered to the onshore assembly site at the harbour. These components include foundations, tower sections, nacelle, rotor, blades, substations and cables. Onshore and offshore substations are usually directly delivered to their installation location and no assembly at the harbour is required. Array and export cable-laying vessels are already loaded with cables and no harbour assembly is also necessary.

2.2.2. Onshore Assembly

The onshore assembly site at the harbour is where, based on the installation strategy, all component assemblies are completed, components are then loaded onto the installation vessel to be transported to the site of the offshore wind farm. Assembly at the harbour only mainly applies to wind turbine components. Based on the installation strategy, different assembly concepts for wind turbine components are possible, some based concepts are listed below:

1. No onshore assembly: All components are transported to the location of the offshore wind farm and then installed one by one.
2. Tower assembly: The tower sections (typically three or four sections) are assembled at the onshore assembly site. Then, the whole tower structure is bolted on the deck of the installation vessel to maximise the vessel's loading capacity.
3. Assembly of two blades and the nacelle: The nacelle, hub and two blades are connected together. This concept is also known as the "bunny ear" concept. When the assembly is done, the nacelle with two blades attached is placed on the deck of the installation vessel.

4. Assembly of three blades and the nacelle: This concept is similar to the bunny ear concept, but with the whole rotor is attached to the nacelle.

2.2.3. Offshore Transport

The last step before the installation of an offshore wind farm is the transportation of all components to the location of the offshore wind farm. Currently, there are several installation vessels customised for the offshore wind industry and more optimised vessels are in the design phase. For each specific installation project, based on the strategy employed, an installation vessel is reconfigured for equipment placement and deck preparation. This step is normally called the mobilisation and takes place before loading the components from the manufacturing facilities or the onshore assembly site at the harbour to the deck of the vessel. When the installation is finished, the deck area is reconfigured for the next offshore wind installation. This step is normally called demobilisation.

After the mobilisation of the installation vessel and loading the components to the deck of the vessel, sea-fastening components are used to secure components to the deck of the transport vessel with the aim of preventing movement while the ship is in transit and subject to motions of the moving vessel. Sea-fastening design is typically specific to the vessel and cargo, however, modular sea-fastening components are often used for offshore wind components due to the unitized nature of the cargo (Ekici et al. 2016). After sea-fastening, the vessel can sail to the location of the wind farm. Sailing out to the location of the wind farm can only take place when the weather conditions at the location of the wind farm are suitable for the next installation step. Otherwise, the vessel will wait at the harbour for suitable weather conditions. This delay is normally known as weather delay or waiting on weather and for far offshore wind farms can be a significant project risk. Therefore, it is advisable that, based on the historical weather data, the weather delay per installation step be calculated. If this calculation is done, the optimal starting date for the installation can be found to minimise the total weather delay (Asgarpour 2016).

2.2.4. Installation

The installation step of offshore wind farms is when the years of planning come to reality. This step starts when the installation vessel with foundations arrives at the location of the wind farm to install the first foundation, and finishes when the cable installation vessels connect the offshore substation to the onshore substation through export cables. Installation of offshore wind farms can be categorised in four stages:

1. Foundation installation
2. Turbine installation
    a. Tower
    b. Nacelle
    c. Rotor
    d. Blade
3. Substation installation

    a. Offshore substation
    b. Onshore substation
4. Cable installation
    a. Array cables
    b. Export cables

A brief description of these steps is given below:

Foundation installation

Depending on the foundation type, the installation vessel and strategy may differ. Currently, approximately 90% of offshore wind turbines are installed on monopiles and the remainder are installed on jackets, tripods or gravity-based support structures. There are also a few demonstration floating turbines, which have no bottom-fixed foundations (Asgarpour 2016).

Monopiles are large hollow steel or concrete tubes, whose thickness and diameter vary with turbine size, soil conditions and water depth. Before installation of a monopile, a layer of scour protection should be applied to avoid seabed erosion around the monopile. This first scour protection layer is made by rock dumping around the monopile position. When the first layer of scour protection is made, monopiles are lifted from the installation vessel and then positioned on the seabed.

Common installation methods of monopiles are pile driving using a hydraulic hammer or pile drilling. On average it takes about one or two days to install a monopile using these methods. If pile driving using a hydraulic hammer is chosen, depending on the seabed conditions and water depth, it takes about 2000-3000 hammer hits to drive the monopile into the ground (Asgarpour 2016). During the pile driving or drilling, the piling depth is continuously monitored to make sure the monopile is placed into the correct depth. Since for hammering or drilling a stable platform is required, normally jack-up barges are used for monopile installation.

If a monopile is used as a foundation, in order to connect and level the turbine tower to the monopile, an extra component, called the transition piece, is necessary. The transition piece is lifted and placed on the top of the monopile and then the space between the monopile and the transition piece (about 10-20 cm thick) is grouted. The top of the transition piece is used as the work platform and the sides are used for boat landing and ladder placement. Moreover, J-shaped tubes are placed on the side of the transition piece to guide the array cables from the tower to the seabed. The installation of the monopile and transition piece is usually limited by a maximum wind speed of 18 m/s and a maximum wave height of 2 m (Paterson et al. 2018). These values may vary based on several factors (i.e., the vessel used for installation).

The installations of jackets and tripods to some levels are similar to each other. Similar to the monopile installation, a first layer of scour protection by rock dumping is required. The jackets or tripods are transported to the location of the wind farm using jack-up barges or floating vessels with mooring line stabilisation. When the installation vessel is positioned, the jacket or tripod is lifted and placed on the seabed. Alternatively, the jacket or tripod can be floated and then, using a crane, be positioned. In that case, a heavy lift crane is no longer

required. When the structure is positioned into the location, for jackets, four piles and for tripods, three piles are driven into the seabed to fix the foundation. The pile-driving methods for jackets and tripods are similar to monopiles. When the foundation installation is finished, the turbine tower can be installed directly on the top side of the jacket or the tripod.

Gravity-based foundations are normally self-buoyant and can be floated or towed out to the location of the offshore wind farm. Since the placement of the gravity-based foundation on the seabed requires a flat area, seabed preparation and scour protection steps are needed. When the seabed is prepared and the foundation is positioned in the right location, the foundation is sunk by the influx of water, and then the base of the foundation is filled with ballast to anchor the foundation. When ballasting is finished, the turbine tower can be directly installed on the topside of the gravity-based foundation.

Turbine installation

The turbine components to be installed are the tower, nacelle, hub and blades. The first installation step starts with the tower. As discussed before, the tower sections are typically assembled at the onshore assembly site at the harbour and the complete tower is transported to the location of the wind farm by the installation vessel. When the installation vessel is in position and stabilised, the tower is lifted and placed on top of the foundation and then bolted. If tower sections are not assembled at the onshore assembly site, the assembly takes place offshore, which logically takes more time and effort due to the harsh weather conditions offshore.

The second turbine component to be installed is the nacelle. Similar to the tower, the nacelle is lifted by the crane off the installation vessel and placed on the top of the tower. If the blades are not already attached to the nacelle, each blade should be lifted separately and connected to the hub. Then, in order to not change the position of the vessel or crane, the rotor is rotated to make space for the installation of a new blade. This operation is iterated up to the moment that all three blades are installed. Turbine installation is usually limited by a maximum wind speed of 8 m/s and a maximum wave height of 2 m (Paterson et al. 2018). These values may vary based on several factors (i.e., the pre-assembly method used and the vessel used for installation)

Substation installation

In order to connect the wind turbine generators to a grid, proper electrical infrastructure is required. During the early stages of the development of offshore wind farm, due to the low installed capacity and small transmission distance to the onshore grid, offshore substations were not required. Currently, there has been a trend in wind power engineering to combine multiple wind generation units (wind turbines), each with the capacity of many megawatts, and to connect them together to the onshore grid. This way, the total capacity of an offshore wind farm can be more than several hundred megawatts (Sulawa, Jami, and Pound 2009; Topham and McMillan 2017; Ederer 2015). In addition, offshore wind farms that are currently under construction or whose construction is planned, are relatively far away from the

onshore grid and thus require an offshore substation which is installed on a special platform (Robak and Raczkowski 2018).

Cable installation

The last step of the offshore wind farm installation is cable installation. Depending on the size and location of the wind farm, array cables connecting the output power of turbines are connected to one or two offshore substation busbars. Then, using export cables, the high-voltage electricity produced by the offshore wind farm is transferred to the onshore substation and from there, to the local electrical grid. The array and export cable routes are planned in such a way as to minimise the total cable length and follow all environmental laws and marine restrictions. Cable installation is usually limited by a maximum wind speed of 15 m/s and wave height of 1.5 m, the burial of the cable by a maximum wind speed of 12 m/s and wave height of 3 m (Paterson et al. 2018). But these values may vary based on many factors (i.e., vessel used). In the following, the installations of array and export cables are discussed separately.

Array cable installation: The array or infield cables are lines of cables connecting several turbines to an offshore substation. If a monopile foundation is used, the array cables are pulled through J-tubes and then are connected to the wind turbine cables in the tower bottom. After cable pulling, a second layer of scour protection by rock dumping may be applied around the foundation.
The array cables should be placed 1 or 2 m under the seabed in the space between wind turbines. This is done using trenching remotely operated vehicles (ROV) departed from an offshore vessel and monitored by an experienced pilot so as to not damage the cables. The trenching ROV buries the array cables 1 or 2 m below the seabed, depending on the environmental requirements and IEC and DNV standards (i.e.,, DNV-RP-J301 guideline). The last turbine in a row is connected to an offshore substation. This operation should be done for each row of connected turbines.

Export cable installation: After connecting array cables to offshore substations using transformers, the voltage is stepped up for onward transmission over a longer distance. The export high-voltage AC or DC cables connect the offshore substations to an onshore substation. The installation of export cables is similar to array cables, but larger cable-laying vessels and trenching ROVs are used. Typically, the cables near shore should be buried deeper than those far from the shore. After export cable installation, pre-commissioning tests can be carried out and then, the offshore wind farm can be commissioned.

2.2.5. Current research

Offshore wind farm installation planning is highly complex, due to the high dependency on weather and the oversized components that impose specific constraints in areas such as transportation and lifting. Currently, there is very little transparency vis-à-vis the logistics challenges in the industry (Vis and Ursavas 2016). Weather plays a decisive role in the

selection of the sites and in the operational planning. The fundamental purpose of installing wind turbines is to utilize wind energy as much as possible (Tsoutsos et al. 2015; Janajreh, Su, and Alan 2013). Accordingly, the offshore sites selected for offshore wind projects are likely to have high wind speeds, which also result in significant wave heights. This affects the installation process significantly. The wind and sea conditions always limit and narrow the time window for safe installation (Vis and Ursavas 2016). Marine operations play a pivotal role throughout all phases of a wind farm's life cycle. In particular, uncertainties associated with offshore installations can extend construction schedules and increase the capital expenditure (CAPEX) required for a given project. Installation costs typically account for approximately 30% of the overall project cost (Paterson et al. 2018).

A categorization of past research, based on the different phases of wind turbine operations, reveals that studies about the maintenance and operation phase are denser compared to the installation phase (Vis and Ursavas 2016). Within the first category, a number of researchers (Kovács et al. 2011; Besnard and Bertling 2010; Besnard, Fischer, and Tjernberg 2013) have worked on scheduling models for the maintenance of offshore wind turbines. A recent paper in renewable energy (Shafiee 2015) comprehensively reviews the past research on maintenance logistics. Dinwoodie et al. (2015) described an approach for verifying simulation models and demonstrated a verification process for four models. A reference offshore wind farm was defined and simulated using these models to provide test cases and benchmark results for verification for wind farm availability and O&M costs. This paper also identified key modelling assumptions that impact the results. The calculated availabilities for the four models showed good agreement apart from cases where maintenance resources were heavily constrained.

This project fits within the definition of the second category, that is, the installation phase. It adds to the existing research by considering the effect the wind profile model used in the simulation tool will have during the installation campaign simulation. The significance of and need for further studies on the installation phase of wind farms has been underlined by industry facts. Installation at sea is complex, and the equipment necessary is highly expensive (Vis and Ursavas 2016). The large components of the turbines' structure are highly vulnerable to wind. Hence, installation processes like lifting are restricted to a certain wind speed range.

The work on the modelling of logistic requirements and installation of offshore wind far has increased over the last five years in an attempt to reduce the uncertainty associated with accessing and completing work at offshore locations. This type of modelling and analysis allows practitioners to review the installation of an offshore wind farm in advance so that developers can prepare for certain outcomes in terms of cost or delay (Paterson et al. 2018).

Irawan, Jones, and Ouelhadj (2017) looked to address the scheduling issues surrounding offshore wind construction by means of an integer linear programming method to identify the optimal installation with lowest costs and shortest schedules, combining weather data and vessel availability. Their investigation in the use of metaheuristic approaches such as Variable Neighbourhood Search (VNS) and Simulated Annealing (SA) was found to offer reasonable results with low computation time. Their approach was compared against a linear programming optimiser known as CPLEX, which was found to identify the optimum solution but computationally more expensive.

Barlow et al. (2015) reviewed which vessels and operations are most susceptible to weather constraints during the installation campaign. Their study aimed to assess the impact

of operational and vessel improvements over recent times, indicating that a non-linear relationship exists between vessel limits and the duration of the installation. It was also concluded that load out operations appear most susceptible in adverse weather conditions.

The modelling approach by Vis and Ursavas (2016) revealed that the key activities impacting performance are the vessel loads, distance to shore and the pre-assembly strategy adopted for the main wind turbine components. They recommend that a pre-assembly strategy should be employed that presents the optimum choice between the lowest number of lifts possible and the maximum number of turbines that can fit on a vessel. The optimal approach will differ for each offshore wind project but careful consideration of these two parameters should help reveal the best solution for a given project.

3. Dataset Overview

The observation data from Forschungsplattform in Nord-und Ostsee 3 (FINO3) used in this study is described in section 3.1. The data was filtered, the wind speed distribution of the filtered data at a certain height was then compared to that of the original data at the same height. This was done to ensure the filtered data is still a proper representation of the wind speed distribution at FINO3. The filtration process and the result of the comparison are presented in section 3.2. The Atmospheric stability of the filtered data was also determined using the bulk-Richardson method. The determination process is described in section 3.3.

After, in section 3.4, the filtered observations are grouped into atmospheric Stability Classes according to intervals of Obukhov length, L. The relative occurrence of these stability classes was then compared to results obtained by M. C. Holtslag, Bierbooms, and van Bussel (2017) from Ijmuiden (similar distance from shore as FINO3). Also, the result from the comparison (FINO3 to Ijmuiden) was compared to the result obtained by Sathe, Gryning, and Peña (2011). They compared the relative occurrence of stability classes at OWEZ (Dutch part of the North Sea were Ijmuiden is also located) to Horns Rev (Danish part of the North Sea were FINO3 is also located). The relative occurrence of the atmospheric stability classes as a function of wind and the normalized mean wind speed profile for each stability at FINO3 is also presented in section 3.4.

3.1. Observation Data

The 120 m high Forschungsplattform in Nord-und Ostsee 3 (FINO3) offshore measurement platform is sited about 80 km west off the coast of the German North Sea island of Sylt (55º 11,7 'N, 007º 9,5' E), in the midst of German offshore wind farms (Butendiek, DanTysk, Sandbank and Nördlicher Grund) and has been in operation since August 2009.

The met mast has a platform at 22 m height and wind speed is measured at several heights between 30 m and 106 m as shown in Figure 3.1a. Other meteorological measurements also being observed consist of wind direction, air temperature, moisture, air pressure, global radiation, relative humidity and precipitation (See Figure 3.1b). More information on this can be found on the FINO3 (“FINO3” n.d.) website.

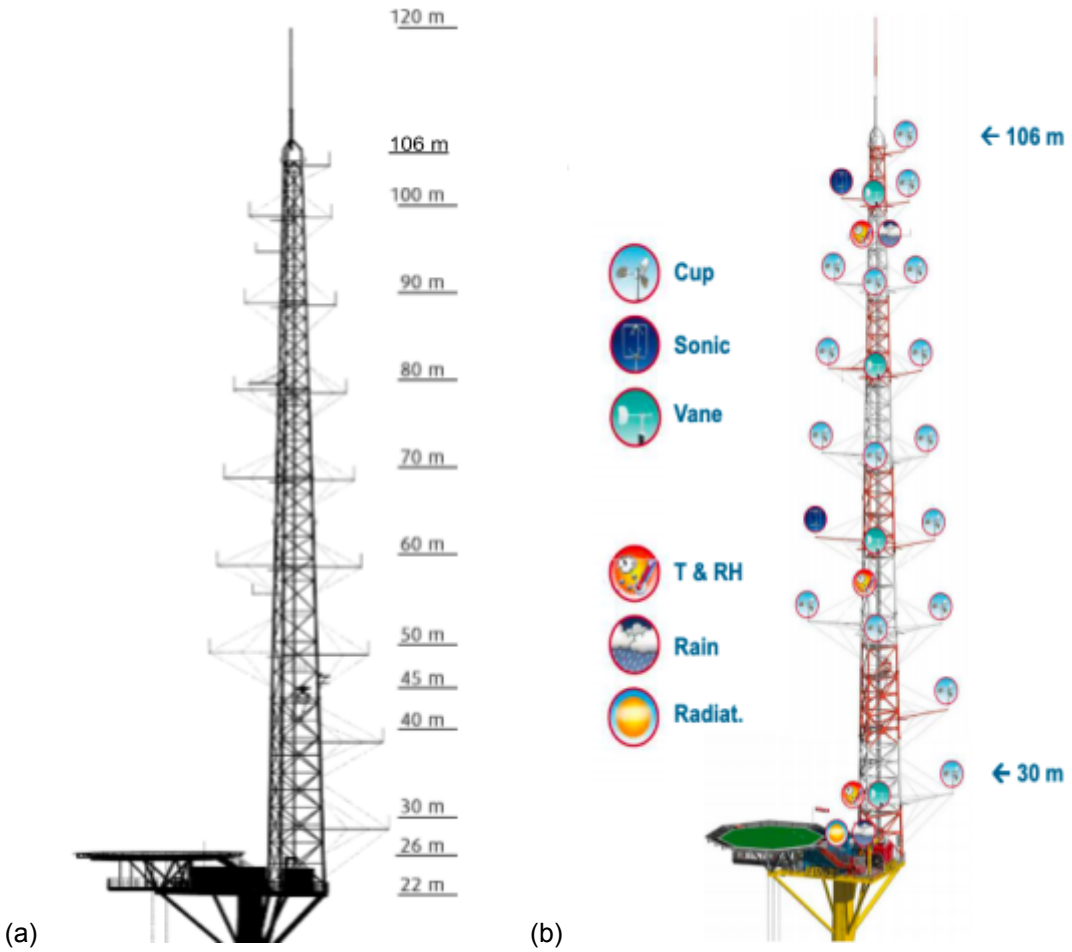

Figure 3.1: FINO3 met mast design and measurement heights.

To minimise mast distortion effects, the platform has a triangular cross-section (2.63 m side) with one, two or three booms at different height level. The boom orientation is shown in Figure 3.2 (225º, 345º and 105º, called respectively A, B and C from here on), this layout allows the selection of wind sectors undisturbed by the mast.

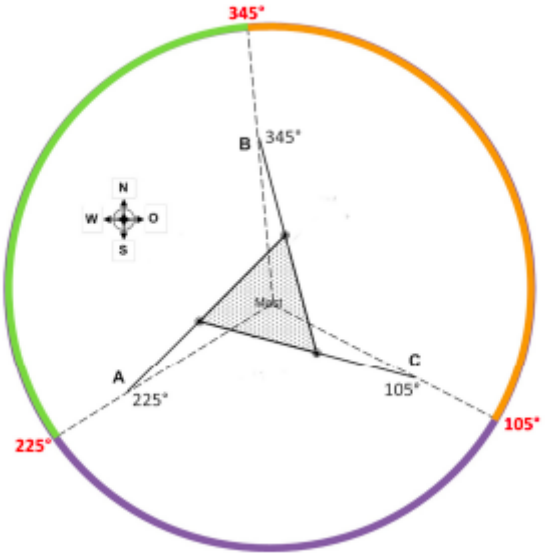

Figure 3.2: Orientation of the three booms at the FINO3 platform.

Oceanographic data on and immediately surrounding the platform is also being measured. A wave buoy records significant wave parameters (wave height, wave direction, up crossing period and wave peak period).

Nine years of observation data from September 2009 to August 2018 taken from the official BSH database website, http://fino.bsh.de, originally in the format of '.dat'. is filtered and utilised in this study.

3.2. Data Filtering

Wind observations are heavily distorted when the corresponding sensor is located in the wake of the met mast. M. C. Holtslag, Bierbooms, and van Bussel (2015) showed that sensors experience significantly reduced wind speeds when located directly behind (∓ 10º) the tower structure and when one sensor is located directly in front of the tower, both remaining sensors located more to the side of the tower experience increased wind speeds while the sensor in the front of the tower experiences a reduced wind speed. The presence of the tower structure causes locally a weak increase in wind speed sideways of the tower and a significant reduction of wind speed behind the tower. It is therefore decided to determine the actual wind speed at various heights based on the wind direction, and select wind speed measurement from booms in wind sectors undisturbed by the mast.

The possible wind directions were divided into six sectors as shown in Figure 3.3a. It is assumed that the wind speed measurements of boom A are undisturbed for wind direction in (105° to 165°) & (285° to 345°) sectors, boom B measurements are undisturbed for wind direction in (45° to 105°) & (225° to 285°) sectors and boom C measurements are undisturbed for wind direction in (165° to 225°) & (345° to 45°) sectors (See Figure 3.3b). The wind direction at 100 m on boom C is used.

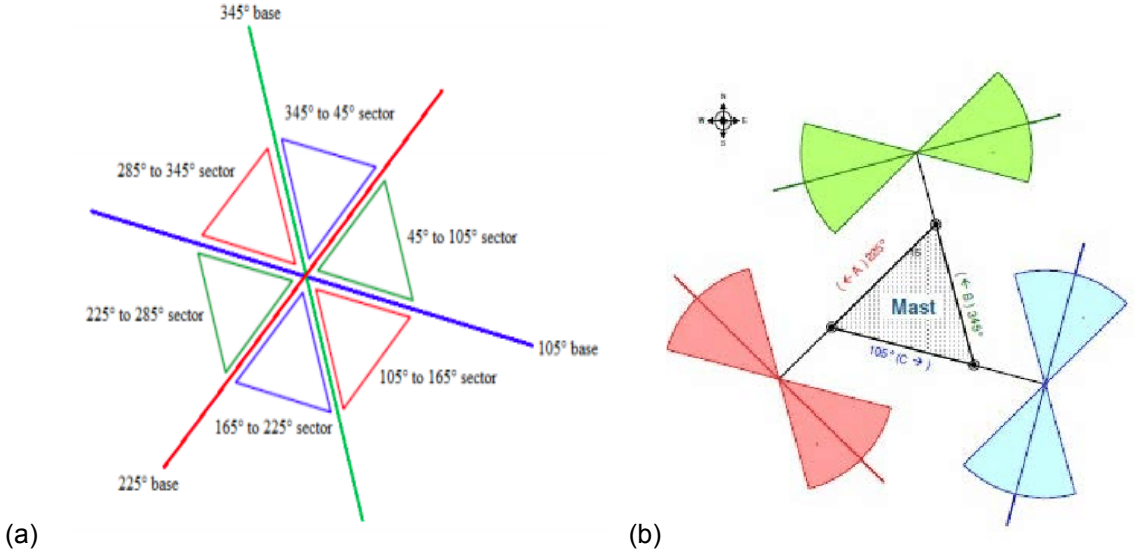

(a) (b)

Figure 3.3: Wind direction at FINO3 divided into six sectors (sectors are shown in (a) and the corresponding undisturbed sectors for each boom are shown in (b)).

A break down of the wind speed measurements data return at the various height from September 2009 to August 2018 based on this selection process is shown in Table 3.1 (Non-available measurements due to technical problems were also filtered out). The possible data return for this period is 473,328 records of 10-minutes average values.

Table 3.1: Data return at the various measurement heights at FINO3 based on 9 years of data from September 2009 to August 2018 (The possible data return for this period is 473,328 records of 10-minutes average values).

Elevation (m)	Boom A (105° to 165°) & (285° to 345°) sectors	Boom B (45° to 105°) & (225° to 285°) sectors	Boom C (345° to 45°) & (345° to 45°) sectors	No of available data	% of possible data return
30	NO	YES	NO	160986	34.01%
40	NO	YES	NO	156467	33.06%
50	YES	YES	YES	428818	90.60%
60	YES	YES	NO	307896	65.05%
70	YES	YES	YES	422025	89.16%
80	YES	YES	NO	309479	65.38%
90	YES	YES	YES	411307	86.90%
100	YES	YES	NO	276674	58.45%
106	NO	YES	NO	153893	32.51%

From table 3.1, the highest elevation with three boom present is the 90 m elevation. A wind rose of data return for the wind speed observations at 90 m height was plotted and is presented in Figure 3.4. This shows that the dominant wind directions are between 225° to 285°.

All observations obtained at the meteorological measurement site are stored as 10-min mean observations. But the required oceanographic data measured by the wavy buoy (significant wave height and mean surface temperature) are stored as 30-min mean observations. Based on the 10-min timestep of the meteorological measurements, the oceanographical data were interpolated to 10-min mean observations by selecting the nearest 30-min mean observations value to the required 10-min timestamp.

The data is then filtered such that if for a given 10-min timestep any of the following data is missing the whole time step is excluded:

1) Wind speed observation (at any height from 30 m to 106 m).
2) Significant wave height observation (significant wave height is required as input when carrying out offshore wind farm installation campaign simulation).
3) Surface temperature observation (required for calculation of Richardson number).
4) Temperature, humidity and air pressure at 29 m height (required for calculation of Richardson number).

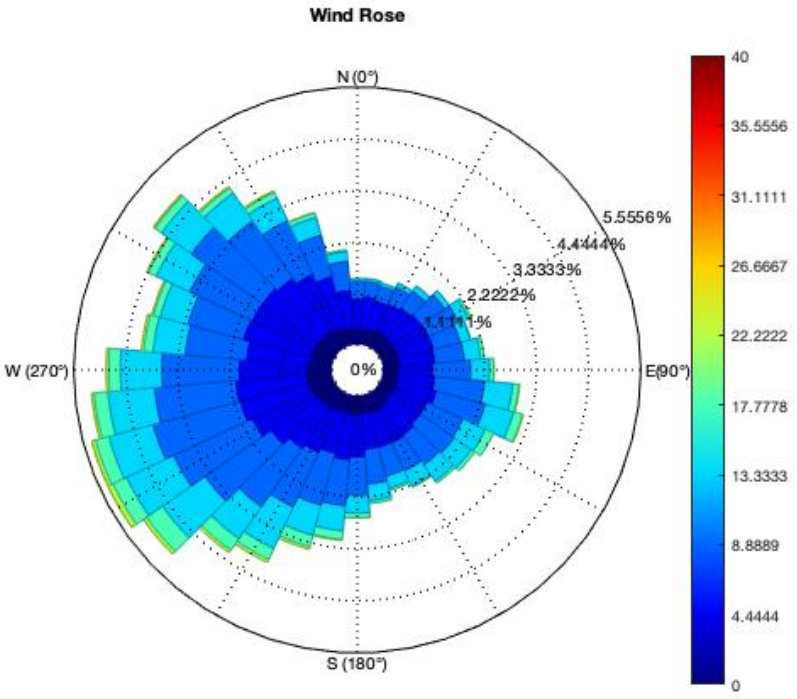

Figure 3.4: Wind rose of data return for the wind speed observations at 90 m height at FINO3 based on 411,307 10-min mean wind speed observations from September 2009 to August 2018.

Besides, we filter for stationary conditions following Obhrai et al. (2012) by removing non-stationary conditions which conformed to the following criteria:

1) A variation in u of more than 10%.
2) A variation in T of more than 0.5°C.
3) A wind direction change of more than 10° between consecutive values.

Also, observation of wind speeds lower than 2 m/s at 30 m height are filtered out.After application of these filters, a total dataset of 119,324 observations remains, which equals approximately 74% of the wind speed data return at 30 m height and approximately 25% of the possible data return for the period of September 2009 to August 2018.

The distribution of the wind speed observation at 90 m height of the original data set (see table 3.1) and the filtered data set at 90 m was compared and found to be similar, especially for wind speed observation above 6 m/s (see Figure 3.5). This is also similar to the results presented in Figure 3 of Obhrai et al. (2012), with significant deviation for wind speed observation lower than 10 m/s, but their distribution was based on two years of data from October 2009 to October 2011. A wind rose of the filtered dataset for wind speed observations at 90 m height is presented in Figure 3.6.

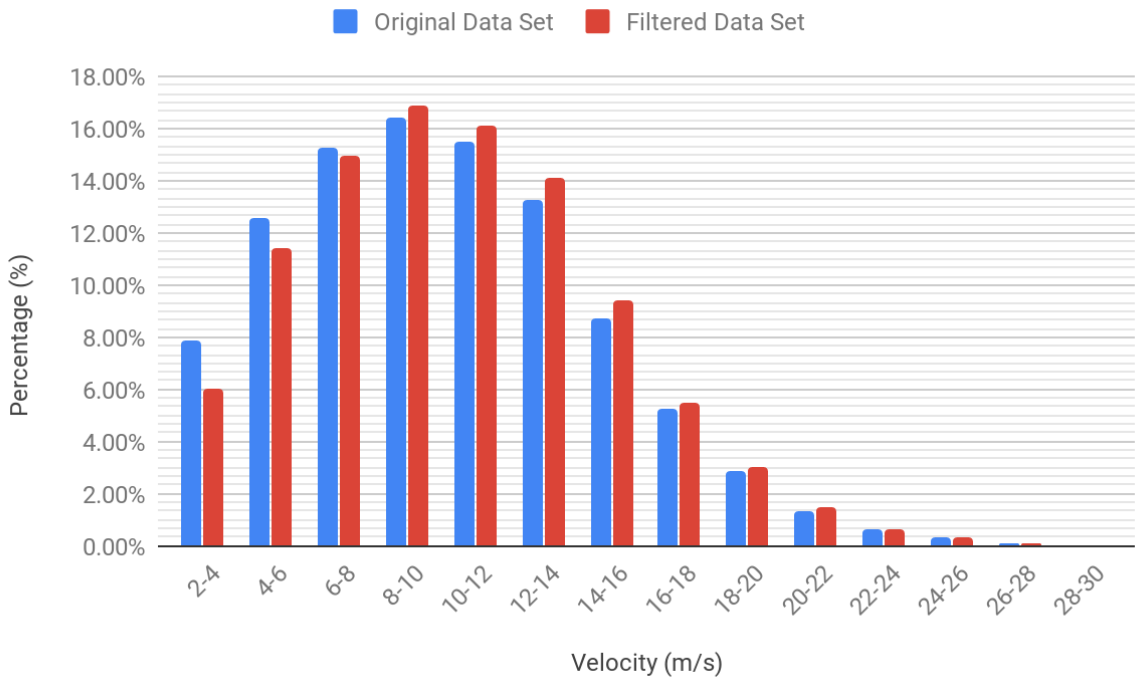

Figure 3.5: Distribution of wind speed observations at 90 m height of the original data set and filtered dataset. (original data set is based on 411,307 10-min mean wind speed observations from September 2009 to August 2018, while the filtered dataset is based on 119,324 10-min mean wind speed observations remaining after applying the filters outlined in this study).

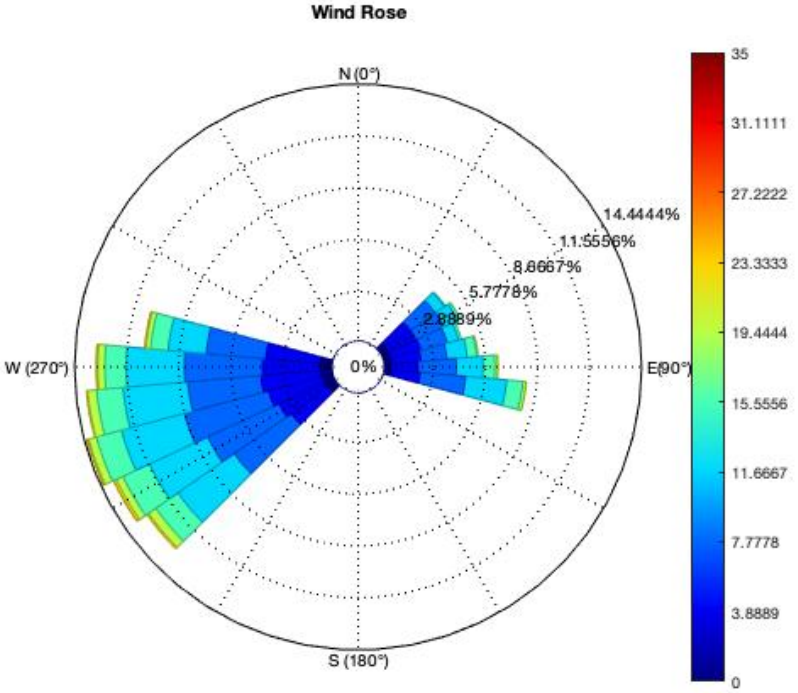

Figure 3.6: Wind rose of the filtered data set for wind speed observations at 90 m height based on 119,324 10-min mean wind speed observation remaining after applying the filters outlined in this study.

3.3. Atmospheric Stability Determination

Since turbulent fluxes of heat and momentum are not measured at FINO3, the Obukhov length cannot be determined with the eddy covariance method. The other methodologies assessed to determine stability are most sensitive to measurement errors when Δu or $\Delta\overline{\theta}_v$ (mean difference between the sea surface temperature and the virtual potential temperature at the reference height) is small. Since both wind speed and temperature gradients between 30 m and 50 m (temperature measurements only available at 50 m, not 40 m) height are far smaller than those between 0 and 30m height, the gradient-Richardson method is most sensitive to measurement errors. This is especially true for near-neutral conditions $(\Delta\overline{\theta}_v \approx 0)$ or very unstable conditions $(\Delta u \approx 0)$ (M. C. Holtslag, W A A, and van Bussel 2014). Besides, the profile methods assume the validity of the logarithmic wind speed and temperature profiles, either up to 30 m height or up to 50 m height. The logarithmic profile is valid in the lowest 10% of the boundary layer (M. C. Holtslag, W A A, and van Bussel 2014). However for very stable conditions the observation heights (especially at 50 m height) are likely no longer located within the surface layer. As such the accuracy of the gradient-Richardson method decreases for increasing atmospheric stability. Since bulk-Richarson method is least sensitive to measurement errors, and does not depend on the assumption of validity of the logarithmic wind and temperature profiles, we follow Grachev and Fairall (1997) and use the Bulk-Richardson number (hereafter RI) to estimate ζ based on mean observation of temperature, humidity and air pressure at 29 m height, mean wind speed observations at 30 m height and mean surface temperature observations obtained with the wave buoy. Both at the surface and at 29 m height the virtual potential temperature is calculated as

$$\theta_v(z) = (T(z) + 0.0098z)(1 + 0.61r) \quad [37]$$

Where T is the observed temperature and r is the mixing ratio, which is a function of the observed air pressure, temperature and relative humidity (Stull 1988a). Note that in the conversion of temperature to potential temperature, we follow M. C. Holtslag, Bierbooms, and van Bussel (2015) and assumed that the air is unsaturated since the dry adiabatic lapse rate of 9.8 K/km is assumed to be valid. At the sea-air interface, it is assumed that the air has a relative humidity of 100%.

Although one should determine RI with the wind speed and temperature observations at similar heights, the met mast measures the temperature at 29 m height and wind speed at 30 m height. It is therefore assumed that the virtual potential temperature calculated at 29 m height is representative for 30 m height as well. This is estimated using equation [38] applied in Grachev and Fairall (1997)

$$RI = -\frac{gz\Delta\overline{\theta}_v}{T_z u_z^2} \quad [38]$$

Where z is the reference height at which the mean temperature T_z and mean wind speed u_z are measured, $\Delta\overline{\theta}_v$ is the mean difference between the sea surface temperature and the virtual potential temperature at the reference height.

And subsequently the dimensionless stability parameter, ζ is calculated depending on the state of the atmosphere:

$$\zeta = 10RI \qquad if\ RI \leq 0 \text{ (stable conditions)} \qquad [39]$$

$$\zeta = \frac{10RI}{1-5RI} \qquad if\ RI \geq 0 \text{ (unstable conditions)} \qquad [40]$$

The singularity at $RI = 0.2$ prevent calculation of ζ, thus for $RI > 0.2$ stability is not calculated (about 0.7% of the filtered observations). Subsequently, L is calculated using the equation [41].

$$L = \frac{z}{\zeta} \qquad [41]$$

3.4. Stability Classification

The filtered observations are grouped with respect to stability, we follow the classification set used by M. C. Holtslag, Bierbooms, and van Bussel (2017) as shown in Figure 3.2.

Table 3.2: Atmospheric Stability Classes according to intervals of Obukhov length, L.

Stability class (-)	Stability regime (m)	L average (m)	Nr. of obs (-)
Very Unstable	-100 <= L < -50	-71.26	20946
Unstable	-200 <= L < -100	-138.94	13889
Near Neutral Unstable	-500 <= L < -200	-303.75	8337
Neutral	||L|| >500	5492.41	8756
Near Neutral Stable	200 < L <= 500	313.7	3844
Stable	100 < L <= 200	147.66	3098
Very Stable	50 < L <= 100	73.04	1858

The relative occurrence of the stability classes was compared to results obtained by M. C. Holtslag, Bierbooms, and van Bussel (2017) from Ijmuiden (similar distance from shore as FINO3 located in the Danish part of the North Sea), located 85 km offshore at 52º 50,89 'N, 003º 26.14' E in the Dutch North Sea area (Werkhoven and Verhoef 2012). The locations of

these sites are shown in Figure 3.7 and the results are presented in Figure 3.8a. Also, the results from the comparison were compared to the results obtained by Sathe, Gryning, and Peña (2011) shown in Figure 3.8b. They compared the relative occurrence of stability classes at OWEZ (Dutch part of the North Sea), located 18 km offshore from the coast of Egmond aan Zee, the Netherlands (52º 36' 22,9"N, 004º 23'22,7" E) to Horns Rev (Danish part of the North Sea), located also 18 km offshore from the coast of Jutland, Denmark (55º 33'9"'N, 007º 47'15" E).

Figure 3.7: Location of FINO3, Ijmuiden, OWEZ and Horns Rev meteorological masts.

.

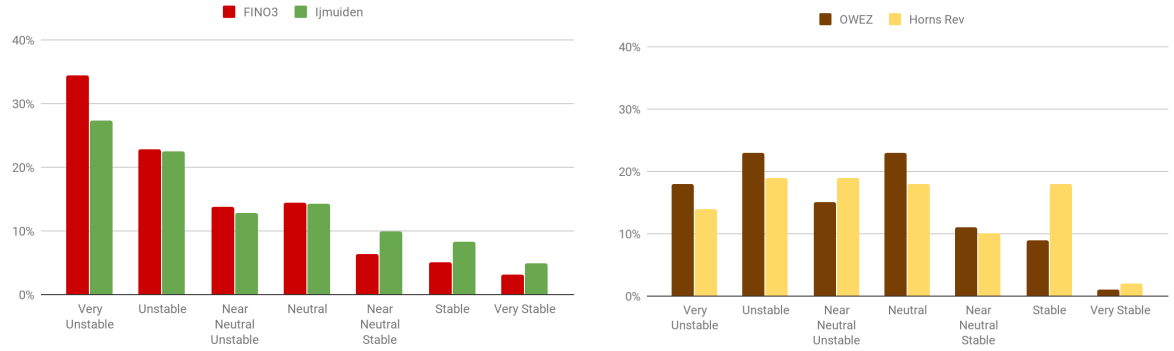

(a) FINO3 and Ijmuiden (b) OWEZ and Horns Rev

Figure 3.8: Overall distribution of atmospheric stability (FINO3 data is based on filtered data from September 2009 to August 2018 as described in this study while Ijmuiden data is based on one year of filtered data from June 2014 to May 2015 as described in M. C. Holtslag, Bierbooms, and van Bussel (2017), OWEZ data is based on filtered data from 2005 to December 2008 as described in Sathe, Gryning, and Peña (2011), Horns Rev data is based on filtered data from April 1999 to December 2006 also as described in Sathe, Gryning, and Peña (2011).

Figure 3.8a shows the overall distribution of atmospheric stability at FINO3 and Ijmuiden. In general, the conditions obtained for FINO3 are mainly very unstable and unstable and are in conformity with the results obtained at Ijmuiden by M. C. Holtslag,

Bierbooms, and van Bussel (2017). The results obtained at OWEZ and Horns Rev by Sathe, Gryning, and Peña (2011) are shown in Figure 4.8b. There result shows that the general conditions at these sites are mainly neutral and unstable. The difference in the results obtained at FINO3 and Ijmuiden to that obtained at OWEZ and Horns Rev is understandable because FINO3 and Ijmuiden are located further offshore (approximately about 80 km offshore) compared to OWEZ and Horns Rev which are located closer to the shore (approximately about 18 km to shore). The further offshore we go, the more unstable atmospheric conditions become. It is also noticeable that there are more very unstable conditions at FINO3 than at Ijmuiden and in general less stable (near neutral stable and very stable included) conditions at FINO3 as compared with that at Ijmuiden. This is also in conformity with the observation of Sathe, Gryning, and Peña (2011) for the Dutch part (more unstable conditions at OWEZ than at Horns Rev) and for the Danish part (less stable conditions at OWEZ as compared with that at Horns Rev).

The relative occurrence of the stability classes at FINO3 as a function of wind speed is presented in Figure 3.9. It is found that very unstable conditions prevail at the site for lower winds speeds (i.e., between 2 m/s to 12 m/s). The occurrence of very unstable conditions decreases with increasing wind speed (i.e., from 8 m/s to 24 m/s). It is also observable that above 24 m/s, there are no very unstable conditions. Unstable conditions are found for wind speeds between 2 m/s and 28 m/s, above 28 m/s there are no unstable conditions. Above 16 m/s, near neutral unstable and neutral conditions start to occur more frequently. Also, there is an increase of neutral conditions with increasing wind speed. Neutral conditions prevail above 22 m/s. Near neutral stable conditions are found to occur for wind speeds between 2 m/s to 28 m/s, they increase gradually from 8 m/s to 24 m/s. Stable conditions are found to occur for wind speeds between 2 m/s to 26 m/s, while very stable conditions occur between 2m/s to 20 m/s.

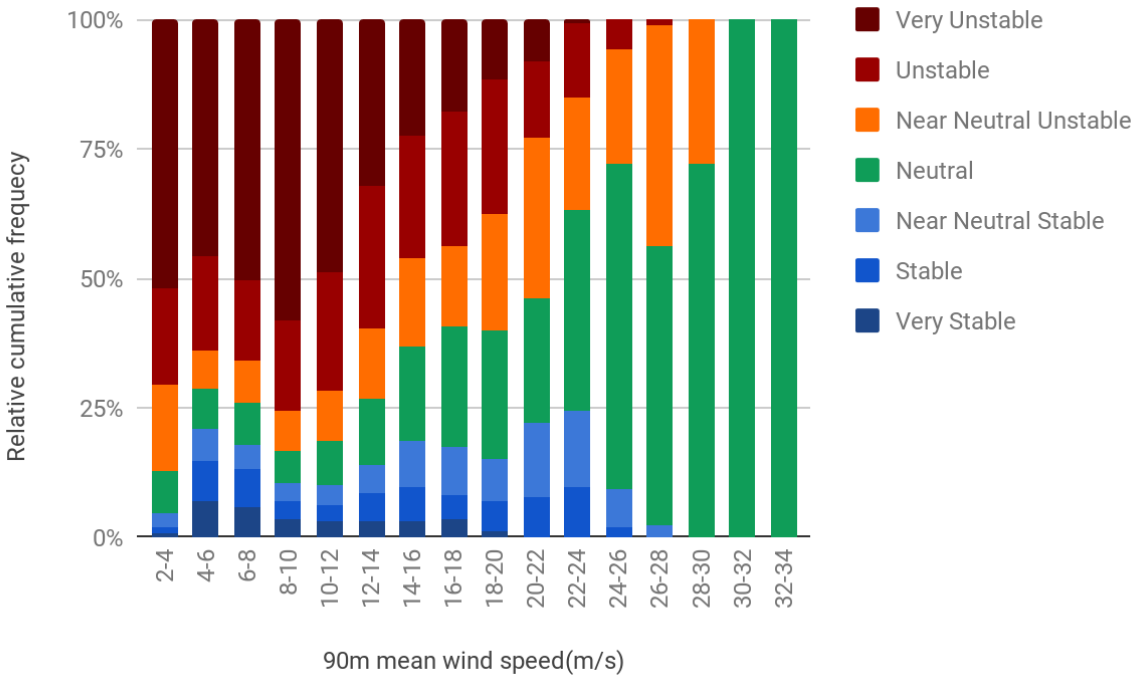

Figure 3.9: Variation of atmospheric stability at 90 m height with respect to wind speed at FINO3 based on filtered 10-min mean wind speed observations from September 2009 to August 2018.

The normalised mean wind speed profile of the filtered observed data is shown in Figure 3.10. These profiles follow clear trends in agreement with the boundary-layer meteorology literature. For example, wind speed shear increases with increasing stability (A. A. M. Holtslag 1984; Van Ulden and Holtslag 1985).

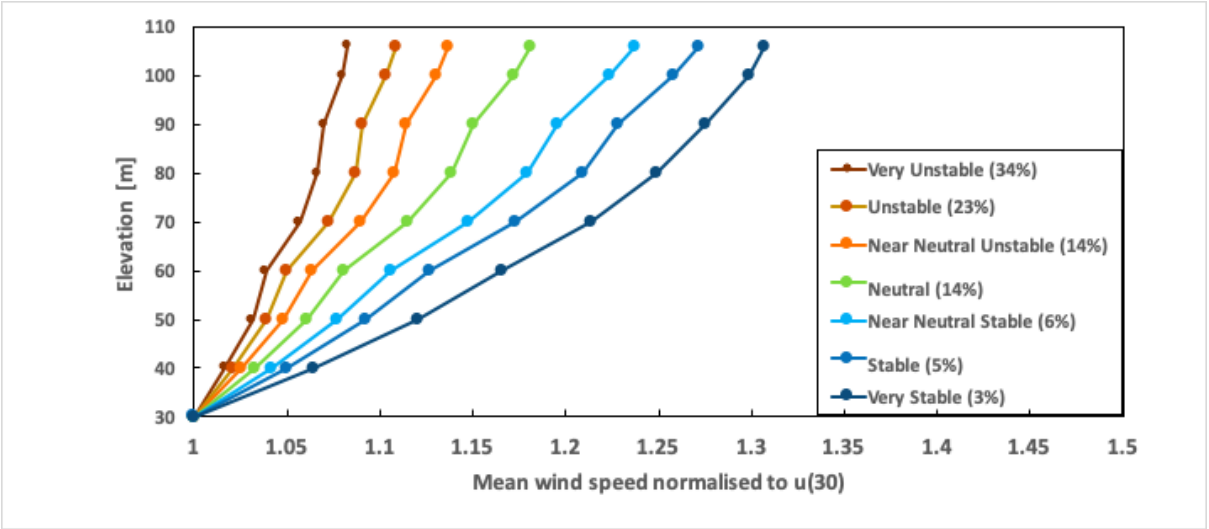

Figure 3.10: Normalized mean wind speed profile for each stability at FINO3 based on filtered 10-min mean wind speed observations from September 2009 to August 2018.

4. Wind Profiles Analysis and Results.

The parameters used for the various wind profile models considered in this study are defined in section 4.1. Using the defined parameters, the various wind profile models were used to extrapolate the measured wind speed observations at 30 m height to the other observations heights at FINO3. The performance of the various wind profile was then assessed, the analysis and results of the assessments carried out are presented in section 4.2.

4.1. WInd profiles parameters

In section 2.1, the wind profiles were defined and parameterized based on theoretic argument, however, in practice typically not all required input parameters are available from observation data. Due to limitations in the available observation data at FINO3 (i.e., no direct observations of z_0, u^*_0, L or h). The parameters used for the various wind profile models considered in this study are defined in this section.

4.1.1. Power law wind profile parameters

The power law wind profile in equation [1] requires α, the power law exponents. In this study, two power law exponents are considered. The power law with an exponent 0.12 as

recommended by the IEC 64100-3 and GL standards and the power law exponent with an exponent of 0.14 which is popularly used in literature. Using equation [1], the observed wind speed at 30 m height was extrapolated to the other observation heights with these two power law exponents.

4.1.2. Logarithmic law wind profile parameters

The Logarithmic wind profile (referred to as Log wind profile from here on) in equation [2] requires the roughness length, z_0. Since we consider offshore conditions, z_0 is parametrized with the Charnock's equation in equation [3], with $A_c = 0.012$ and g is the gravitational acceleration of 9.81 m/s^2. The friction velocity is iteratively calculated, assuming the validity of the Log wind profile in the lowest 30 m of the atmosphere (i.e, the lowest wind speed observation height], as

$$z_0 = \left[\frac{A_c}{g}\right] \left[\frac{\varkappa \overline{U}(z)}{In\left(\frac{z}{z_0}\right)}\right]^2 \quad [42]$$

The observed wind speed at 30 m height is then extrapolated to the other observation heights.

4.1.3. Stability corrected logarithmic wind profile parameters

The observed wind speed at 30 m is extrapolated to the other observation heights using the stability corrected logarithmic wind profile in equation [4]. The stability correction functions proposed by Businger and Dyer (Businger et al. 1971; Dyer 1974) are used in this study, which is defined for unstable (equation [43]) and stable(equation [45]) conditions respectively as

$$\psi(L \leq 0) = 2ln\left(\frac{1+x}{2}\right) + ln\left(\frac{1+x^2}{2}\right) - 2\,arctan\,(x) + \frac{\pi}{2} \quad [43]$$

$$x = \left(1 - \gamma_{BD}\frac{z}{L}\right)^{1/4} \quad [44]$$

$$\psi(L \geq 0) = -\beta\frac{z}{L} \quad [45]$$

The parameters β and γ_{BD} were first determined as 4.7 and 15 based on the Kansas experiments (Businger et al. 1971). In literature, various other values of β and γ_{BD} are found. In this study, the correction proposed by Högström (Högström 1988) is adopted ($\beta = 6$ and $\gamma_{BD} = 19.3$) for the stability corrected logarithmic wind profile (referred to as Businger Dyer wind profile from here on).

4.1.4 The extended wind profile parameters

The observed wind speed at 30 m was extrapolated to the other observation heights using the extended wind profile. The parametrized extended wind profile is a function of the aerodynamic roughness length, the friction velocity, atmospheric stability and boundary layer height, and neither of these parameters is directly observed at the site considered as stated earlier. Since we consider offshore conditions, z_0 is parametrized with Charnock's equation as was done for the Bus. Dyer wind profile. The friction velocity is iteratively calculated, assuming the validity of surface layer scaling in the lowest 30 m of the atmosphere (i.e., the lowest wind speed observation height), as

$$u*_0 \left[ln\left(\frac{zg}{A_c u_{*0}^2}\right) - \psi(\zeta) \right] = \varkappa \overline{U}(z) \quad [46]$$

Where the ψ-functions of Equations [16] and [17] are used. The observation dataset has no direct estimates of the boundary layer height h, hence we follow Gryning and consider the Rossby- Montgomery equation

$$h = c\frac{u*_0}{f} \quad [47]$$

Where c has to be parametrized. Although, as discussed in Section 2.1, h is in reality dependent on other parameters as well, here we adopt Rossby number similarity theory and assume h is defined as a function of $u*_0$, f and L alone. Subsequently, c is parametrized as a continuous function of stability using equation [38] and [39] in M. C. Holtslag, Bierbooms, and van Bussel (2017) which are defined for stable and unstable conditions respectively as

$$c = 0.04 + 0.05\left(1 + 2\frac{100}{L}\right)^{-1} \quad [48]$$

$$c = 0.17 - 0.08\left(1 - 0.5\frac{100}{L}\right)^{-3} \quad [49]$$

4.2. Analysis and results on wind profile models

4.2.1 Wind profile extrapolation analysis and results based on stability classes.

The measured wind speed observations at 30 m height were extrapolated to the other observation heights at FINO3 using the wind profile models considered in this study. The performance of the wind profile models for the different stability classes (see Table 3.2) was then assessed. First, for each stability class, the average wind speed at the various heights

was normalised using the average wind speed at 30 m height. Then, the normalised average wind speeds obtained for the measured wind speed observations were compared to the normalised average wind speeds obtained for the extrapolated data from the wind profile models. The results for this comparison for each stability class are presented in Figure (4.1-4.7)a. To give an indication of the magnitude of the over/underestimation of the wind speeds at the various observation heights, the RMSEs (root mean square error) at the various heights for each wind profile model was evaluated. The results of the RMSEs at the various observation heights are presented in Figure (4.1-4.7)c. Finally, for an indication of the overall performance of the wind profile for a stability class, the average RMSE for each wind profile model was evaluated. The results of the average RMSE are presented in Figure (4.1-4.7)b. The RMSE between the estimated wind speed $\hat{u}_i$ by the wind profile models and measured wind speed observations was calculated as.

$$RMSE = \sqrt{\frac{\sum_{i=1}^{n} (\hat{u}_i - u_i)^2}{n-1}} \qquad [50]$$

For very unstable conditions (Figure 4.1) it is found that the Businger-Dyer and the extended wind profiles correspond well to the observations up to approximately 60 m height but for higher altitudes, the wind speed is underestimated (See Figure 4.1a). As stated earlier the RMSE gives an indication of the over/underestimation. The RMSEs of the Businger-Dyer and the extended wind profiles were similar for all observation heights and it increased gradually with increasing altitude (See Figure 4.1c). It is noticeable though, that for higher altitudes (i.e above 70 m) the extended wind profile had slightly lower RMSEs compared to the Businger-Dyer wind profile. Hence, the extended wind profile had the lowest average RMSE of 0.5398 m/s compared to the Businger-Dyer wind profile with RMSE of 0.5424 m/s (See Figure 4.1b).

The Log and the power law (both exponents) wind profiles overestimated the wind speed for all observation heights, the magnitude of the overestimation increased gradually with increasing altitude (See Figure 4.1a). The RMSEs of the Log wind profile were lower for all observation heights compared to the RMSEs of the power law (both exponents) wind profiles (See Figure 4.1c). The power law (with an exponent of 0.14) wind profile had the highest RMSEs for all observation heights and hence, the highest overestimation of the wind speed. It should be noted that though the Businger-Dyer and the extended wind profiles underestimate the wind speed, the average RMSE approximately 0.54 m/s for both was lower compared to the Log, the power law (with an exponent of 0.12) and the power law (with an exponent of 0.14) wind profiles with average RMSEs of 0.60 m/s, 0.86 m/s and 1.04 m/s respectively (See Figure 4.1b).

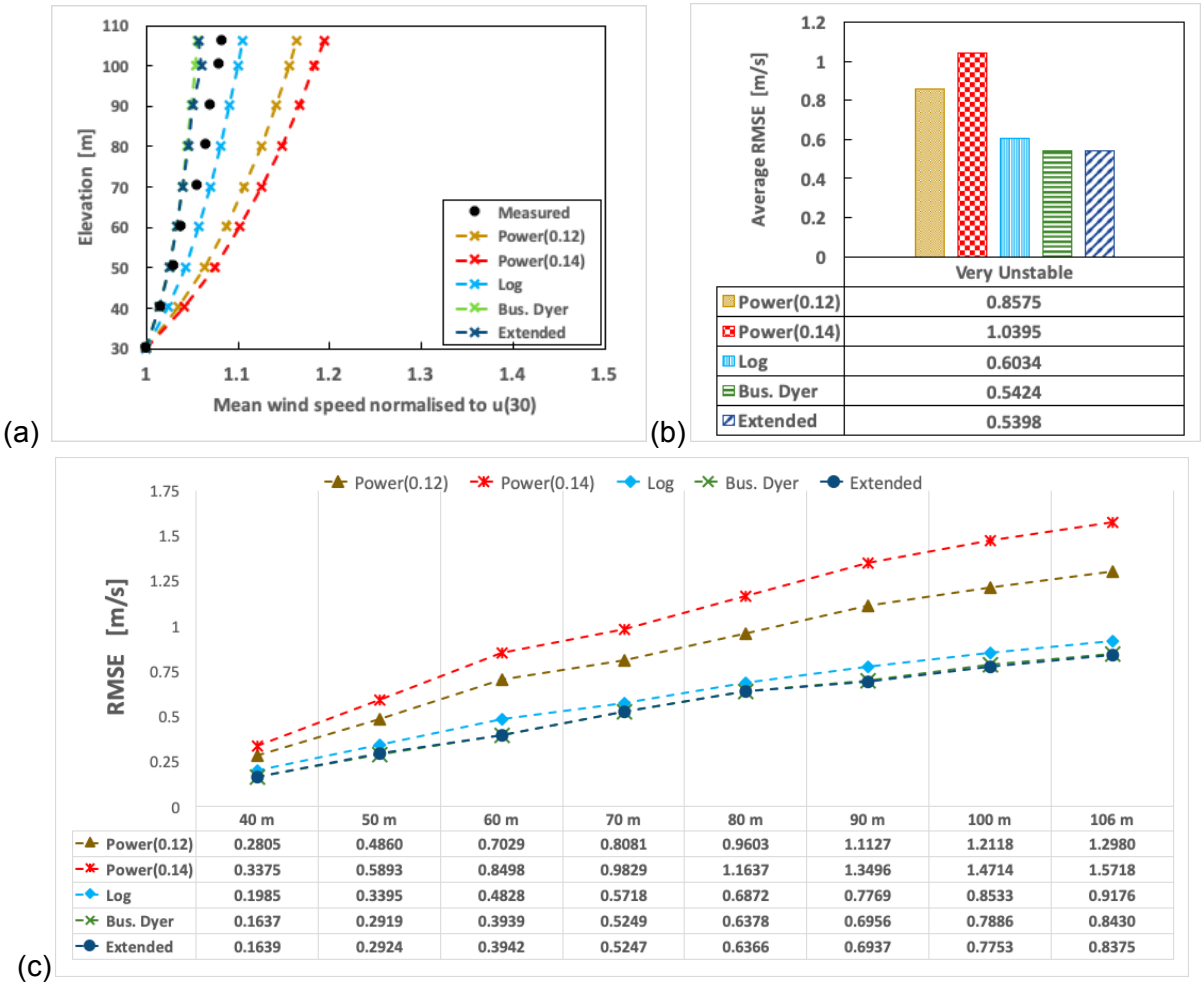

Figure 4.1: Very unstable conditions (The normalised average wind speed of the measured wind speeds and the wind profile models (a), Average RMSE of the wind profile models (b), RMSE at the various heights of the wind profile model(c)).

Figure 4.1: Very unstable conditions (The normalised average wind speed of the measured wind speeds and the wind profile models (a), Average RMSE of the wind profile models (b), RMSE at the various heights of the wind profile model(c)).

For unstable conditions (Figure 4.2), the Businger-Dyer and the extended wind profiles give similar results to in very unstable conditions, but the underestimation is of higher magnitude. Also, it is more noticeable in unstable conditions that the RMSEs of the extended wind profile is lower for all observation heights compared to the RMSEs of the Businger-Dyer wind profile (See Figure 4.2c). The average RMSE of the extended wind profile 0.6194 m/s is significantly lower than that of the Businger-Dyer wind profile 0.6366 m/s (See Figure 4.2b).

The Log wind profile model corresponds well to the observations for all heights. It should be noted that though Figure 4.2a shows that the log wind profile corresponded well to measurements, this is a plot of the average wind speed at the observation heights which means that the wind profile is most likely overestimating for some observation and underestimating for others, both the average corresponds well to the average of the measured wind speed. The power law wind profiles (both exponents) also gives similar

results as in very unstable conditions, but the overestimation is of lower magnitude. The average RMSE of the power law with an exponent of 0.12 and power law with an exponent of 0.14 was approximately 0.81 m/s and 0.99 m/s respectively. The RMSEs at all observation heights of the Businger-Dyer and the extended wind profiles are lower than the RMSEs of the power law wind profiles (both exponents). The Log wind profile had the lowest RMSEs for observation heights above 60 m and also, the lowest average RMSE 0.6115 m/s but not significantly lower than the extended wind profile with an average RMSE of 0.6194 m/s.

(a)

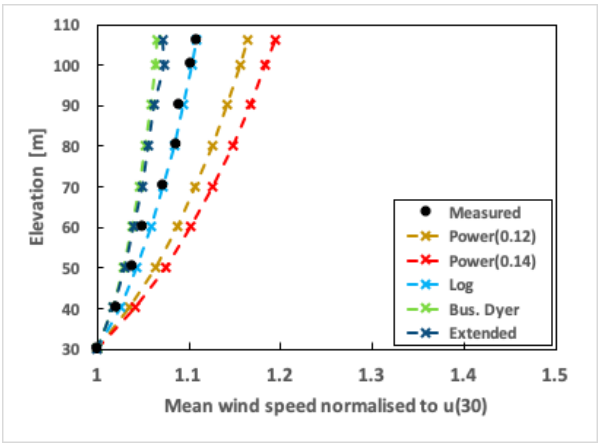

(b)

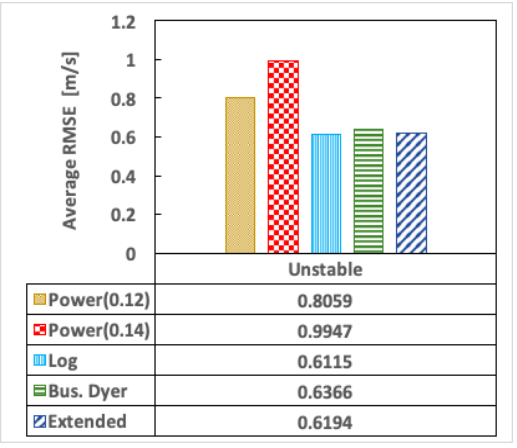

	Unstable
Power(0.12)	0.8059
Power(0.14)	0.9947
Log	0.6115
Bus. Dyer	0.6366
Extended	0.6194

(c)

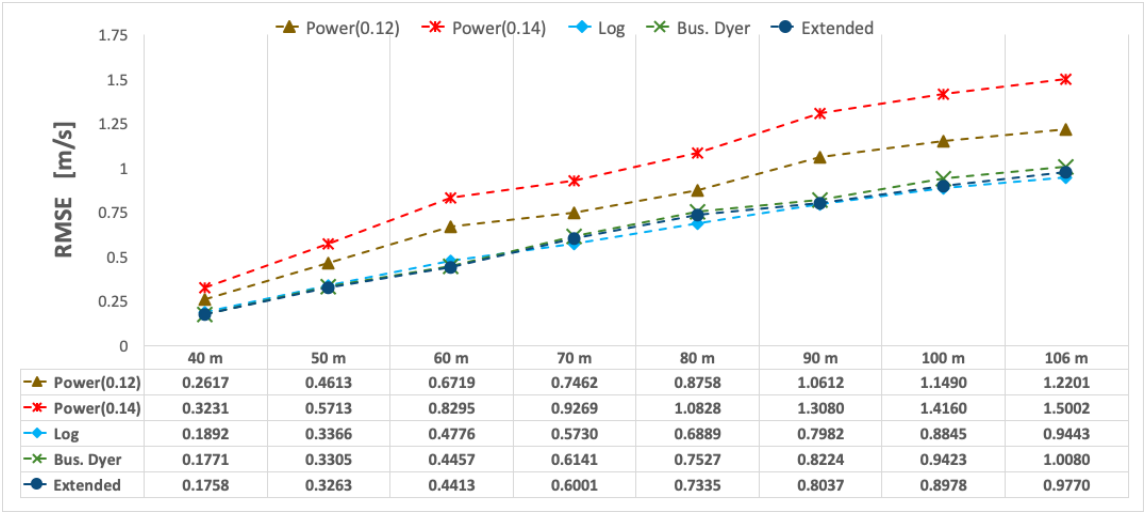

	40 m	50 m	60 m	70 m	80 m	90 m	100 m	106 m
Power(0.12)	0.2617	0.4613	0.6719	0.7462	0.8758	1.0612	1.1490	1.2201
Power(0.14)	0.3231	0.5713	0.8295	0.9269	1.0828	1.3080	1.4160	1.5002
Log	0.1892	0.3366	0.4776	0.5730	0.6889	0.7982	0.8845	0.9443
Bus. Dyer	0.1771	0.3305	0.4457	0.6141	0.7527	0.8224	0.9423	1.0080
Extended	0.1758	0.3263	0.4413	0.6001	0.7335	0.8037	0.8978	0.9770

Figure 4.2: Unstable Conditions (The normalised average wind speed of the measured wind speeds and the wind profile models (a), Average RMSE of the wind profile models (b), RMSE at the various heights of the wind profile model(c)).

For near neutral unstable conditions (Figure 4.3), the Businger-Dyer and the extended wind profiles underestimated the wind speed for all observation heights. The magnitude of the underestimation increased gradually with increasing altitude. The RMSEs of the Businger-Dyer wind profile model are higher for all observation heights compared to the RMSEs of the extended wind profile model, especially above 60 m altitudes. The average RMSE of the extended wind profile, approximately 0.71 m/s was lower than that of the Businger-Dyer wind profile, approximately 0.77 m/s.

The Log wind profile model corresponds well to the observations for heights up to 60 m, but for higher altitudes, the wind speed is underestimated. The power law wind profiles (but exponents) gives similar results as in unstable conditions, but the overestimation is of lower magnitude. The Log and extended wind profile model had similar RMSEs up to 60 m

height, but above this altitude, it is noticeable that the Log wind profile has lower RMSEs. Hence, the average RMSE of the Log wind profile model, approximately 0.69 m/s was lower than that of the extended wind profile model, approximately 0.72 m/s.

The power law wind profile had the highest RMSEs for all observation heights and also, the highest average RMSE, approximately 0.93 m/s. The Businger-Dyer wind profile compared to the power law wind profile with an exponent of 0.12 has lower RMSEs for heights up to 60 m but above this altitude, the power law with an exponent of 0.12 had lower RMSEs. Hence the average RMSE of the power law with an exponent of 0.12 approximately 0.76 m/s is lower than that of the Businger-Dyer wind profile model approximately 0.77 m/s.

(a)

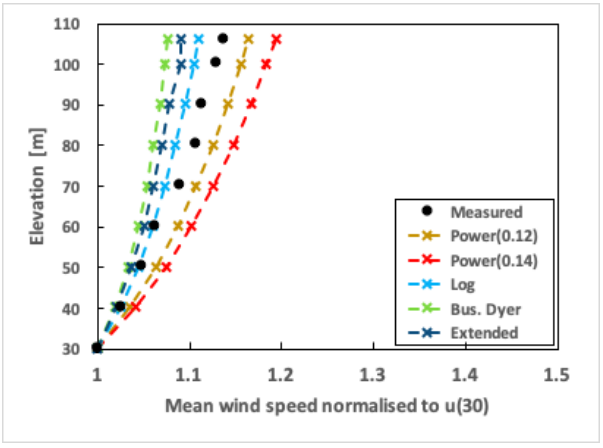

(b)

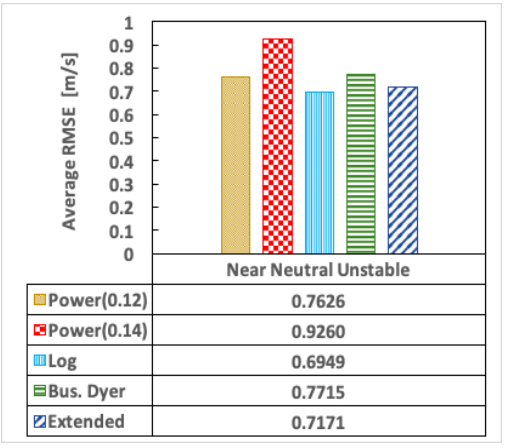

	Near Neutral Unstable
Power(0.12)	0.7626
Power(0.14)	0.9260
Log	0.6949
Bus. Dyer	0.7715
Extended	0.7171

(c)

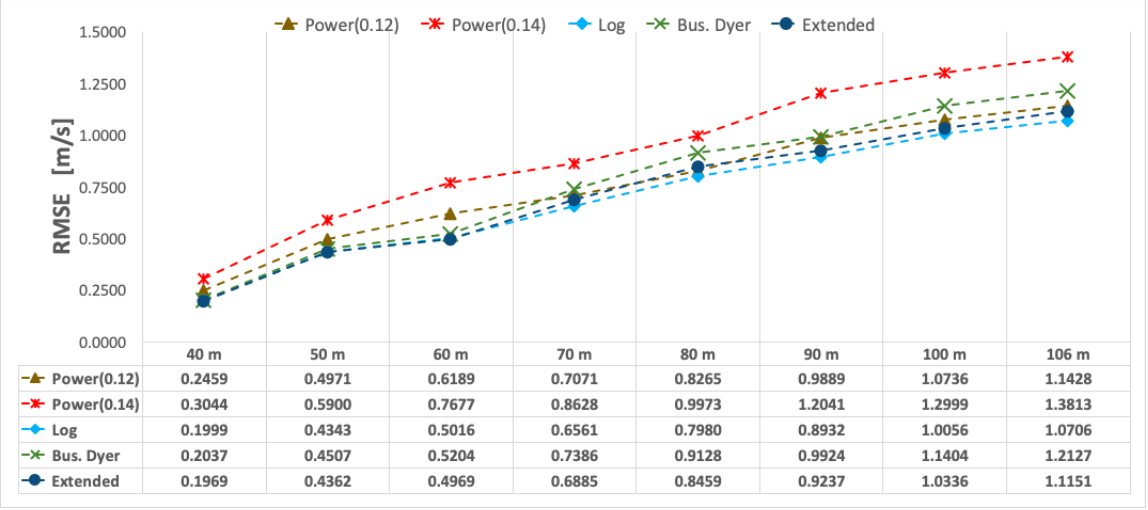

	40 m	50 m	60 m	70 m	80 m	90 m	100 m	106 m
Power(0.12)	0.2459	0.4971	0.6189	0.7071	0.8265	0.9889	1.0736	1.1428
Power(0.14)	0.3044	0.5900	0.7677	0.8628	0.9973	1.2041	1.2999	1.3813
Log	0.1999	0.4343	0.5016	0.6561	0.7980	0.8932	1.0056	1.0706
Bus. Dyer	0.2037	0.4507	0.5204	0.7386	0.9128	0.9924	1.1404	1.2127
Extended	0.1969	0.4362	0.4969	0.6885	0.8459	0.9237	1.0336	1.1151

Figure 4.3: Near neutral unstable conditions (The normalised average wind speed of the measured wind speeds and the wind profile models (a), Average RMSE of the wind profile models (b), RMSE at the various heights of the wind profile model(c))

For neutral conditions (Figure 4.4), the Log, the Businger-Dyer and the extended wind profile underestimated the wind speed, the magnitude of the underestimation increased gradually with increasing elevation. The Log and the Businger-Dyer wind profile had similar RMSEs for all observation heights, the RMSEs of the extended wind profile was lower for all heights compared to the RMSEs of the Log and the Businger-Dyer wind profile. The average RMSEs of the extended, the Businger-Dyer and the Log wind profiles were approximately 0.76 m/s, 0.86 m/s and 0.88 m/s respectively.

The power law with an exponent of 0.12 corresponds well to the observations up to approximately 60 m height but for higher altitudes, the wind speed was underestimated. The power law wind profiles with an exponent of 0.14 overestimated the wind speed for all observation heights. For heights up to 60 m, the extended wind profile had lower RMSEs compared to the power law wind profile with an exponent of 0.12, but for higher altitudes, the RMSEs of the extended wind profile is higher. Also, the power law wind profile with an exponent of 0.12 had a lower average RMSE, approximately 0.73 m/s compared to the extended wind profile with an average RMSE of approximately 0.76 m/s. The RMSEs of the Log and the Businger-Dyer wind profile were lower compared to the RMSEs of the power law wind profile with an exponent of 0.14 for observation heights up to 60 m, but for height altitudes, the RMSEs of the power law with an exponent of 0.14 was lower. Hence, the power law with an exponent of 0.14 had a lower average RMSE of approximately 0.79 m/s compared to that of the Log and the Businger-Dyer wind profile.

(a)

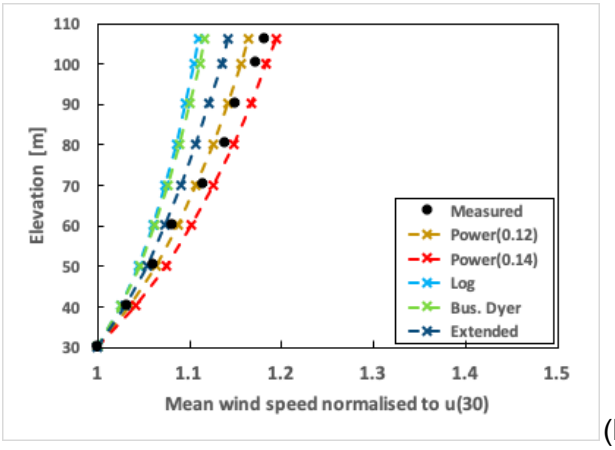

(b)

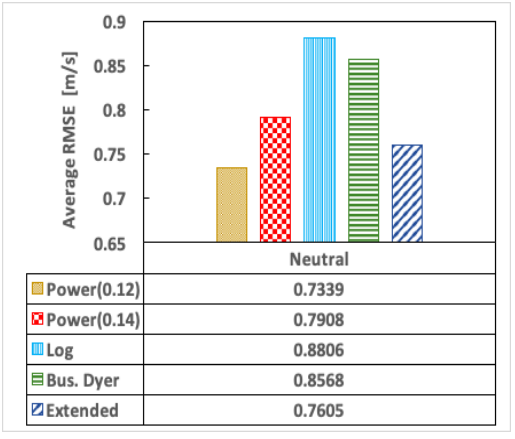

(c)

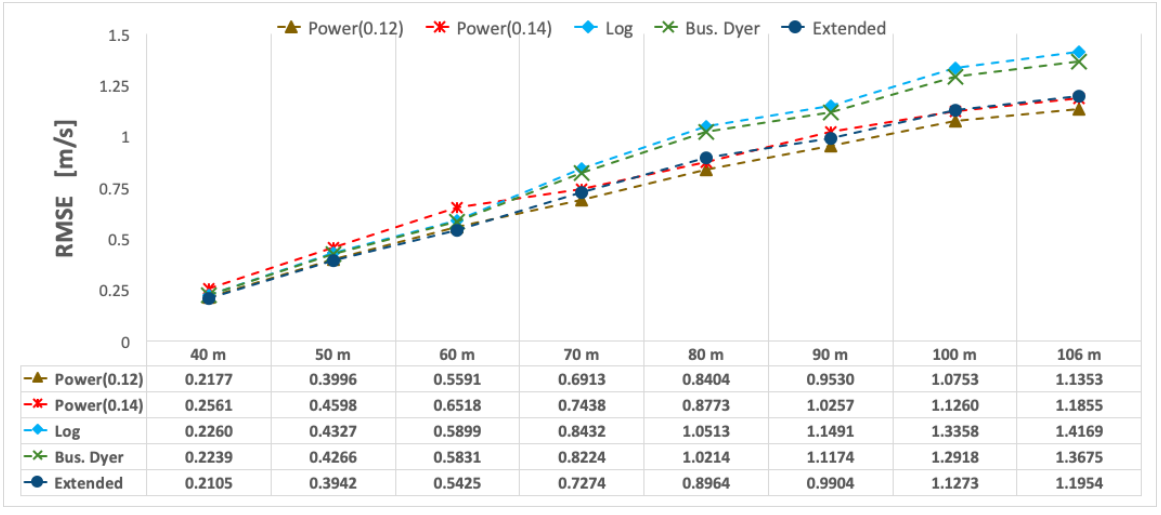

	40 m	50 m	60 m	70 m	80 m	90 m	100 m	106 m
Power(0.12)	0.2177	0.3996	0.5591	0.6913	0.8404	0.9530	1.0753	1.1353
Power(0.14)	0.2561	0.4598	0.6518	0.7438	0.8773	1.0257	1.1260	1.1855
Log	0.2260	0.4327	0.5899	0.8432	1.0513	1.1491	1.3358	1.4169
Bus. Dyer	0.2239	0.4266	0.5831	0.8224	1.0214	1.1174	1.2918	1.3675
Extended	0.2105	0.3942	0.5425	0.7274	0.8964	0.9904	1.1273	1.1954

Figure 4.4: Neutral conditions (The normalised average wind speed of the measured wind speeds and the wind profile models (a), Average RMSE of the wind profile models (b), RMSE at the various heights of the wind profile model(c)).

For near neutral stable conditions (Figure 4.5), the Log wind profile model and the power law wind profile model with an exponent of 0.12 underestimated the wind speed. The RMSEs of the Log wind profile were higher for all observation heights compared to the

power law wind profile with an exponent of 0.12. Hence, the average RMSE of the Log wind profile, approximately 1.21 m/s was higher than that of the power law with an exponent of 0.12 which had an average RMSE of approximately 0.93 m/s.

The power law wind profile model with an exponent 0.14 corresponds well to the observations up to approximately 60 m but for higher altitudes, the wind speed was underestimated, the magnitude of the underestimation increased with increasing altitude. The Businger-Dyer wind profile model and the extended wind profile model corresponds well to the observations up to approximately 60 m, but for higher altitudes, the wind speed is slightly underestimated. The extended wind profile model had the lowest RMSEs for all observation heights compared to the RMSEs of the Businger-Dyer wind profile and the power wind profile with an exponent of 0.14. The average RMSE of the extended wind, approximately 0.84 m/s was also the lowest. The average RMSE of the Businger-Dyer wind profile and the power law wind profile model with an exponent of 0.14 were approximately 0.93 m/s and 0.85 m/s respectively.

(a)

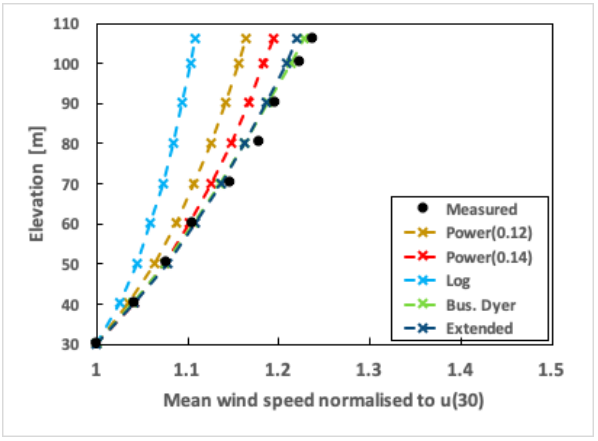

(b)

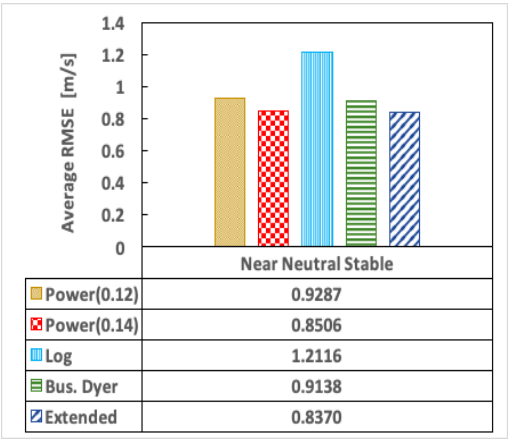

	Near Neutral Stable
Power(0.12)	0.9287
Power(0.14)	0.8506
Log	1.2116
Bus. Dyer	0.9138
Extended	0.8370

(c)

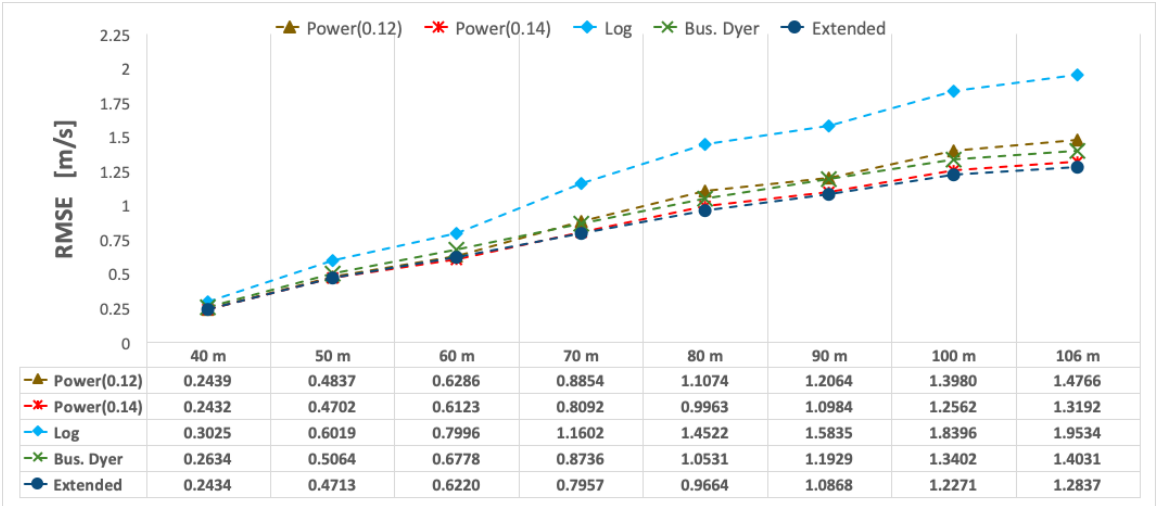

	40 m	50 m	60 m	70 m	80 m	90 m	100 m	106 m
Power(0.12)	0.2439	0.4837	0.6286	0.8854	1.1074	1.2064	1.3980	1.4766
Power(0.14)	0.2432	0.4702	0.6123	0.8092	0.9963	1.0984	1.2562	1.3192
Log	0.3025	0.6019	0.7996	1.1602	1.4522	1.5835	1.8396	1.9534
Bus. Dyer	0.2634	0.5064	0.6778	0.8736	1.0531	1.1929	1.3402	1.4031
Extended	0.2434	0.4713	0.6220	0.7957	0.9664	1.0868	1.2271	1.2837

Figure 4.5: Near neutral stable conditions (The normalised average wind speed of the measured wind speeds and the wind profile models (a), Average RMSE of the wind profile models (b), RMSE at the various heights of the wind profile model(c)).

For stable conditions, the Log wind profile model and the power law wind profile (both exponents) models underestimated the wind speed. The magnitude of the underestimation was high, especially for higher altitude. The average RMSE of the Log wind profile, the

power law wind profile with an exponent of 0.12 and the power law wind profile with an exponent of 0.14 were approximately 1.41 m/s, 1.11 m/s and 0.98 m/s respectively. It is important to note that for these wind profile models the RMSEs increased rapidly with increasing altitude, for the log wind profile the RMSE at 106 m height was approximately 2.25 m/s.

The Businger-Dyer wind profile corresponds well to the observations up to approximately 60 m but for higher altitudes, the wind speed was overestimated. The magnitude of the overestimation increases with height. The extended wind profile model corresponds well to the observations for all observation heights. The extended wind profile had the lowest RMSEs for all observation height and also, the lowest average RMSE approximately 0.85 m/s. The average RMSE of the Businger-Dyer wind profile was approximately 1.00 m/s.

(a)

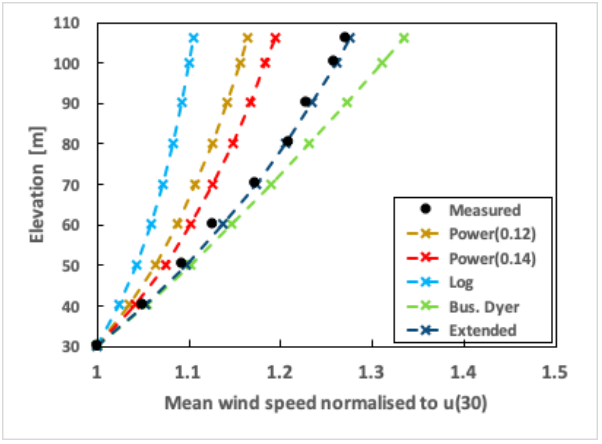

(b)

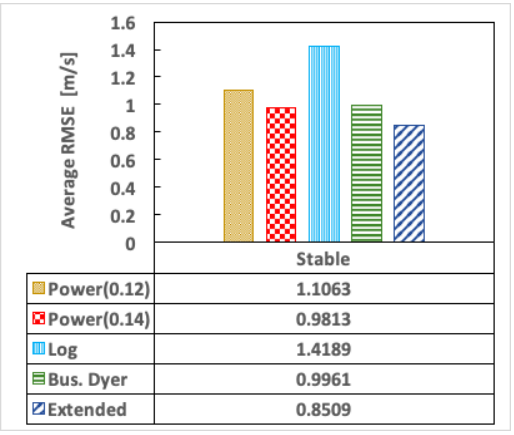

	Stable
Power(0.12)	1.1063
Power(0.14)	0.9813
Log	1.4189
Bus. Dyer	0.9961
Extended	0.8509

(c)

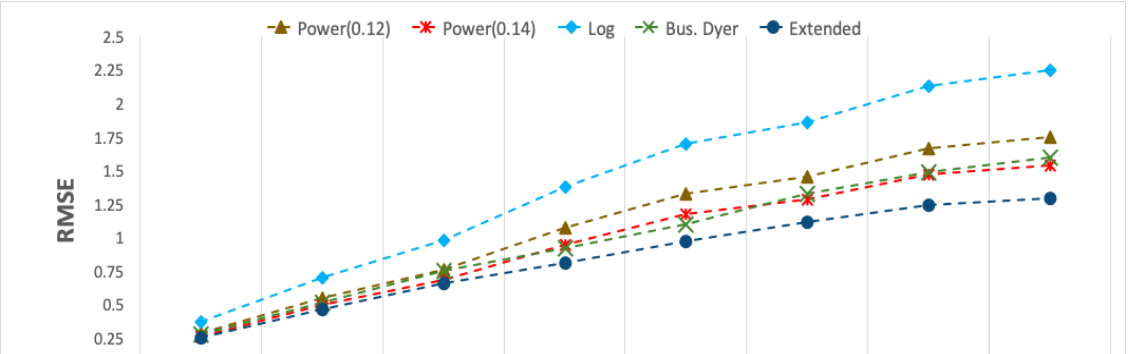

	40 m	50 m	60 m	70 m	80 m	90 m	100 m	106 m
Power(0.12)	0.2879	0.5478	0.7602	1.0702	1.3281	1.4511	1.6601	1.7451
Power(0.14)	0.2617	0.4938	0.6874	0.9474	1.1725	1.2862	1.4651	1.5362
Log	0.3684	0.7030	0.9752	1.3739	1.6973	1.8605	2.1286	2.2446
Bus. Dyer	0.2752	0.5172	0.7538	0.9179	1.0970	1.3258	1.4891	1.5932
Extended	0.2499	0.4635	0.6602	0.8123	0.9728	1.1182	1.2370	1.2932

Figure 4.6: Stable conditions (The normalised average wind speed of the measured wind speeds and the wind profile models (a), Average RMSE of the wind profile models (b), RMSE at the various heights of the wind profile model(c)).

For very stable conditions, the neutral wind profile model and the power law wind profile (both exponents) give similar results as in stable conditions, but the underestimation is of higher magnitude. The average RMSE of the Log wind profile, the power law wind

profile with an exponent of 0.12 and the power law wind profile with an exponent of 0.14 were approximately 1.72 m/s, 1.43 m/s and 1.30 m/s respectively. Note that for these wind profile models, the RMSEs increased rapidly with increasing altitude, for the log wind profile the RMSE at 106 m height was approximately 2.48 m/s.

The Businger-Dyer wind profile overestimated the wind speed, the magnitude of the overestimation increased rapidly with increasing altitude. The RMSE at 106 m elevation was 2.57 m/s. The extended wind profile model corresponds well to the observations up to approximately 70 m but for higher altitudes, the wind speed was slightly overestimated. The extended wind profile had the lowest RMSEs for all observation heights and also, the lowest average RMSE approximately 1.01m/s. The average RMSE of the Businger-Dyer wind profile was approximately 1.46 m/s.

(a)

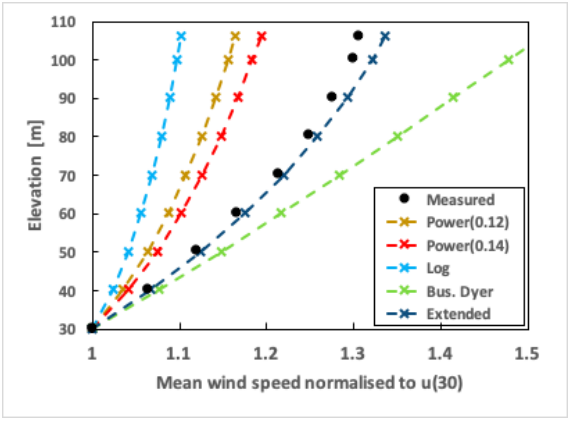

(b)

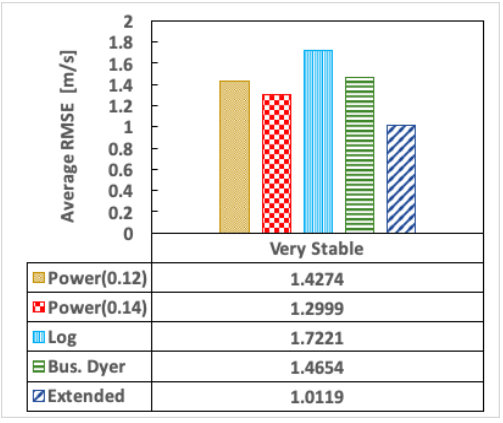

	Very Stable
Power(0.12)	1.4274
Power(0.14)	1.2999
Log	1.7221
Bus. Dyer	1.4654
Extended	1.0119

(c)

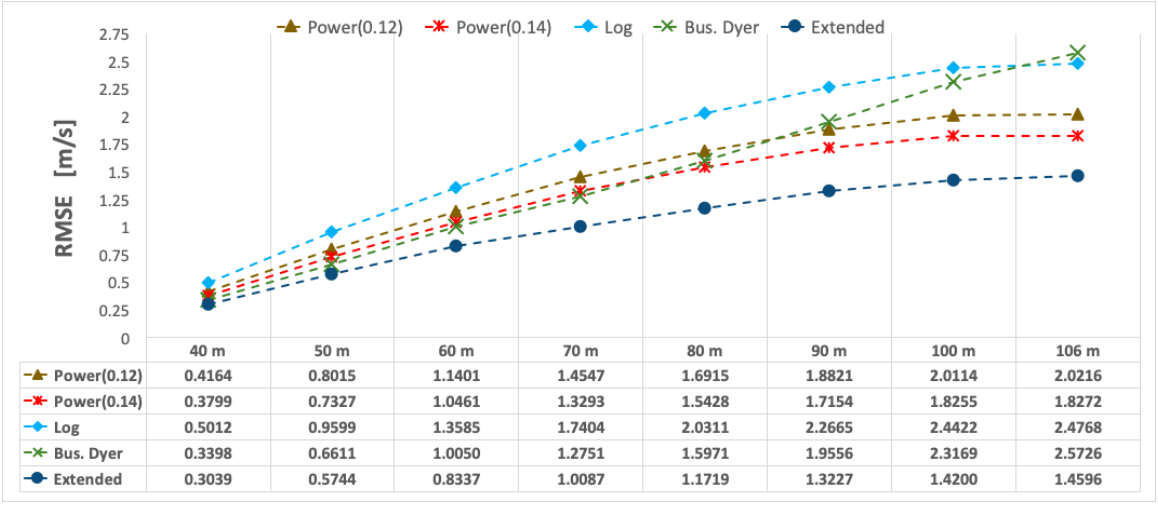

	40 m	50 m	60 m	70 m	80 m	90 m	100 m	106 m
Power(0.12)	0.4164	0.8015	1.1401	1.4547	1.6915	1.8821	2.0114	2.0216
Power(0.14)	0.3799	0.7327	1.0461	1.3293	1.5428	1.7154	1.8255	1.8272
Log	0.5012	0.9599	1.3585	1.7404	2.0311	2.2665	2.4422	2.4768
Bus. Dyer	0.3398	0.6611	1.0050	1.2751	1.5971	1.9556	2.3169	2.5726
Extended	0.3039	0.5744	0.8337	1.0087	1.1719	1.3227	1.4200	1.4596

Figure 4.7: Very stable conditions (The normalised average wind speed of the measured wind speeds and the wind profile models (a), Average RMSE of the wind profile models (b), RMSE at the various heights of the wind profile model(c)).

For neutral and unstable (all) conditions it is found that the extended wind profile model underestimates the wind speed, hence it is decided to examine all the stability conditions for the extended wind profile in more detail. The observations for all stability conditions is further classified as a function of the friction velocity to assess if the wind profile performs better for specific conditions. The results are presented in the next subsection .

4.2.2. Results of further analysis on the extended wind profile

The observations for all stability conditions is further classified as a function of the friction velocity to assess if the extended wind profile performs better for specific conditions. The results are presented shown in Figure 4.8 (a-g). Also, the average boundary layer height for each friction velocity regime under the various stability conditions is presented in Table 4.3.

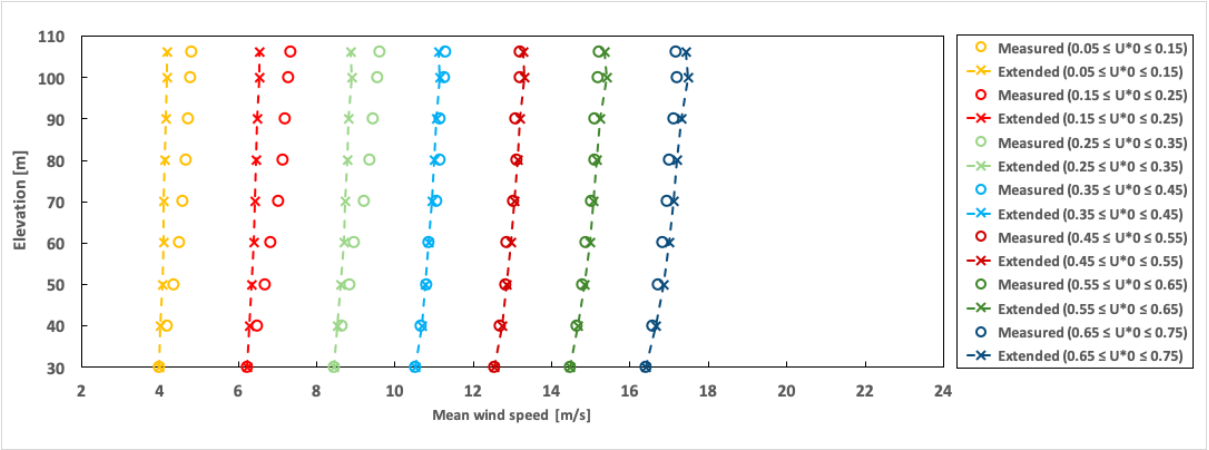

(a) Very unstable

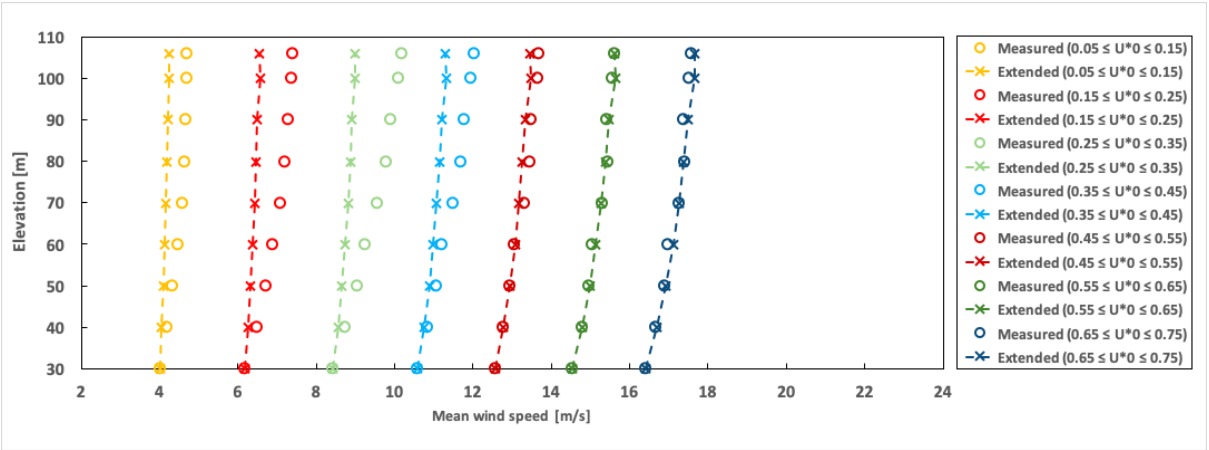

(b) Unstable

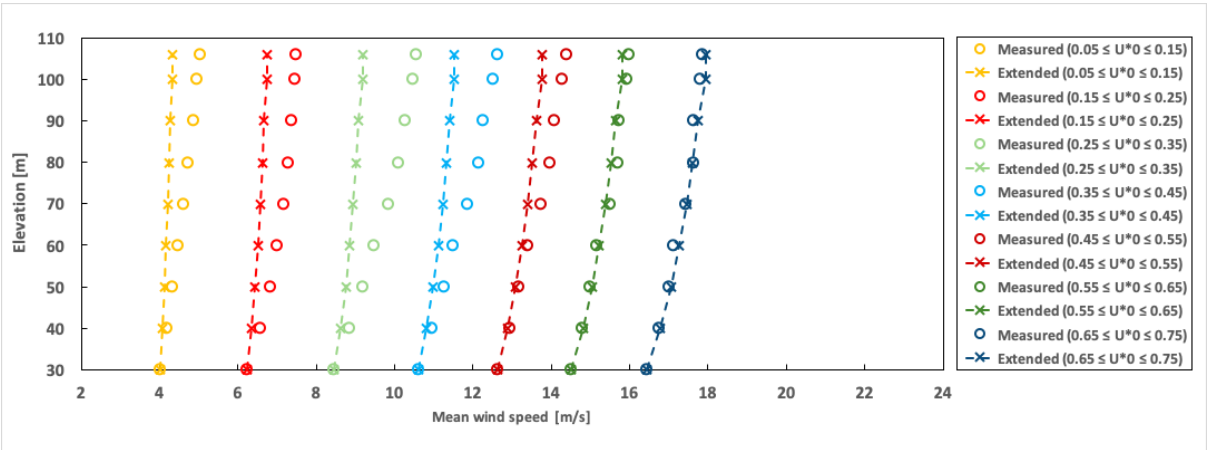

(c) Near neutral unstable

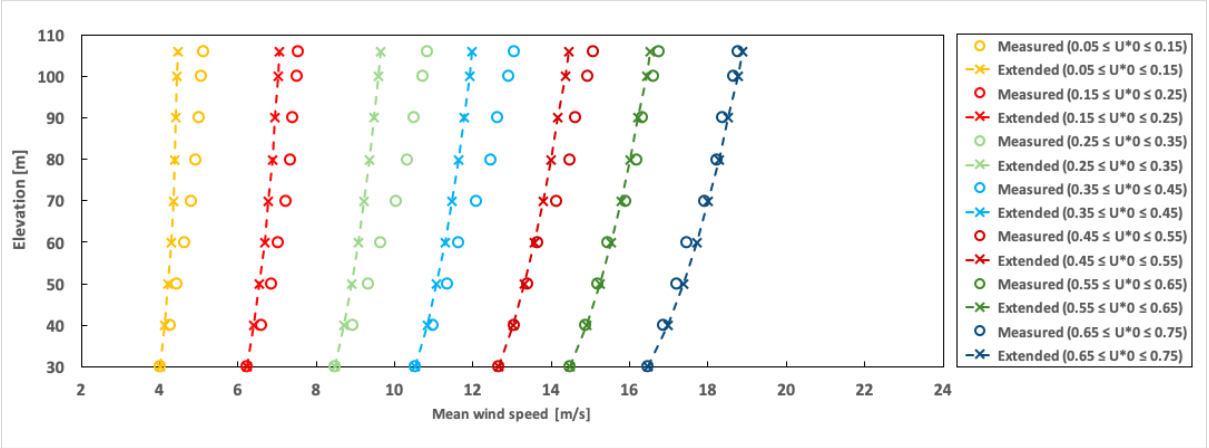

(d) Neutral

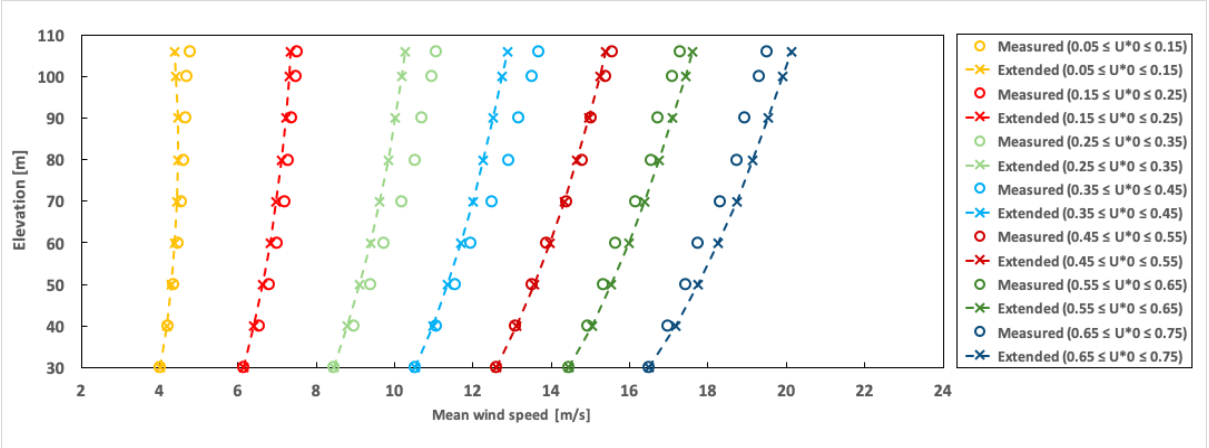

(e) Near neutral stable

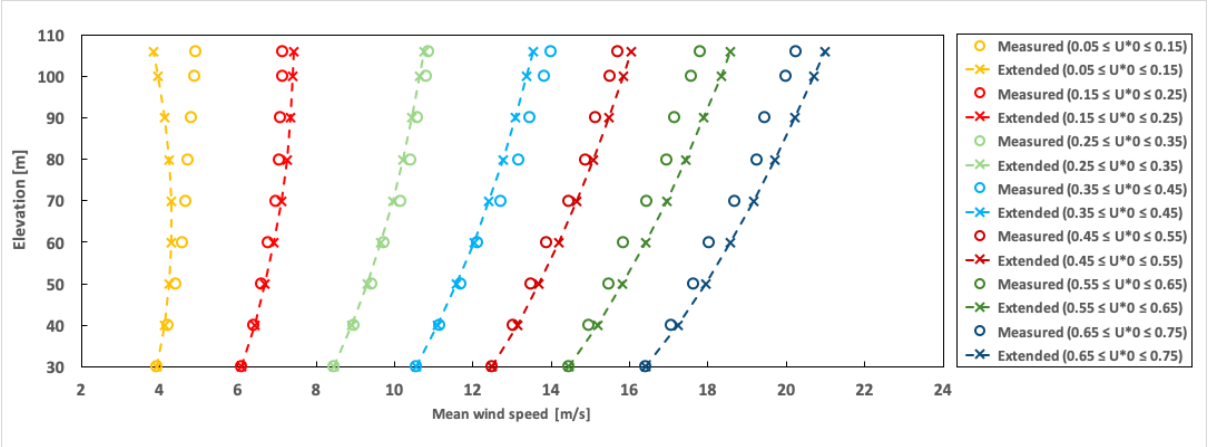

(f) Stable

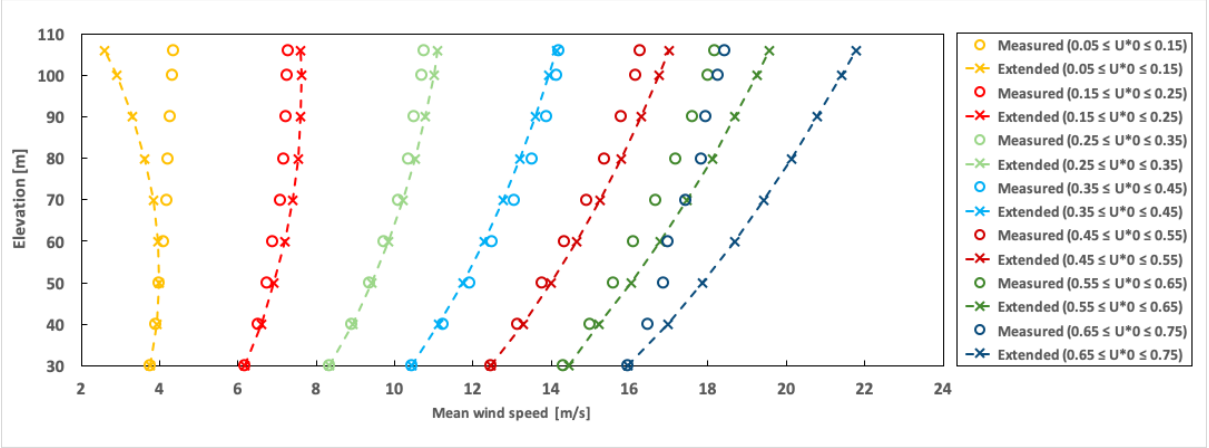

(g) Very stable

*Figure 4.8: Average wind speed at various observation height compared to estimates of extended wind profile as a function of friction velocity. Note the y-axis uses a logarithmic scale.(very unstable(a), unstable(b), near neutral unstable(c), neutral(d), near neutral stable(e), stable(f), very stable(g)). Note that the plot for 0.65< u*o< 0.75 are based on two observations, hence the deviation*

For very unstable conditions (Figure 4.8a), the extended wind profile nearly coincides well with observations for u_{*o} < 0.35 at all heights but for lower friction velocity it underestimates the wind speed. For unstable conditions (Figure 4.8b), the extended wind profile nearly coincides well with observations for u_{*o} < 0.35. Though for 0.35< u_{*o} < 0.45 regime, underestimation of the wind speed is noticed for altitude above 60 m.

For near neutral unstable conditions (Figure 4.8c), the extended wind profile nearly coincides well with observations for u_{*o} < 0.45. Though for 0.45< u_{*o} < 0.55 regime, underestimation of the wind speed is noticed for altitude above 60 m. For neutral conditions (Figure 4.8d) similar results are found as for near neutral unstable conditions, though the magnitude of the underestimation is lower.

For all stable conditions (near neutral stable and very stable included). The extended wind profile curves to the left and underestimates the wind speed for 0.05< u_{*o} < 0.15 regime, the magnitude of the underestimation increases with increasing stability. For near neutral stable conditions (Figure 4.8e), the extended wind profile coincides well with observations for 0.45< u_{*o} < 0.55 regime, underestimates the wind speed below u_{*o} < 0.45 and overestimates the wind speed above u_{*o} > 0.55.

For stable conditions (Figure 4.8f), the extended wind profile coincides well with observations for 0.15 < u_{*o} < 0.55 regime up to 60 m height, but for 0.45 < u_{*o} < 0.55 regime slight underestimation is noticed for altitude above 60 m. Above u_{*o} > 0.55 overestimation of the wind speed is noticed. For very stable conditions (Figure 4.8g), similar results are found as for stable conditions, though with different orders of magnitude. Note that the plot for 0.65< u_{*o} < 0.75 are based on two observations, hence the deviation. The result obtained in this current study for stable and very stable conditions is similar to the results presented in Figure 5 by M. C. Holtslag, Bierbooms, and van Bussel (2017).

Table 4.1: The average boundary layer height for each friction velocity regime under the various stability conditions shown in figure 4.8.

Friction velocity regime	Very Unstable h (m)	Unstable h (m)	Near Neutral Unstable h (m)	Neutral h (m)	Near Neutral Stable h (m)	Stable h (m)	Very Stable h (m)
0.05< u_{*_o} ≤ 0.15	160	145	126	95	73	61	51
0.15< u_{*_o} ≤ 0.25	273	242	213	163	121	104	93
0.25< u_{*_o} ≤ 0.35	393	354	306	238	179	155	133
0.35< u_{*_o} ≤ 0.45	513	467	407	312	233	204	177
0.45< u_{*_o} ≤ 0.55	637	578	503	388	293	252	219
0.55< u_{*_o} ≤ 0.65	757	693	598	457	349	301	262
0.65< u_{*_o} ≤ 0.75	892	798	701	533	411	358	302

From Table 4.1, it can be observed that the average boundary layer height increases with increasing friction velocity and decreases with increasing stability. Aslo, comparing Table 4.1 to Figure 4.8 it is observed that the extended wind profile seems to perform better for certain average boundary range for unstable (all) conditions (i.e. 637 m to 892 m) and also, certain average boundary layer range for stable (all) conditions (i.e. 293 m to 349 m). It is then decided to evaluate the performance of the extended wind profile for a continuous range of boundary layer height, and to see if the other wind profiles considered in this study perform better than the extended wind profile for certain boundary layer heights, the boundary layer height h, ranging from 50 m to 1200 m for unstable conditions and ranging from 50 m to 900 m for stable conditions with a bin size of 25 m are considered. As such we consider 45 narrow bin for unstable conditions and 35 for stable conditions, which serves as an approximation of the boundary layer height on a continuous scale. For observations of a boundary layer height bin, the average RMSE between the measured filtered data and the extrapolated data obtained from the wind profile models considered in this study is calculated. Figure 4.9 shows the average RMSE found as a function of boundary layer height for the various wind profiles.

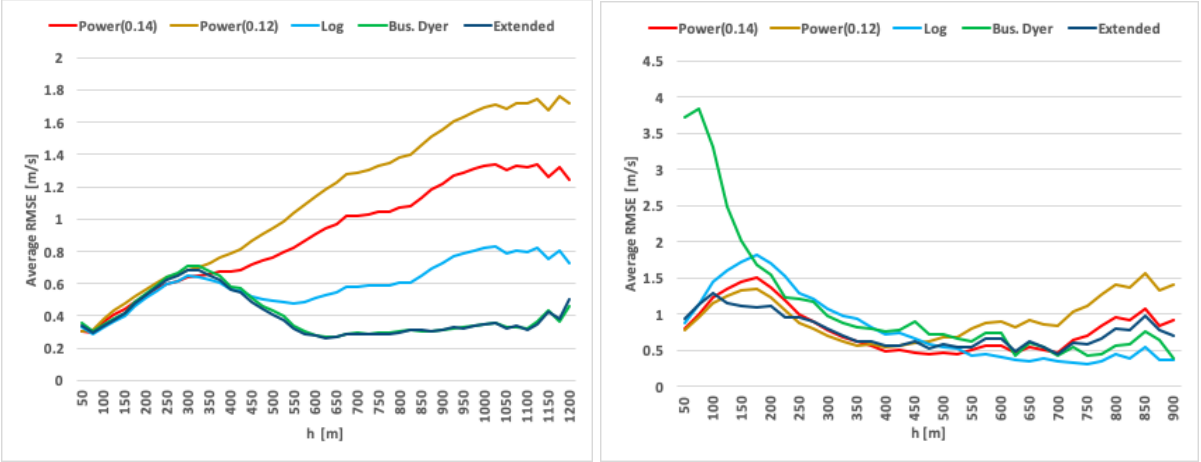

Figure 4.9: Average RMSE of the various wind profile as a function of boundary layer height, h for unstable (left panel) conditions and stable (right panel) conditions.

From Figure 4.9, it can be observed that does indeed perform better for certain boundary layer height for unstable and stable conditions. The extended wind profile and the Businger Dyer wind profile has similar performance for unstable conditions and they perform better than the other wind profile models. However, for stable conditions the Businger Dyer wind profile has a very poor performance for low boundary layer heights. The extended wind profile performance better for the majority of the boundary layer height (i.e from about 100 m to 550 m) but for boundary layer heights (i.e. above 700m), the log and the Businger Dyer wind profile seems to perform better. It should be noted that the Log wind profile is most likely underestimating the wind speed for these boundary layer heights whereas the extended wind profile is overestimating it.

4.2.3. Wind profile extrapolation analysis and results for all filtered data.

As was done in section 4.2.1 for stability classes, the measured wind speed observations at 30 m height were extrapolated to the other observation heights at FINO3 using the wind profile models considered in this study. The performance of the wind profile models for all the measured filtered was then assessed. First, the average wind speed at the various heights was normalised using the average wind speed at 30 m height. Then, the normalised average wind speeds obtained for the measured wind speed observations were compared to the normalised average wind speeds obtained for the extrapolated data from the wind profile models. The results for this comparison for each stability class are presented in Figure 4.10a. To give an indication of the magnitude of the over/underestimation of the wind speeds at the various observation heights, the RMSEs (root mean square error) at the various heights for each wind profile model was evaluated. The results of the RMSEs at the various observation heights are presented in Figure 4.10c. Finally, for an indication of the overall performance of the wind profile, the average RMSE for each wind profile model was evaluated. The results of the average RMSE are presented in Figure 4.10b. The RMSE between the estimated wind speed $\hat{u}_i$ by the wind profile models and measured wind speed observations was calculated with equation [50].

(a)

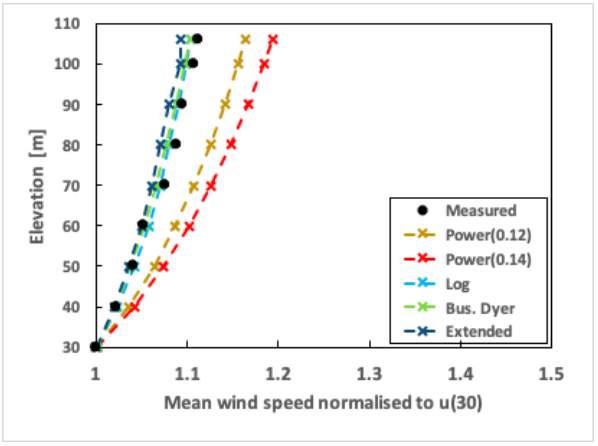

(b)

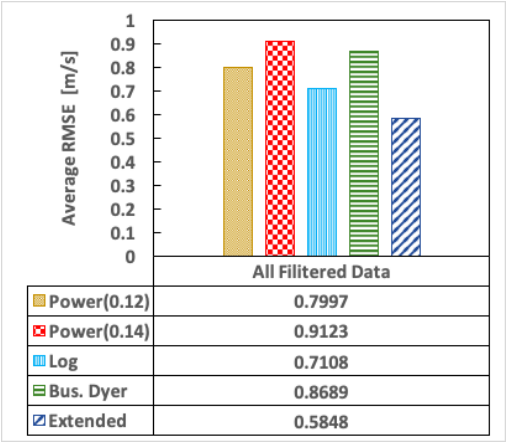

	All Filitered Data
Power(0.12)	0.7997
Power(0.14)	0.9123
Log	0.7108
Bus. Dyer	0.8689
Extended	0.5848

(c)

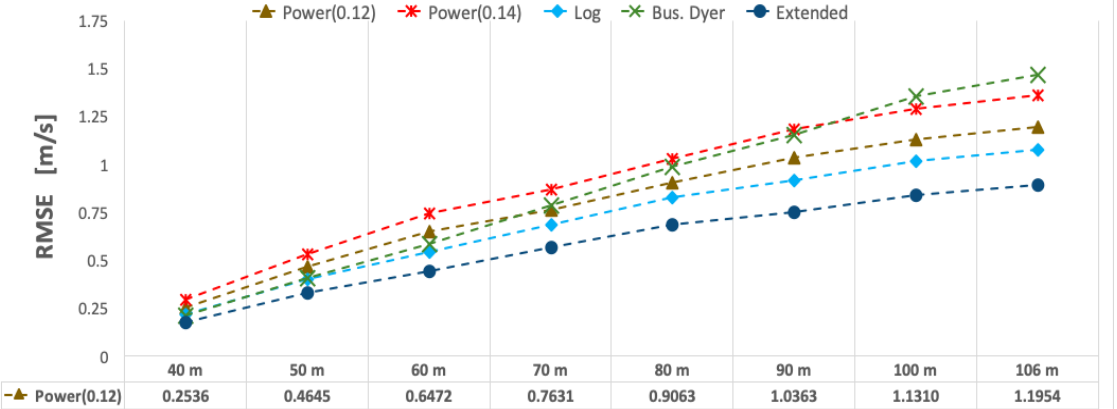

	40 m	50 m	60 m	70 m	80 m	90 m	100 m	106 m
Power(0.12)	0.2536	0.4645	0.6472	0.7631	0.9063	1.0363	1.1310	1.1954
Power(0.14)	0.2923	0.5316	0.7460	0.8688	1.0263	1.1835	1.2881	1.3618
Log	0.2152	0.4020	0.5456	0.6874	0.8254	0.9179	1.0181	1.0748
Bus. Dyer	0.2093	0.4102	0.5873	0.7867	0.9849	1.1550	1.3516	1.4664
Extended	0.1754	0.3309	0.4417	0.5683	0.6826	0.7527	0.8368	0.8896

Figure 4.10: All filtered data (The normalised average wind speed of the measured wind speeds and the wind profile models (a), Average RMSE of the wind profile models (b), RMSE at the various heights of the wind profile model(c)).

Also, to assess the performance of the wind profile model for a continuous range of stability conditions, It is decided to adopt a similar approach as was used for the boundary layer height in Section 4.4, hence stability conditions of 100/L ranging from 5 to 2 with a 0.1 bin size are considered. As such we consider here 71 narrow stability classes, compared to the 7 general classes used in the previous section, which serves as an approximation of stability on a continuous scale. For observations of a stability class bin, the average RMSE between the measured filtered data and the extrapolated data obtained from the wind profile models considered in this study is calculated. Figure 4.11 shows the average RMSE found as a function of stability for the various wind profiles.

From Figure 4.10, it is observed that the power law (both exponents) wind profiles overestimated the wind speed for all observation heights, the magnitude of the overestimation increased gradually with increasing altitude (See Figure 4.10a). As stated earlier the RMSE gives an indication of the over/underestimation. The power law (with an exponent of 0.14) wind profile had the highest RMSEs for all observation heights up to 90 m, but for higher altitudes the Businger Dyer wind profile had the highest RMSEs .(See Figure 4.10b). The average RMSEs of the power law (with an exponent of 0.12) and the power law

(with an exponent of 0.14) wind profiles were approximately 0.80 m/s and 0.91 m/s respectively (See Figure 4.10b).

The Log wind profile model corresponds well to the observations for all heights (See Figure 4.10a). It should be noted that though Figure 4.10a shows that the log wind profile corresponded well to measurements, this is a plot of the average wind speed at the observation heights which means that the wind profile is overestimating for some observations and underestimating for others as was shown in section 4.2, both the average corresponds well to the average of the measured wind speed. The Log wind profile had an average RMSE of 0.71 m/s (See Figure 4.10b)

The Businger-Dyer and the extended wind profiles correspond well to the observations up to approximately 60 m height but for higher altitudes, the wind speed is underestimated (See Figure 4.10a). The underestimation by the extended wind profile is slightly lower than that of the Businger Dyer wind profile, this is because as shown in section 4.2 the Businger dyer largely over estimates the wind speed during stable conditions. Since they both have very similar performance during unstable conditions and an average value is considered in figure 4.10a, the overestimation by the Businger Dyer wind profile during stable condition will hence indicate a lower underestimation. It is also observed that the RMSE of the Businger wind profile for the various observation heights increased at a higher rate than the other wind profile models.

The extended wind profile had the lowest RMSEs for all observation heights and hence, the lowest average RMSE, approximately 0.58 m/s of all the wind profiles considered. The Businger dyer wind profile had an average RMSE of approximately 0.86 m/s,

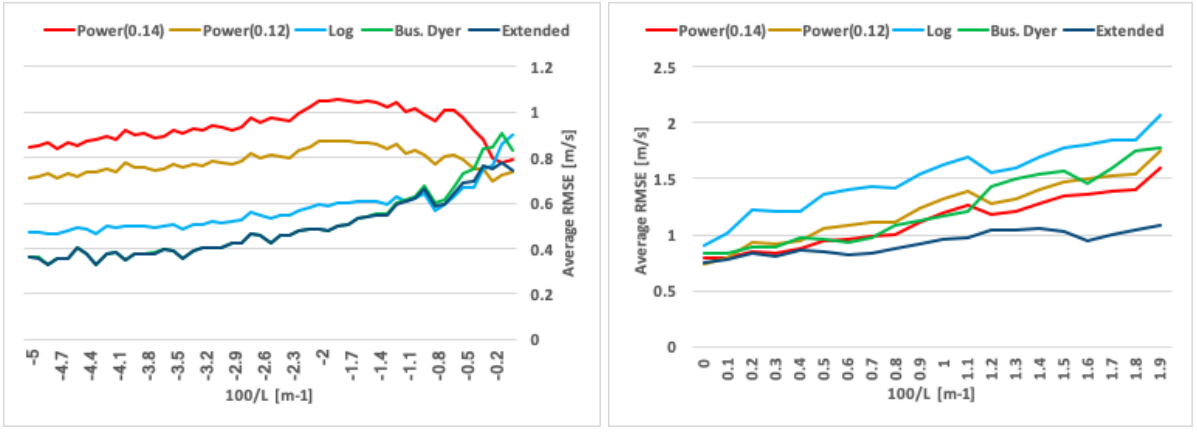

Figure 4.11: Average RMSE of the various wind profile as a function of stability for unstable (left panel) conditions and stable (right panel) conditions.

It can be observed from Figure 4.11 that for unstable conditions, the extended wind profile performs approximately as good as the Businger Dyer wind profile. Only for near neutral conditions the extended wind profile starts to perform better compared to the Businger Dyer wind profile. The log wind profile performs less good for unstable conditions. Due to the absence of stability correction the log profile overestimates the wind shear as has been shown in section 4.2. The power law wind profile (both exponents) performs very poor for unstable conditions since wind shear is strongly overestimated with the exponents of 0.12 and 0.14 considered here.

For stable conditions, the extended wind profile performs better than any of the other wind profile models considered in this study. Here it is found that the power law wind profile with an exponent of 0.14 performs reasonably well, since wind shear is strong for stable conditions, which is also achieved when the power law wind profile is used with an exponent of 0.14. Though is has been shown in section 4.2 that the wind speed are still largely underestimated for high altitude (i.e. at 108 m elevation). The Businger Dyer wind profile have similar or better performance to the power law wind profile (both exponents) for $100/l$ range between 0 and 1.1, but above this the power law wind profile (both exponents) starts to perform better. Though as shown in section 4.2. The power law wind profile underestimates the wind shear, while the Businger Dyer wind profile overestimates the wind shear.

Combined, it is found that for all stability conditions considered in this assessment, the extended wind profile performs either as well as the other wind profiles considered in this study for unstable conditions. Except near neutral unstable conditions where the power law wind profile performs better. For stable conditions it performs better. As such, incorporating the extended wind profile in wind turbine installation campaign simulations should result in a better representation of the atmospheric conditions for the far offshore site considered in this study.

5. Impact on installation campaign simulation.

The impact of the wind profile model used for extrapolation during offshore wind farm installation campaign simulation is shown for the accumulated waiting on weather (AWoW) and possible power production. This assessment is done for all the wind profiles considered in this study (section 4). The intelligent simulation tools, SIMSTALL of Shoreline is used to obtain the accumulated waiting on weather from installation simulations and MAINTSYS, also from Shoreline is used to obtain the possible power production.

For the installation simulations, it was necessary to define a base case which represents a typical offshore wind farm. The base case considered in this study used the layout and location of the NORCOWE reference wind farm (Bak et al. 2015). This location also coincides with the FINO 3 met mast location where we have obtained the weather data for this study. The base case with specified relevant values is described in Section 5.1. The measured filtered data and the extrapolated data obtained from the wind profile models considered in this study were then analysed for the various wind weather windows defined in the base case. This was done to give an initial indication of how well the wind profile models will perform for these wind weather windows during the installation campaign simulation. The number of available weather windows in the extrapolated data from the wind profile models was compared to that available in the measured filtered data; the results from this are presented and analysed in Section 5.2. Then, a new approach to wind profile usage in wind farm installation campaign simulation is then proposed and defined Section 5.3.

After, the base case was then run with the measured filtered data as weather input. The sensitivity of the AWoW to the installation campaign start month, the wind speed limit of installation operations and the duration of the installation operation is then accessed. The analysis and the results from these are presented in Section 5.4. Then, the base case was run with the extrapolated data obtained from the wind profile models as weather input. The results obtained are then compared to the results obtained when using the measured filtered data as weather input. Concurrently, the suggested approach in this study is validated. The results of the comparison and the validation of the suggested approach are presented in Section 5.5. The measured filtered data and extrapolated data from the wind profile models are also used as weather input to estimate the possible power production, the results of over/underestimation of possible power production by the extrapolated data from the wind profile models are presented in Section 5.6.

5.1. Description of the base case

A hypothetical wind farm consisting of 80 (10MW) wind turbines, each sitting atop monopile foundations and assumed to have a hub height of 108 m was established for all simulations in this study. The wind farm is assumed to be located at the location of the FINO3 met mast, 80 km west of the island of Sylt at the Danish-German border. The closest turbine is located at an approximate distance of 86 km from the harbour at Esbjerg port. The mean water depth at the location of the wind farm is 22.5 m.

The Curvilinear baseline turbine layout of the NORCOWE reference wind farm (T. Bak et al. 2015) as shown in Figure 5.1 was also assumed.

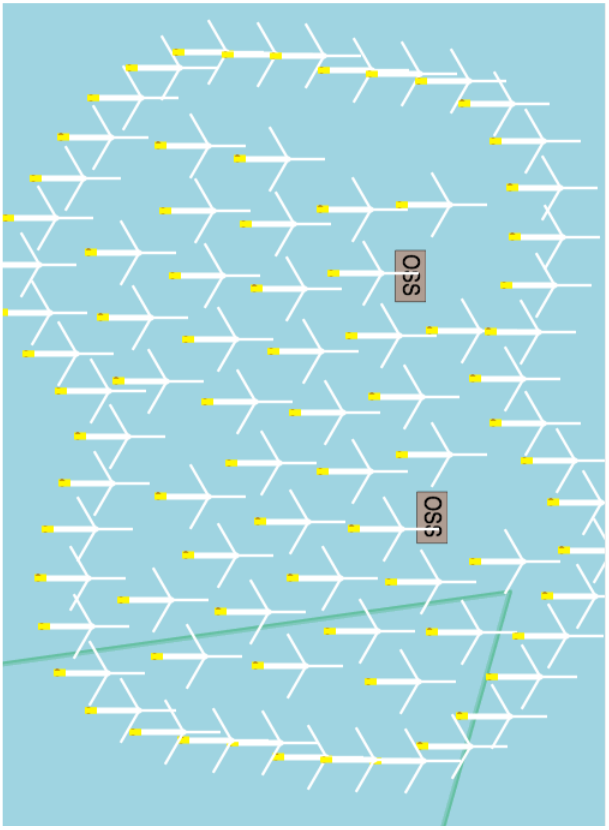

Figure 5.1: Curvilinear baseline offshore wind turbine layout.

5.1.1. Installation Simulation Campaign

In this study, the Shoreline intelligent simulation tool ("Shoreline" n.d.), SIMSTALL was used for all installation campaign simulations. SIMSTALL is used to Simulate the entire process of installation, completion, commissioning and testing for sustainable energy projects, including estimating costs and the financial performance of the early production. SIMSTALL can also be used to assess weather and project schedule risks and predict where obstacles could arise. The SIMSTALL simulation tool was configured to carry out the installation campaign as described below:

As described in section 2.2, logistics operations within the installation campaign of an offshore wind farm involves activities such as delivering of the wind turbine components, preassembly of components, offshore transportation, offshore installation and testing and commissioning. The offshore installation activity was divided into four phases: the installation of the foundations, turbines, substations and cables. The installation campaign in this study considers the foundation and turbine installation phases only.

In practice, different logistical methods can be used during the installation campaign of an offshore wind farm. For example, the wind turbine components can be delivered in several ways as discussed in section 2.2. The ways in which these components are delivered plays an important role in the installation campaign (Beinke, Alla, and Freitag 2017). In this study, it is assumed that all the wind turbine components are delivered to the harbour and components are always available for loadout at the staging port at any point in time. The components are loaded onto the wind turbine installation vessel (WTIV) which

requires a high lift that is restricted by wind speed. The WTIV used for simulation in this study is assumed to have maximum capacities as indicated in Table 1 in the Appendix .
For safety reasons, the activities by the WTIV are constrained by wave height and wind speed. When the vessel reaches maximum load capacity and the weather is good, it can journey to the installation site.

Before lifting at sea, the WTIV needs to be jacked up. Sealifting is also restricted by the weather, and the weather forecasts are checked. This also applies between lifting the components during installation on site, the availability of the required weather window needs to be evaluated. After all the components onboard the WTIV are installed, the ship returns to the port to load again.

In the installation campaign in this study, the foundations are installed first by pile driving method, the installation of the transition pieces begins when all foundations have been installed. The installation of wind turbine components starts as soon as all the transition pieces have been installed. Different levels of preassembly of components can be employed at the harbour instead of assembly on site as described in Section 2.2**.** The purpose of preassembly is to partly overcome challenges from the dependence on weather conditions, which is the main cause of project delays (York 2007). Through the effective and correct use of the preassembly concept, installation time can be reduced (Herman 2002). In this study, the wind turbine components are assumed to be preassembled in 5 parts, the tower (all sections), the nacelle (the hub is assembled with the nacelle), blade 1, blade 2 and blade 3. The tower sections are installed first followed by the installation of the nacelle, each blade is then attached to the hub which was preassembled to the nacelle.
The installation phases in the installation campaign are illustrated in Figure 5.2.

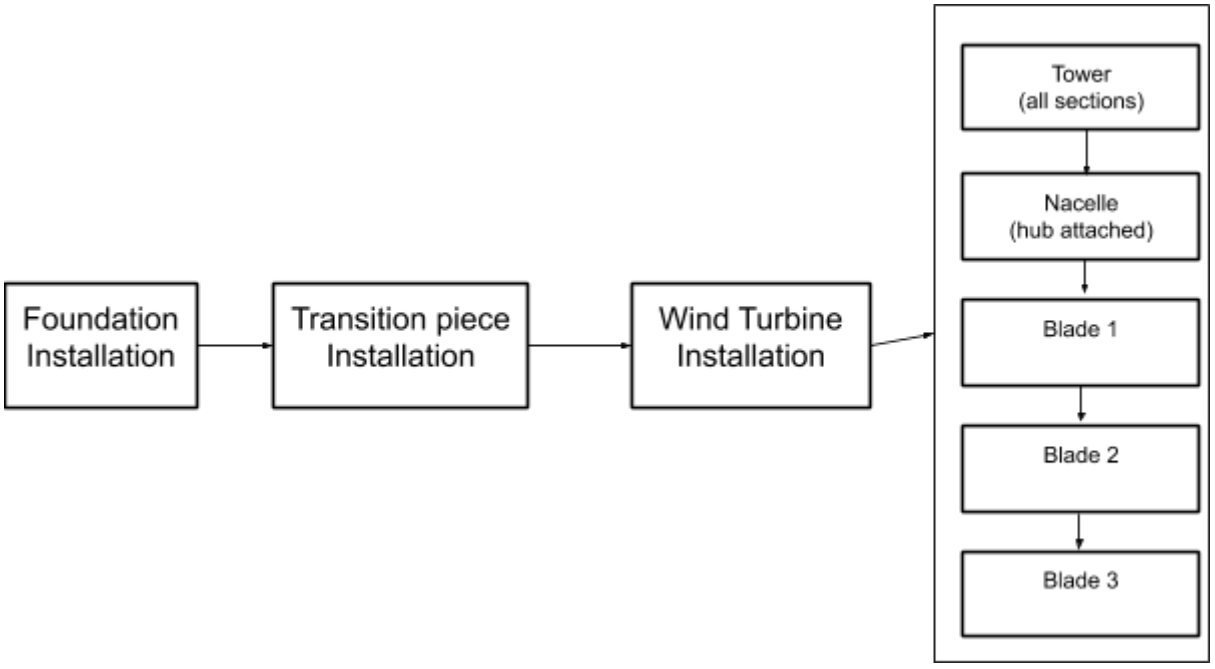

Figure 5.2: The installation phases considered.

5.1.2. Operation duration and limiting criteria

As stated earlier, wind speed and wave height were used as the limiting criteria for operations during the installation campaign simulations. The operation duration and limiting criteria for the different operations during the installation campaign of an offshore wind farm in available literature generally varied, also they considered different phases of offshore wind farm installation campaign. The variation is understandable as there are lots of factors that affect these values for different wind farm installation campaign projects. To account for these variations while accessing the performance of the wind profile model, a sensitivity study was carried out on the operation duration and wind speed limit criteria.

A summary of the operation duration, wind speed and wave limits criteria for each operation during the wind farm installation campaign used as input for the base case in this study are given in Table 2 in the Appendix. The required weather window duration is taken to be twice the operation duration as recommended in DNV-OS H101.

The variation is understandable as there are lots of factors that affect these values for different wind farm installation campaign projects. To account for this variation a sensitivity study was carried out on the operation duration and wind speed limit criteria.

5.1.3. Power Curve

The power curve of the DTU 10-MW Reference wind turbine (C. Bak et al. 2013) was assumed as input for the base case in this study. Table 5.1 gives the design summary of the DTU 10 MW wind turbine and Figure 5.3 show the power curve used.

Table 5.1: The DTU 10 MW Reference wind turbine design summary as used in this study. (*Note Hub height of 108 m was used in this study as opposed to 119 m specified in (C. Bak et al. 2013).

*Table 5.1: The DTU 10 MW Reference wind turbine design summary as used in this study. (*Note Hub height of 108 m was used in this study as opposed to 119 m specified in (C. Bak et al. 2013).*

Description	Value
Rating	10MW
Rotor orientation, configuration	Upwind, 3 blades
Rotor, Hub Diameter	178.3 m, 5.6 m
Hub height	108 m
Cut-in Speed	4 m/s
Rated wind speed	11.4 m/s
Cut-out wind speed	25 m/s

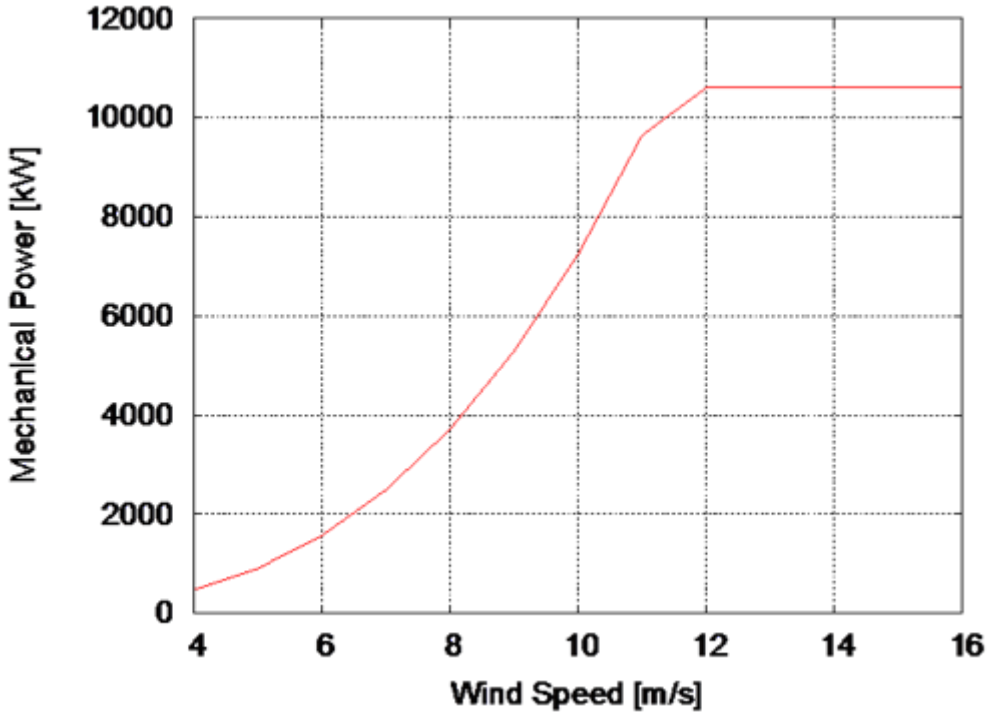

Figure 5.3: The power curve of the DTU 10 MW reference wind turbine (C. Bak et al. 2013).

5.2. Wind weather window

A summary of the wind weather windows required for the various installation operations during the installation campaign of the base case offshore wind farm is presented in Table 5.2. Note that the significant wave height limit is not considered in the analysis in this section. This is because our major focus in this section is on the wind profile models performance and besides, the wave data will be the same for all installation campaign simulations. The number of these wind weather window available in the measured filtered data compared to that available in the extrapolated data from the wind profile models are presented in Figure 5.4.

Table 5.2: Summary of the various wind weather windows in the base case installation campaign.

Code	Weather Window Duration (Hours)	Wind Speed Limit (m/s)	Reference Height (m)	Operations
H5W12a	5	12	92	• Loading of the blade set
H3W14a	3	14	92	• Loading of tower
H4W14a	4	14	92	• Loading of each transition piece • Loading of nacelle
H4W18a	4	18	92	• Loading of each pile
H4W8b	4	8	108	• Installation of the blade (per blade)
H6W10b	6	10	108	• Installation of nacelle
H2W12b	2	12	108	• Positioning (during jack up) • Preparing transition piece for tower installation • Preparing for lifting (during WTG installation)
H8W12b	8	12	108	• Full tower installation • Securing WTG
H2W18b	2	18	108	• Stabbing of monopile
H4W18b	4	18	108	• Upending monopile from the deck
H6W18b	6	18	108	• Piling • Transition piece installation
H12W18b	12	18	108	• Airtight Platform and bolting (during transition piece installation)

From Figure 5.4, it can be observed that the number of available weather windows varies depending on the duration of the weather window and the wind speed limit. As the duration of the weather window increases the number of available weather window tends to decrease, also as the wind speed limit decreases the number of available windows also tends to decrease. For the measured data, H4W8b (Installation of each Blade) had the least number of windows. Also, H6W10b (Installation of nacelle), H8W12b (Full tower installation, Securing WTG) and H12W18b (Airtight Platform and bolting during transition piece installation) had a low number of available window., Attention should be paid to these operations with a low number of windows since they will contribute the most to the accumulated waiting on weather (AWoW) during the installation campaign.

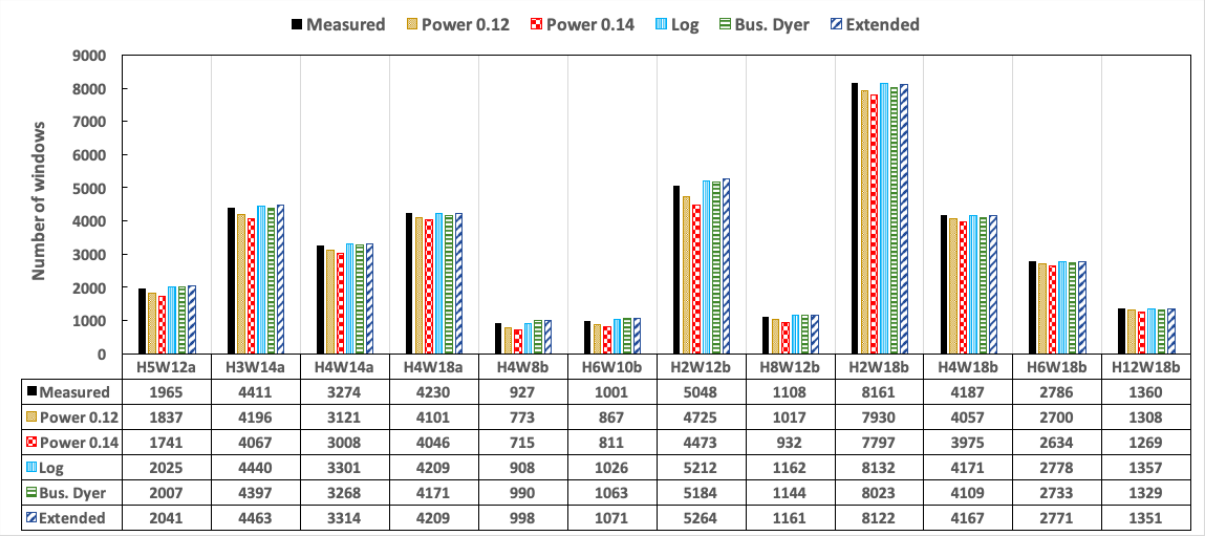

	H5W12a	H3W14a	H4W14a	H4W18a	H4W8b	H6W10b	H2W12b	H8W12b	H2W18b	H4W18b	H6W18b	H12W18b
Measured	1965	4411	3274	4230	927	1001	5048	1108	8161	4187	2786	1360
Power 0.12	1837	4196	3121	4101	773	867	4725	1017	7930	4057	2700	1308
Power 0.14	1741	4067	3008	4046	715	811	4473	932	7797	3975	2634	1269
Log	2025	4440	3301	4209	908	1026	5212	1162	8132	4171	2778	1357
Bus. Dyer	2007	4397	3268	4171	990	1063	5184	1144	8023	4109	2733	1329
Extended	2041	4463	3314	4209	998	1071	5264	1161	8122	4167	2771	1351

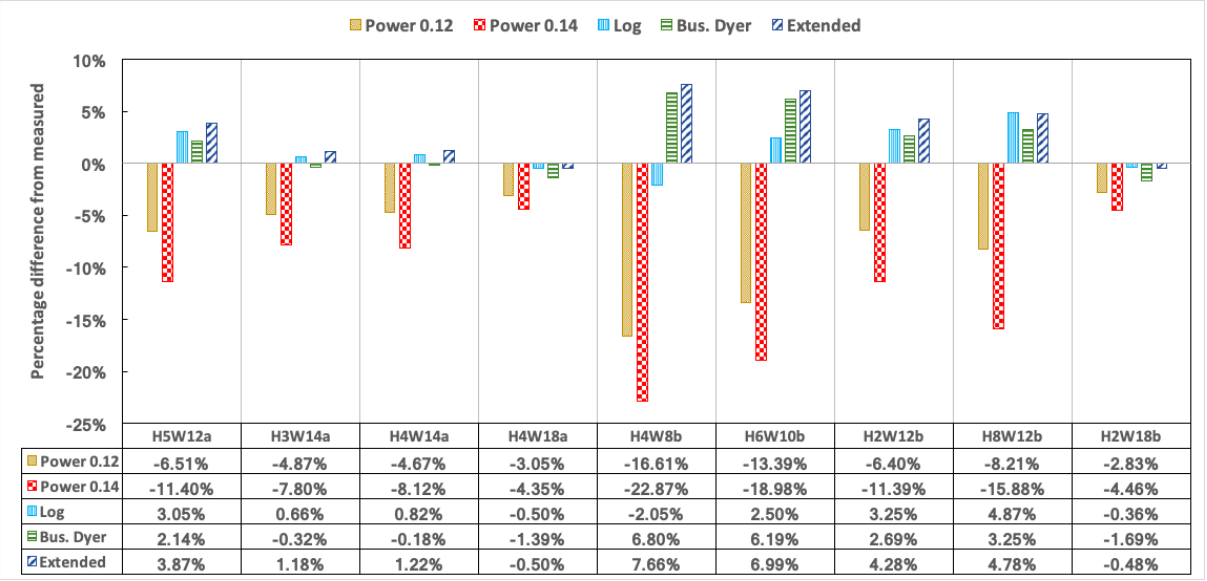

	H5W12a	H3W14a	H4W14a	H4W18a	H4W8b	H6W10b	H2W12b	H8W12b	H2W18b
Power 0.12	-6.51%	-4.87%	-4.67%	-3.05%	-16.61%	-13.39%	-6.40%	-8.21%	-2.83%
Power 0.14	-11.40%	-7.80%	-8.12%	-4.35%	-22.87%	-18.98%	-11.39%	-15.88%	-4.46%
Log	3.05%	0.66%	0.82%	-0.50%	-2.05%	2.50%	3.25%	4.87%	-0.36%
Bus. Dyer	2.14%	-0.32%	-0.18%	-1.39%	6.80%	6.19%	2.69%	3.25%	-1.69%
Extended	3.87%	1.18%	1.22%	-0.50%	7.66%	6.99%	4.28%	4.78%	-0.48%

Figure 5.4: Number of available wind weather windows in measured data compared to extrapolated data from wind profile models.

*The number after "H" represents the duration of the weather window, the number after "W" represents the wind speed limit. a= Height of 92 m and b= height of 108 m. i.e H5W12a implies a weather window with a duration of 5 hours and a wind speed limit of 12 m/s at 72 m.

Also, from Figure 5.4 it can be observed that the extrapolated data from the power law (both exponents) underestimates the number of available wind weather windows. This is because as shown in section 4.2, during unstable conditions which prevail far from shore the power law (both exponents) tends to overestimate the wind speed at the required heights. The magnitude of these underestimations in the number of available wind weather windows are higher for wind weather windows with a low wind speed limit (i.e. 8 m/s), this is due to the prevalence of unstable stable conditions at lower wind speeds (see section 3.4). Compared to the measured, these underestimations varied approximately between 3% to 17% and between 4% to 23% for the extrapolated data obtained from the power law wind profile with an exponent of 0.12 and power law wind profile with an exponent of 0.14 respectively.

Though the extrapolated data from power law wind profile (both exponents) underestimates the number of available wind weather windows for the various installation operations, it does not indicate that it is a good representation of the atmospheric conditions or that it provides a better safety margin. Because there is a high possibility of it indicating a false weather wind weather window. As shown in section 4.2 the power law wind profile model (both exponents) tend to underestimate the wind speed during stable conditions. In fact, for the power law wind profile with an exponent of 0.12, the RMSE at 108 m elevation during very stable conditions (see Figure 4.7c) was approximately 2 m/s. This means the average underestimation in the wind speed in very stable condition by the power law wind profile model with an exponent of 0.12 is about 2 m/s. Though as shown in section 3.4 that the occurrence of stable conditions far offshore is minimal, they can occur in wind speed from 2 m/s up to 26 m/s (see Figure 3.9) and underestimation of the wind speed by up to 2 m/s during weather sensitive installation operations (i.e installation of blade or nacelle) can be disastrous. It is important that the high wind shear during stable conditions is accounted for in the extrapolated data when analysis pertaining to wind weather windows are carried out to avoid the indication of false weather windows for installation operations.

The extrapolated data from the log wind profile both underestimates and overestimates the number of available wind weather windows for the various installation operations. The accuracy of the estimation of the number of wind weather windows by the extrapolated data obtained from the log wind profile model ranged between -2% and 5%. Though it seems to have the highest accuracy compared to the other wind profile models, a lot of false weather windows will be indicated by extrapolated data obtained from the log wind profile model. Because as shown in section 4.2 the underestimation of the wind speed at the required heights by the extrapolated data obtained from the log wind profile model were evident from near neutral unstable conditions. The RMSE which gives an indication of the average underestimation of the wind speed by the log profile during very stable condition at 108 m elevation was 2.5 m/s (see Figure 4.7c). And as discussed for the power law wind profile this can be dangerous.

The extrapolated data obtained from the extended and the Businger Dyer wind profile tends to overestimate the number of available windows for wind weather window with a wind speed limit less than 14 m/s. Overestimation of up to approximately 7% and 8% were observed for the extrapolated data from the extended and the Businger Dyer wind profile respectively. This is understandable because as shown in section 4.2, the extended wind profile model tends to underestimate the wind speed for low wind speeds (i.e. < 14 m/s). It is also observable that the overestimation by the extrapolated data obtained from the extended wind profile is higher than that of the Businger Dyer wind profile. This is because as shown in section 4.2 the Businger dyer wind profile model largely overestimates the wind speed at the required heights, especially during very stable conditions. For instance, the average overestimation of the wind speed by the Businger Dyer wind profile during very stable condition at 108 m as indicated by the RMSE was approximately 2.6 m/s (see Figure 4.7c). The fact that it largely overestimates the wind speed during stable conditions means that some true available wind weather window may be considered false by the data obtained from the Businger dyer wind profile model, hence reducing the number of available wind weather windows. Also, during unstable conditions, the underestimation of the wind speed

by the Businger Dyer wind profile is slightly higher than that of the extended wind profile. This can also lead to the lower overestimation in the number of available wind weather window by the Businger Dyer wind profile compared to the extended wind profile model.

For the other required wind weather windows (i.e. with wind speed limit equals or greater than 14 m/s), the number of available wind weather windows in the data obtained from the extrapolation by the extended and the Businger dyer Wind profile seem to correspond well to that of the measured data. The accuracy in estimating the number of available wind weather wind range from - 0.5% to 1.22% and - 0.18 to 1.69% for the extrapolated data from the extended and Businger Dyer wind profile respectively.

Generally, the extended wind profile is a better representation of the atmospheric conditions as has been shown in this study so far but it has the limitation of underestimating the wind speed at low wind speeds (i.e lower than 14 m/s) especially during unstable conditions. And if the extended wind profile is to be adopted for used in offshore installation campaign simulation, especially for a far offshore site where unstable conditions prevail. There is a need to understand how these extended wind profile performs and accounts for its shortcomings. An approach to account for these shortcomings is proposed in the next section.

5.3. Suggested approach.

5.3.1 Need for a new approach

Most offshore installation campaign simulation tools make use of the power law wind profile model to extrapolate near-surface wind speed observations to the required heights. To account for high wind shear that occurs during stable conditions the exponent of the power law is usually increased (i.e from 0.12 to 0.14). It has been shown in this study (see section 4.2) that increasing the exponent of the power law wind profile from 0.12 to 0.14 increases the overestimations in the wind speeds for unstable conditions (very stable and near neutral stable included). For instance, using a power law wind profile with an exponent of 0.14 to extrapolate from 30 m elevation lead to RMSE of approximately 1.6 m/s at 108 m elevation (see Figure 4.1c). This indicates that overestimations of the wind speed for the majority of the observation are approximately about 1.6 m/s. Also, the power law wind profile with an exponent of 0.14 still underestimated the wind speed for stable (near neutral stable and very stable included) conditions. In fact, for very stable conditions using a power law with an exponent of 0.14 to extrapolate from 30 m elevation lead to RMSE of approximately 1.8 m/s at 108 m elevation (see Figure 4.1c). This also indicates that underestimations of the wind speed for the majority of the observation are approximately about 1.8 m/s.

It has also been shown in the study that stable conditions (near neutral stable and very stable included) can occur in wind speed between 2 m/s to 28 m/s (see Figure 3.9) and that very unstable and unstable conditions prevail at FINO3 (further from shore). This implies that using a power law wind profile for such sites would lead to underestimation of the number of available weather windows due to the high magnitude of overestimation during unstable conditions, but also indicate false weather windows due to the high magnitude of underestimation in the wind speed during stable conditions. Therefore, Increasing the value

of the power law exponent during offshore wind farm installation campaign simulation may indicate less number of available winds, but this does not make them safer or better because of the underestimation that may still be experienced during stable conditions. They will only increase the estimated accumulated waiting on weather unnecessarily.

The result from the number of available windows shows the power law (both exponent) and log wind profile model data underestimates the number of available winds as expected. Based on the results of the analysis carried out thus far in this study a new approach based on the extended wind profile is suggested in this study.

The extended wind profile has been studied extensively in section 4.3. It has been shown that the extended wind profile performs well for stable conditions except for very low wind speeds where it underestimates the wind speed. For unstable conditions, it was also shown that the extended wind profile performs well for wind speed above 14 m/s but for lower wind speed it underestimates the wind speed. This was also observed in the results of the number of available weather windows in section 5.2, where the extended wind profile had an accuracy of approximately $\pm 1\%$ for wind weather windows with wind speeds above 14 m/s. Based on these observations and the results from the analysis on the extended wind profile in section 4.3 a new approach is suggested for wind profile usage in wind farm installation campaign simulation.

5.3.1 Suggested approach defined and validated for wind weather windows

The suggested approach in this study for wind profile usage in wind farm installation campaign simulation is based on the use of the extended wind profile model. Near-surface wind speed observation can be extrapolated using the extended wind profile model as done in this study. The wind speed limits for installation operations with a low wind speed limit (i.e. lower than 14 m/s) should then be adjusted by a compensation factor to account for the underestimation of the wind speed by the extended wind profile, especially during unstable conditions. For instance, if the maximum wind speed for which the installation of each blade can be carried out is 8 m/s, to account for the underestimation of the wind speed by the extended wind profile this limit can be set to 7.75 m/s during the offshore installation campaign simulation (i.e the wind speed limit is reduced by a compensation factor of 0.25 m/s). This factor can be decided based on the safety margin required.

To validate the suggested approach a new wind profile data is defined referred to as “suggested”. For suggested, extrapolated data from the extended wind profile is used but the required wind weather windows for all installation operations with a wind speed limit below 14 m/s is reduced by a compensation factor of 0.25.

The suggested approach was used to carry out the analysis done for the number of available windows in section 5.2 for wind weather windows with a wind speed limit less than 14 m/s. The result is presented in Figure 5.5.

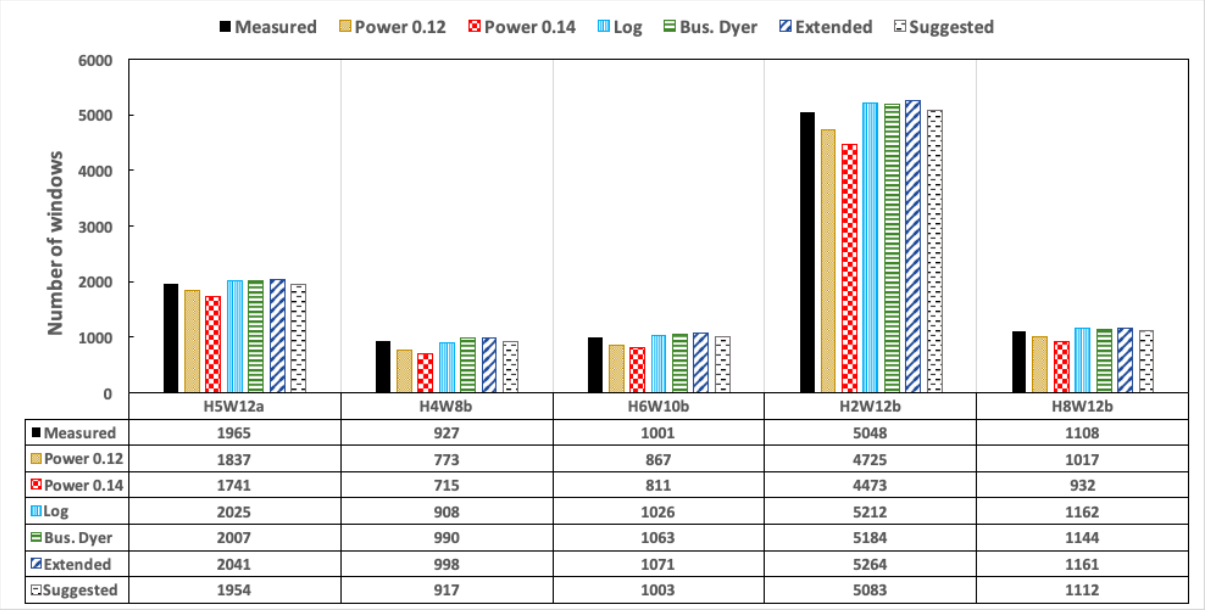

	H5W12a	H4W8b	H6W10b	H2W12b	H8W12b
Measured	1965	927	1001	5048	1108
Power 0.12	1837	773	867	4725	1017
Power 0.14	1741	715	811	4473	932
Log	2025	908	1026	5212	1162
Bus. Dyer	2007	990	1063	5184	1144
Extended	2041	998	1071	5264	1161
Suggested	1954	917	1003	5083	1112

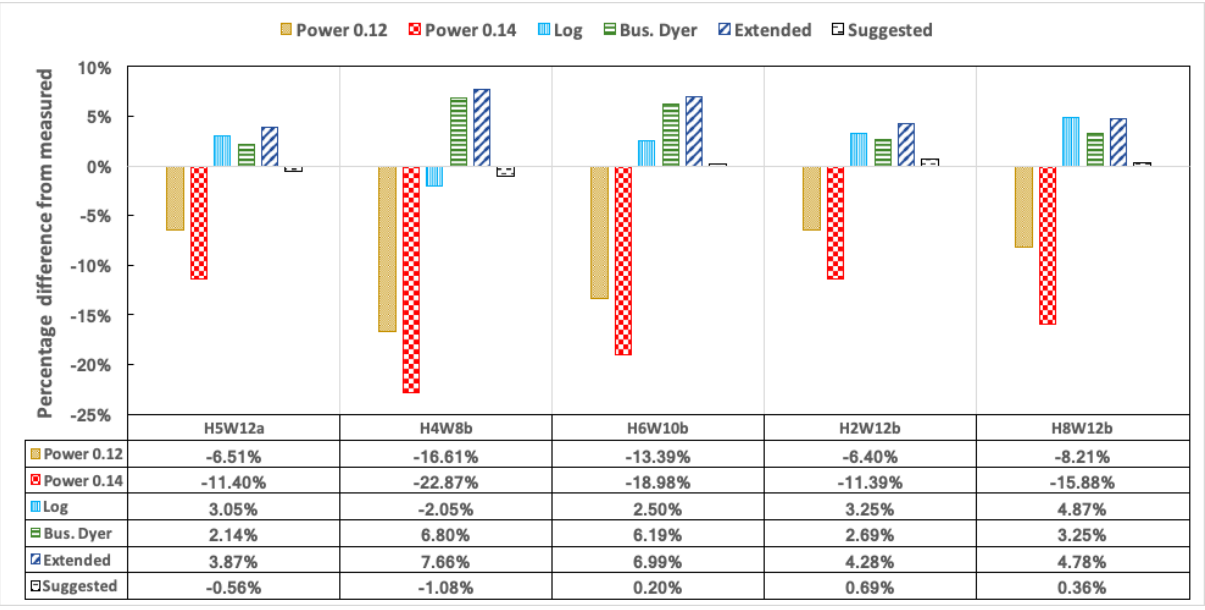

	H5W12a	H4W8b	H6W10b	H2W12b	H8W12b
Power 0.12	-6.51%	-16.61%	-13.39%	-6.40%	-8.21%
Power 0.14	-11.40%	-22.87%	-18.98%	-11.39%	-15.88%
Log	3.05%	-2.05%	2.50%	3.25%	4.87%
Bus. Dyer	2.14%	6.80%	6.19%	2.69%	3.25%
Extended	3.87%	7.66%	6.99%	4.28%	4.78%
Suggested	-0.56%	-1.08%	0.20%	0.69%	0.36%

Figure 5.5: Number of available wind weather windows in measured data compared to extrapolated data from wind profile models and the suggested approach.

*The number after "H" represents the duration of the weather window, the number after "W" represents the wind speed limit. a= Height of 92 m and b= height of 108 m. i.e H5W12a implies a weather window with a duration of 5 hours and a wind speed limit of 12 m/s at 72 m.

It can be observed from Figure 5.5 that the suggested approach has to some extent accounted for the shortcomings of the extended wind profile. It improved the accuracy of estimating the number of available wind windows for wind weather windows with a wind speed limit less than 14 m/s that ranged initially between approximately 4% to 8% to within an accuracy of approximately $\pm 1\%$. The overall accuracy of the suggested approach for all the required wind weather windows for the various installation operation is also within $\pm 1\%$ since the accuracy of wind weather wind with a wind speed limit greater than or equal to 14 m/s will be equivalent to that of the extended wind profile as shown in Figure 5.4. Though slight overestimation (< 1%) of the number of available wind weather wind was still be

observed, they can be eliminated by increasing the compensator factor (i.e from 0.25 m/s to 0.5 m/s) to increase the safety margin. The suggested approach is further assessed for its performance in estimating the accumulated waiting on weather in section 5.5

5.4. Sensitivity study on Accumulated waiting on weather

A total of 240 assets need to be installed at our reference wind farm in our base case defined in section 5.1, which consists of 80 monopile foundations, 80 transition pieces and 80 wind turbines. Each installation simulation is run for a 1000 iterations to obtain sufficiently accurate results and the simulation time for each simulation was about 30 minutes. All P values results were the same since the next installation phases start only when the previous was completed. For the base case (i.e with no weather restriction), the total time to complete the installation campaign was 286.39days and 446 hours of this was spent on transportation. This corresponds approximately to an installation rate of 3.6 days per wind turbine set.

Using the measured filtered data as weather input for the installation campaign simulation, sensitivity studies of accumulated waiting on weather (AWoW) to the installation campaign start Month, limiting criteria (wind speed limit) of installation operations and operation duration of installation operations were performed, the results from these are presented in the subsections below. These sensitivity studies were carried out because of the variations in input parameters (i.e. wind speed limit and installation duration for operations) in available literature as stated earlier and also, this sensitivity studies will give us the opportunity to assess the consistency in the performance of the wind profile model and the suggested approach in this study in estimating the accumulated waiting on weather.

5.4.1 Installation campaign start month sensitivity study

First, the start month of the installation campaign was varied as shown in Table 5.3. This was done in order to see how the start month of an installation campaign can affect the AWoW and hence the total installation time. Note that the start month in this simulation does not correspond to an actual start month because the actual data has been filtered and the filtered data represents the simulation time series (i.e April in the sensitivity start month study might not correspond to an actual April month (season) in real life).

Table 5.3: Installation start Month sensitivity study.

Scenario	Start Month	Installation Duration of base case with no weather data (Days)	Installation Duration of base case with measured data (Days)	AWoW (Hours)	Percentage Increase in installation duration due to AWoW (%)
SM1	January	286.39	559.77	6560	95.46%
SM2	February	286.39	581.46	7081	103.03%
SM3	March	286.39	594.06	7384	107.43%
SM4	April	286.39	576.63	6966	101.34%
SM5	May	286.39	575.78	6946	101.05%
SM6	June	286.39	566.87	6732	97.94%
SM7	July	286.39	562.25	6622	96.32%
SM8	August	286.39	572.86	6875	100.03%
SM9	September	286.39	570.94	6829	99.36%
SM10	October	286.39	580.04	7047	102.54%
SM11	November	286.39	571.92	6852	99.70%
SM12	December	286.39	587.16	7219	105.02%

From Table 4.3 the variation in AWoW depending on the installation campaign start month can be observed. In particular, the percentage increase in total installation time due to AWoW. The increase in the total installation time due to AWoW varied between 95% to 107% for different start month scenarios. The least AWoW was obtained for scenario SM1, with a value of 6560 hours, this may have occurred due to the fact that the operations with a lower number of windows as discussed in section 5.2 occurred during a period when the weather conditions were most favourable. Scenario SM3 had the highest AWoW value of 7384 hours, an increase of 824 hours (about 34 days) relative to scenario SM1. This shows that there is room for optimization when planning a wind farm installation campaign. The most weather sensitive phase of a wind farm installation campaign (i.e the wind turbine installation phase) can be scheduled for the optimal time of the year when the weather condition is favourable to reduce the AWoW and hence, the total installation time which will reduce the overall cost of the wind farm installation project. This phase includes installation of the blades and nacelle which involves weather sensitive heavy lift operations. The installation of the blades and nacelle typically occur 150 days after the start of the installation campaign in this study. The variation in installation campaign start month resulted in a variation in AWoW of up to 13% which also lead to a variation in the total installation time of about 6%. Our results show that proper scheduling of the start of an installation campaign can help reduce the total installation time required to complete a wind farm installation campaign. Proper scheduling

can be achieved by using intelligent simulation software to schedule the most weather sensitive operation for the optimum time when the weather conditions are favourable.

5.4.2. Wind speed limit sensitivity study

The wind speed limit (WSL) for each installation operation in the base case was then varied in steps of 5% from 85% of the base case WSL to 115% of the base WSL as shown in Table 5.4. Note that the wind speed limit sensitivity study was carried out with SM12 scenario (this was selected because as will be seen in section 5.5, SM12 scenario was the SM scenario for which the extended wind profile performed the worst).

Table 5.4: wind speed limit sensitivity study.

Scenario	Percentage of WSL of base case (%)	Installation Duration with no weather data (Days)	Installation Duration with measured data (Days)	AWoW (Hours)	Percentage Increase in installation duration due to AWoW (%)
WL85	85	286.39	733.99	10741	156.29%
WL90	90	286.39	674.4	9310	135.48%
WL95	95	286.39	605.6	7660	111.46%
WL100	100	286.39	587.16	7219	105.02%
WL105	105	286.39	555.94	6469	94.12%
WL110	110	286.39	523.25	5685	82.71%
WL115	115	286.39	506.12	5274	76.72%

It can be observed from Table 5.4 that when the wind speed limit of the installation operation was varied from 85% to 115% (WL85 to LC115 scenarios), the increase in the total installation duration due to AWoW varied from about 76% to 156% (WL85 to WL115 scenarios). Our result implies that increasing the wind speed limits allowed for installation operations will reduce the AWoW, thereby reducing the total installation duration required. A 10% increase in the wind speed limit (i.e WL100 scenario compared to LC110) lead to a decrease in AWoW from 7219 hours to 5685 hours, a decrease of about 64 days (21%) in the AWoW and hence, a reduction of about 11% in the total installation duration. A 10% decrease in the wind speed limit (i.e WL100 scenario compared to WL90) lead to an increase in AWoW from 7219 hours to 9310 hours, an increase of about 87 days (29%) in the AWoW and hence, an increase of about 15% in the total installation duration. This shows that technologies that can help increase the allowable wind speed limit that installation operation can be carried out will be beneficial to the wind industries. Also, the benefits can also be weighed against the cost of such technologies using intelligent simulation tools to

compare various alternative. For instance, whether it will be beneficial to carry out the installation operations with a more expensive vessel with higher wind limit allowance (i.e. if the time gained from reduced AWoW by using such vessel does or does not outway the cost).

5.4.3 Operation duration sensitivity study

The operation duration (OD) of each installation operation with a wind speed limit in the base case was varied in steps of 25% from 50% of the base case OD to 200% of the base OD as shown in Table 5.5. Also, note that the wind speed limit sensitivity study was carried out with SM12 scenario (this was selected because as will be seen in section 5.5, SM12 scenario was the SM scenario for which the extended wind profile performed the worst).

Table 5.5: Operation duration sensitivity study.

Scenario	Percentage of OD of base case (%)	Installation Duration with no weather data (Days)	Installation Duration with measured data (Days)	AWoW (Hours)	Percentage Increase in installation duration due to AWoW (%)
OD50	50	211.39	414.85	4884	96.25%
OD75	75	248.88	501.32	6059	101.43%
OD100	100	286.39	587.16	7219	105.02%
OD125	125	323.88	684.21	8649	111.25%
OD150	150	361.39	777.99	9999	115.28%
OD175	175	396.21	901.62	12129	127.56%
OD200	200	436.39	1043.06	14560	139.02%

It can be observed from Table 5.5 that when the installation duration for each operation was varied from 50% to 200% (OD50 to OD200), the increase in total installation time due to AWoW varied between about 96% to 139% a range of about 43%. This shows how sensitive the AWoW is to the duration of each installation operation used for the simulation. For a 50% reduction in operation duration (scenario OD100 compared to OD50), the AWoW reduced from 7219 hours to 4884 hours which is about a 32% reduction. For a 50% increase in operation duration (scenario OD100 compared to OD150), the AWoW increased from 7219 hours to 9999 hours an increase of about 39%. A 100% increase in operation duration (scenario OD100 compared to OD200) lead to an increase in AWoW from 7219 hours to 14560 hours, which is an increase of about 102%. Our result shows that a reduction in

operation duration required for installation operations can help reduce the increase in total installation time due to AWoW during an installation campaign. There is also room for optimization in the installation of a wind farm buy evaluating the cost of a costlier faster alternative to the benefits. This can also be achieved using intelligent simulation tools.

5.5. Accumulated waiting on weather estimation

To evaluate the performance of the wind profile models and to validate the suggested approach in this study in the estimation of the AWoW, the same set of simulations carried out with the measured filtered data in section 5.4 were carried out with the extrapolated data from the wind profile model and using the suggested approach in this study. The results of the estimate of the AWoW of these simulations were compared to the actual AWoW obtained from the simulations carried out with the measured filtered data in section 5.4. The results for the comparison of the installation start month scenarios are presented in Figure 5.6, the comparison of the wind speed limits scenarios are presented in Figure 5.7 and that of the operation duration scenarios are presented in Figure 5.8.

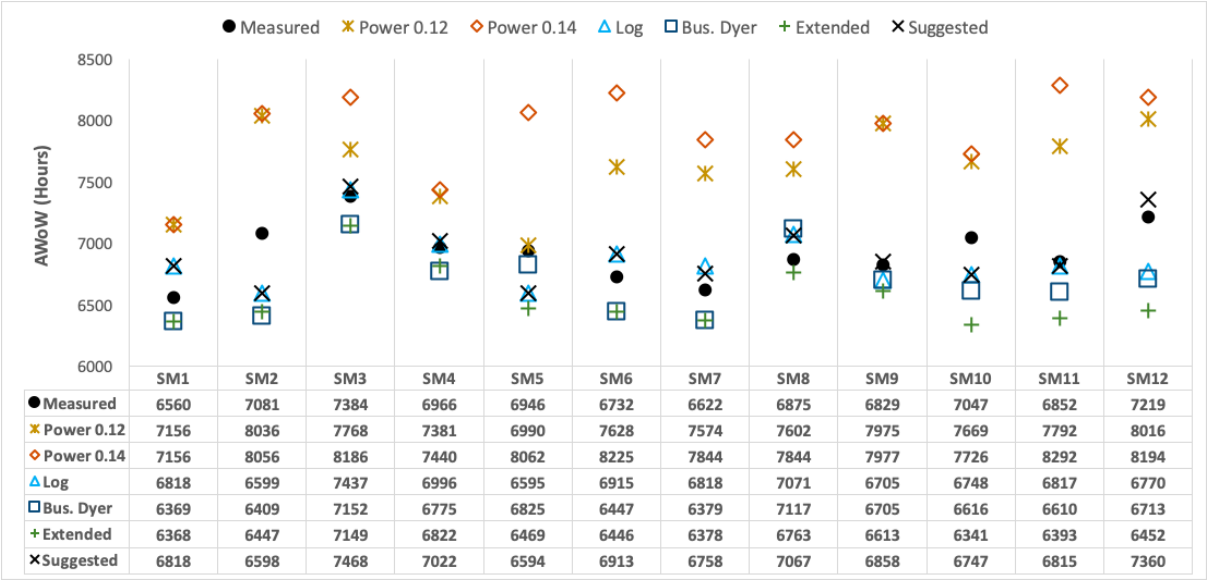

	SM1	SM2	SM3	SM4	SM5	SM6	SM7	SM8	SM9	SM10	SM11	SM12
Measured	6560	7081	7384	6966	6946	6732	6622	6875	6829	7047	6852	7219
Power 0.12	7156	8036	7768	7381	6990	7628	7574	7602	7975	7669	7792	8016
Power 0.14	7156	8056	8186	7440	8062	8225	7844	7844	7977	7726	8292	8194
Log	6818	6599	7437	6996	6595	6915	6818	7071	6705	6748	6817	6770
Bus. Dyer	6369	6409	7152	6775	6825	6447	6379	7117	6705	6616	6610	6713
Extended	6368	6447	7149	6822	6469	6446	6378	6763	6613	6341	6393	6452
Suggested	6818	6598	7468	7022	6594	6913	6758	7067	6858	6747	6815	7360

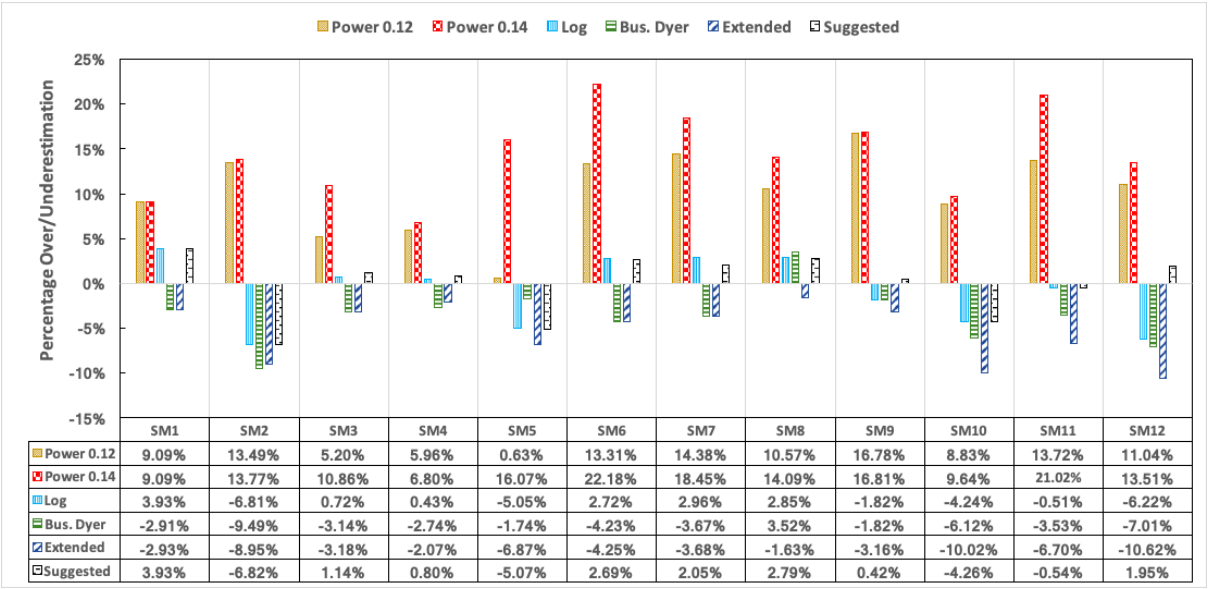

	SM1	SM2	SM3	SM4	SM5	SM6	SM7	SM8	SM9	SM10	SM11	SM12
Power 0.12	9.09%	13.49%	5.20%	5.96%	0.63%	13.31%	14.38%	10.57%	16.78%	8.83%	13.72%	11.04%
Power 0.14	9.09%	13.77%	10.86%	6.80%	16.07%	22.18%	18.45%	14.09%	16.81%	9.64%	21.02%	13.51%
Log	3.93%	-6.81%	0.72%	0.43%	-5.05%	2.72%	2.96%	2.85%	-1.82%	-4.24%	-0.51%	-6.22%
Bus. Dyer	-2.91%	-9.49%	-3.14%	-2.74%	-1.74%	-4.23%	-3.67%	3.52%	-1.82%	-6.12%	-3.53%	-7.01%
Extended	-2.93%	-8.95%	-3.18%	-2.07%	-6.87%	-4.25%	-3.68%	-1.63%	-3.16%	-10.02%	-6.70%	-10.62%
Suggested	3.93%	-6.82%	1.14%	0.80%	-5.07%	2.69%	2.05%	2.79%	0.42%	-4.26%	-0.54%	1.95%

Figure 5.6: Estimate of the AWoW compared to the actual AWoW obtained from the measured filtered data for installation start month scenarios.

From Figure 5.6 it can be observed that for all start month scenarios, the extrapolated data obtained from the power law wind profile (both exponents] always overestimated the AWoW. Compared to the AWoW obtained when the measured filtered data was used, the overestimation by extrapolated data obtained from the power law with an exponent of 0.14 was the highest for all SM scenarios, the overestimations ranged between about 7% (SM4 scenario) to 22% (SM6 scenario) and the overestimation by the extrapolated data obtained from the power law with an exponent of 0.12 range between about 1% (SM5 scenario) to 17% (SM9 scenario).

The extrapolated data obtained from the log wind profile overestimated the AWoW for some of the SM scenarios and underestimated it for others. Compared to the AWoW obtained when the filtered measured data was used, the under/overestimations ranged between about - 7% (SM2 scenario) and 4% (SM1 scenario).

The extrapolated data from the extended wind profile and the Businger Dyer wind profile underestimated the AWoW, except for SM8 scenario where the extrapolated data from the Businger Dyer wind profile overestimated the AWoW. For the majority of the SM scenario, the underestimation of the AWoW by the extrapolated data from the extended wind profile was higher than the underestimation of the AWoW when the extrapolated data from the Businger Dyer wind profile was used. This occurs because as analysed in section 5.2, the overestimation of the number of available weather windows for the various installation operations by the extrapolated data from the extended wind profile was higher than that of the Businger Dyer wind profile. Compared to the AWoW obtained when the filtered measured data was used, the underestimation of the AWoW by the extrapolated data obtained from the extended wind profile model ranged between approximately about 2% (SM8 scenario) to 11% (SM12 scenario), while the over/underestimation of the AWoW when the extrapolated data from the Businger Dyer wind profile was used ranged between about -9% (SM2 scenario) to 4% (SM8 scenario).

When the suggested approach in this study was used with a compensation factor of 0.25 m/s (see section 5.3) the AWoW was overestimated for the majority of the start month scenarios. Compared to the AWoW obtained when the filtered measured data was used, the overestimation ranged between approximately about 0% (SM9 scenario) to 4% (SM1 scenario).

For four of the start month scenarios (SM2, SM5, SM10 and SM11 scenarios) the AWoW was still underestimated, but underestimation was lower than when the extrapolated data from the extended wind profile was used. Compared to the AWoW obtained when the filtered measured data was used, the underestimations ranged between about 1% (SM11 scenario) to 7% (SM2 scenario). Increasing the compensation factor can eliminate these underestimations. In this study, an increase in the compensation factor from 0.25 m/s to 0.50 m/s eliminated the underestimations for these scenarios.

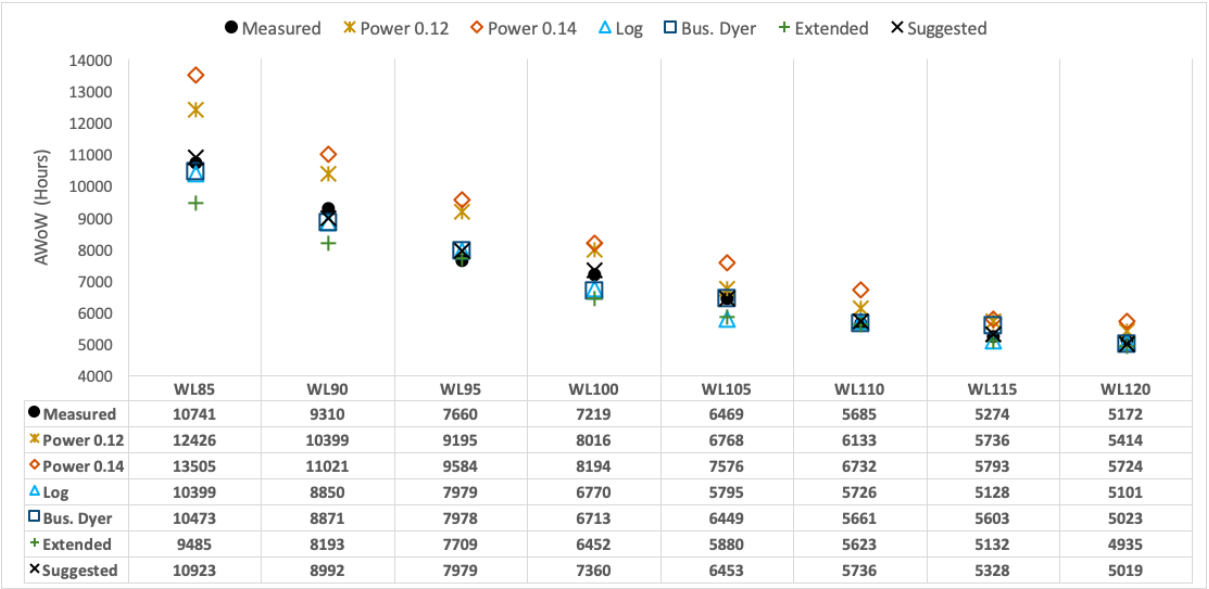

	WL85	WL90	WL95	WL100	WL105	WL110	WL115	WL120
Measured	10741	9310	7660	7219	6469	5685	5274	5172
Power 0.12	12426	10399	9195	8016	6768	6133	5736	5414
Power 0.14	13505	11021	9584	8194	7576	6732	5793	5724
Log	10399	8850	7979	6770	5795	5726	5128	5101
Bus. Dyer	10473	8871	7978	6713	6449	5661	5603	5023
Extended	9485	8193	7709	6452	5880	5623	5132	4935
Suggested	10923	8992	7979	7360	6453	5736	5328	5019

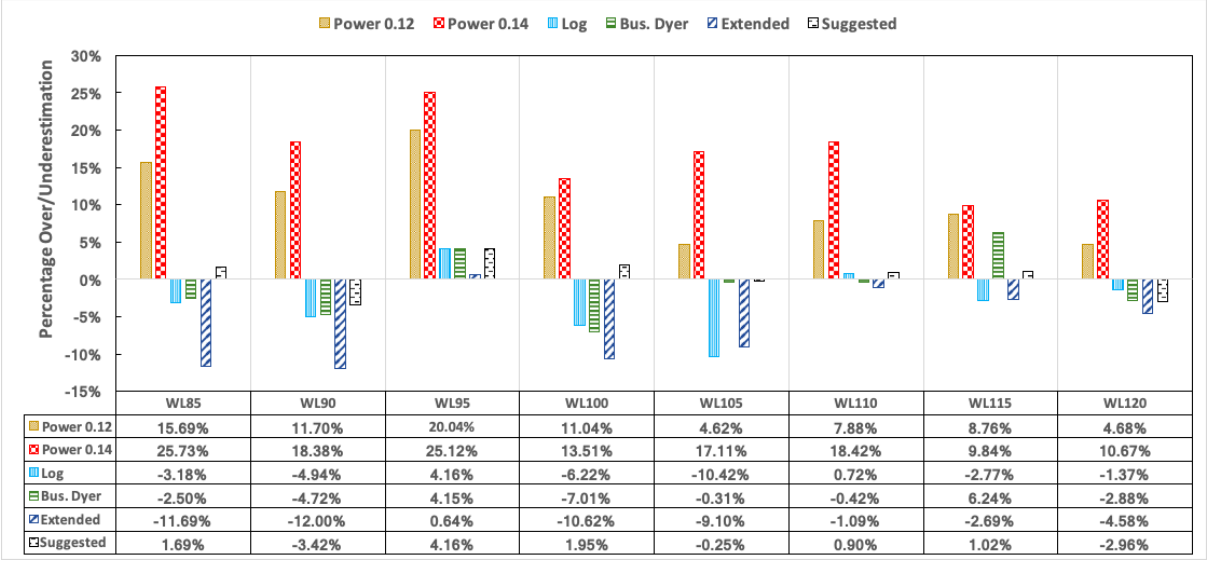

	WL85	WL90	WL95	WL100	WL105	WL110	WL115	WL120
Power 0.12	15.69%	11.70%	20.04%	11.04%	4.62%	7.88%	8.76%	4.68%
Power 0.14	25.73%	18.38%	25.12%	13.51%	17.11%	18.42%	9.84%	10.67%
Log	-3.18%	-4.94%	4.16%	-6.22%	-10.42%	0.72%	-2.77%	-1.37%
Bus. Dyer	-2.50%	-4.72%	4.15%	-7.01%	-0.31%	-0.42%	6.24%	-2.88%
Extended	-11.69%	-12.00%	0.64%	-10.62%	-9.10%	-1.09%	-2.69%	-4.58%
Suggested	1.69%	-3.42%	4.16%	1.95%	-0.25%	0.90%	1.02%	-2.96%

Figure 5.7: Estimate of the AWoW compared to the actual AWoW obtained from the measured filtered data for wind speed limit scenario scenarios.

From Figure 5.7 it can be observed that for all wind speed limit (WSL) scenarios, the extrapolated data obtained from the power law wind profile (both exponents] always overestimated the AWoW. Compared to the AWoW obtained when the measured filtered data was used, the overestimation by the power law with an exponent of 0.14 was the highest for all WSL scenarios, the overestimations ranged between about 10% (WL115 scenario) to 26% (WL85 scenario) and the overestimation by the power law with an exponent of 0.12 range between about 5% (WL105 scenario) to 20% (WL95 scenario).

The extrapolated data obtained from the log wind profile overestimated the AWoW for some of the WSL scenarios and underestimated it for others. Compared to the AWoW obtained when the filtered measured data was used, the under/overestimations ranged between about - 10% (WL105 scenario) and 4% (WL95 scenario).

The extrapolated data obtained from the Businger Dyer wind profile also overestimated the AWoW for some of the WSL scenarios and underestimated it for others. Compared to the AWoW obtained when the filtered measured data was used, the under/overestimations ranged between about - 7% (WL100 scenario) to 6% (WL115 scenario). The extrapolated data from the extended wind profile underestimated the AWoW, except for WL95 scenario where the AWoW was overestimated by about 1%. Compared to the AWoW obtained when the filtered measured data was used, the underestimation of the AWoW by the extrapolated data obtained from the extended wind profile model ranged between about 1% (WL110 scenario) to 12% (WL85 scenario).

When the suggested approach in this study was used with a compensation factor of 0.25 m/s (see section 5.3) the AWoW was overestimated for the majority of the operation duration scenarios. Compared to the AWoW obtained when the filtered measured data was used, the overestimation ranged between about 1% (WL110 scenario) to 4% (WL85 scenario).

For WL105 scenario, Compared to the AWoW obtained when the filtered measured data was the AWoW was slightly underestimated (less than 1%). For WL90 and WL120 scenarios, the AWoW was underestimated by about 3%. Increasing the compensation factor

can eliminate these underestimations. In this study, an increase in the compensation factor from 0.25 m/s to 0.50 m/s eliminated the underestimations for these scenarios.

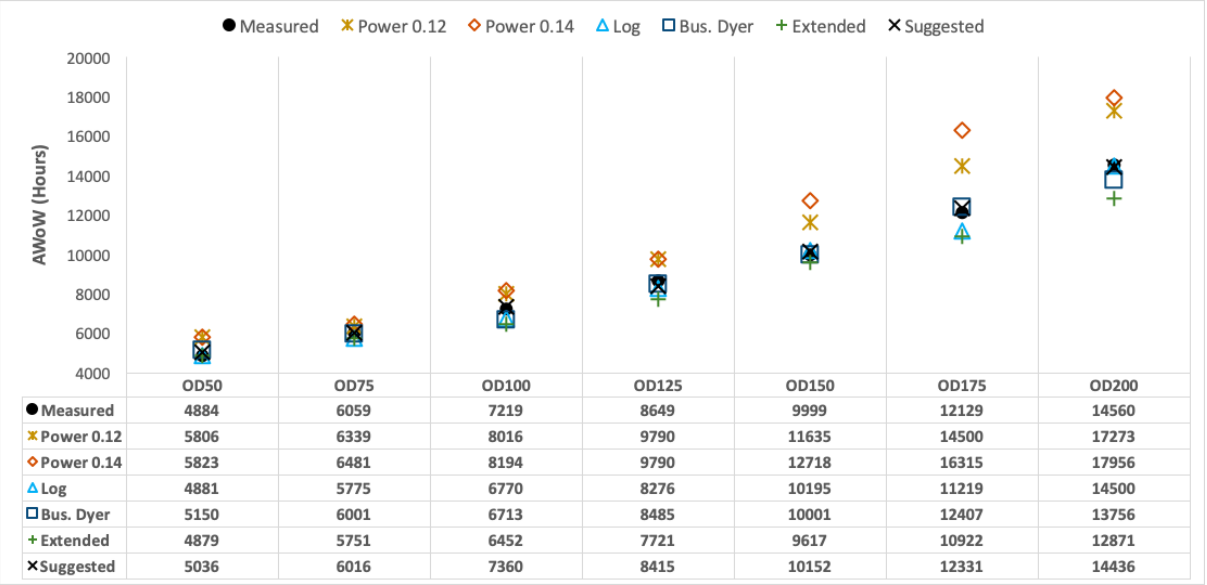

	OD50	OD75	OD100	OD125	OD150	OD175	OD200
Measured	4884	6059	7219	8649	9999	12129	14560
Power 0.12	5806	6339	8016	9790	11635	14500	17273
Power 0.14	5823	6481	8194	9790	12718	16315	17956
Log	4881	5775	6770	8276	10195	11219	14500
Bus. Dyer	5150	6001	6713	8485	10001	12407	13756
Extended	4879	5751	6452	7721	9617	10922	12871
Suggested	5036	6016	7360	8415	10152	12331	14436

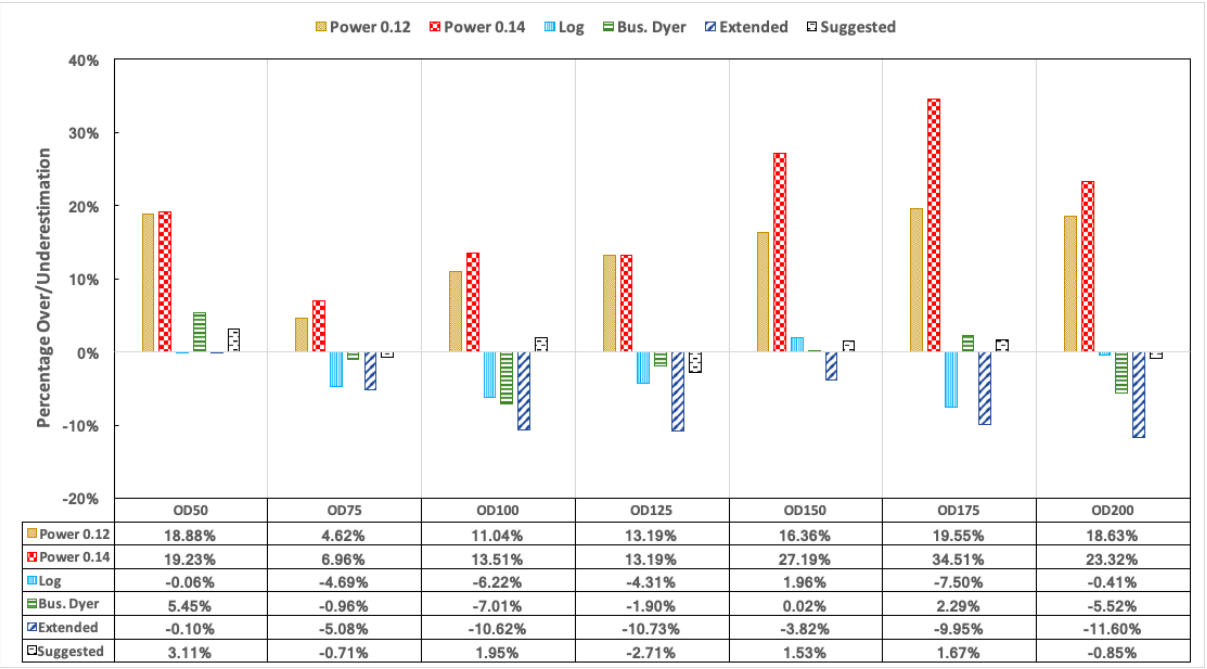

	OD50	OD75	OD100	OD125	OD150	OD175	OD200
Power 0.12	18.88%	4.62%	11.04%	13.19%	16.36%	19.55%	18.63%
Power 0.14	19.23%	6.96%	13.51%	13.19%	27.19%	34.51%	23.32%
Log	-0.06%	-4.69%	-6.22%	-4.31%	1.96%	-7.50%	-0.41%
Bus. Dyer	5.45%	-0.96%	-7.01%	-1.90%	0.02%	2.29%	-5.52%
Extended	-0.10%	-5.08%	-10.62%	-10.73%	-3.82%	-9.95%	-11.60%
Suggested	3.11%	-0.71%	1.95%	-2.71%	1.53%	1.67%	-0.85%

Figure 5.8: Estimate of the AWoW compared to the actual AWoW obtained from the measured filtered data for operation duration scenarios.

From Figure 5.8 it can be observed that for all operation duration (OD) scenarios, the extrapolated data obtained from the power law wind profile (both exponent) always overestimated the AWoW. Compared to the AWoW obtained when the measured filtered data was used, the overestimation by the power law with an exponent of 0.14 was the highest for all OD scenarios, the overestimations ranged between about 7% (OD75 scenario) to 35% (OD175 scenario) and the overestimation by the power law with an exponent of 0.12 range between about 5% (OD75 scenario) to 20% (OD175 scenario) .

The extrapolated data obtained from the log wind profile overestimated the AWoW for some of the OD scenarios and underestimated it for others. Compared to the AWoW obtained when the filtered measured data was used, the under/overestimations ranged between about - 8% (OD175 scenario) and 2% (OD150 scenario).

The extrapolated data obtained from the Businger Dyer wind profile also overestimated the AWoW for some of the OD scenarios and underestimated it for others. Compared to the AWoW obtained when the filtered measured data was used, the under/overestimations ranged between about - 7% (OD100 scenario) to 5% (OD50 scenario). The extrapolated data from the extended wind profile underestimated the AWoW, Compared to the AWoW obtained when the filtered measured data was used, the underestimation of the AWoW by the extrapolated data obtained from the extended wind profile ranged between about 0% (OD50 scenario) to 12% (OD200 scenario).

When the suggested approach in this study was used with a compensation factor of 0.25 m/s (see section 5.2) the AWoW was overestimated for the majority of the operation duration scenarios. Compared to the AWoW obtained when the filtered measured data was used, the overestimation ranged between about 2% (OD50 scenario) to 3% (OD150 scenario).

For two of the operation duration scenarios (OD75 and OD200 scenarios), Compared to the AWoW obtained when the filtered measured data was used, the AWoW was slightly underestimated (less than 1%). For OD125 scenario the AWoW was underestimated by about 3%. Increasing the compensation factor can eliminate these underestimations. In this study, an increase in the compensation factor from 0.25 m/s to 0.50 m/s eliminated the underestimations for these scenarios.

In general, when extrapolated data obtained from the power law wind profile with an exponent of 0.12 and the power law wind profile with an exponent of 0.14 were used, overestimations of the AWoW of up to about 20% and 35% respectively were obtained. When extrapolated data from the Log wind profile was used, overestimations of the AWoW of up to about 9% was obtained and also, underestimation of the AWoW of up to about 6% was obtained. For the extrapolated data obtained from the Businger Dyer wind profile, overestimations of the AWoW of up to about 4% was obtained and also, underestimation of the AWoW of up to about 10% was obtained. When the extrapolated data from the extended wind profile was used, overestimations of the AWoW of up to about 1% was obtained and also, underestimation of the AWoW of up to about 12% was obtained.

When the suggested approach in this study was used with a compensation factor of 0.25 m/s, overestimations of the AWoW of up to about 4% was obtained and also, underestimation of the AWoW of up to about 6% were still obtained. Increasing the compensation factor can eliminate these underestimations. In this study, an increase in the compensation factor from 0.25 m/s to 0.50 m/s eliminated the underestimations.

5.6 Possibile power production estimation.

Assuming zero failure of wind turbine components, the Possible power production for the base case using the measured filtered data as the weather was obtained from the intelligent simulation software, MAINTSYS of Shoreline. This was done in order to see if the

adoption of the extended wind profile will also be beneficial in the estimation of the possible power production. The result was compared to the result obtained when using the extrapolated data from the wind profile model as weather input. The result of the comparison is presented in Figure 5.9.

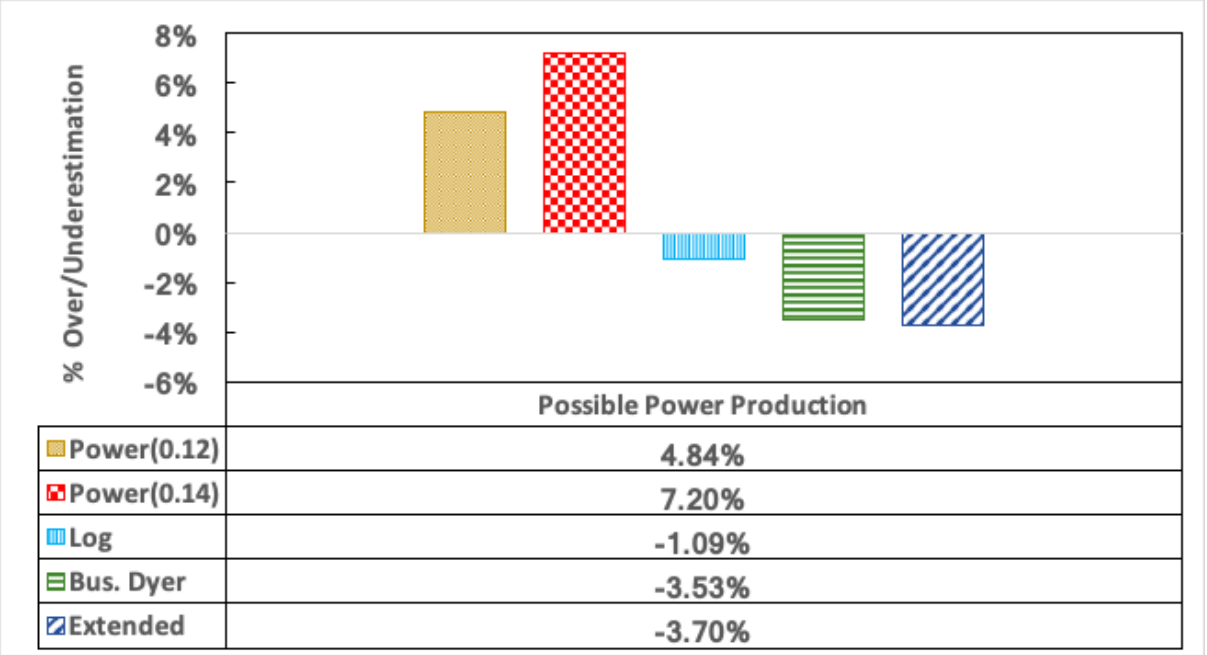

Figure 5.9: Percentage Over/Underestimation of the possible power production

The extrapolated data obtained using the power law wind profile with an exponent of 0.12 and an exponent of 0.14 overestimated the possible power production by 4.84% and 7.20% respectively. This is understandable because from the analysis carried in section 4.2 the power overestimates the wind speed at the hub height during unstable conditions which prevail at the FINO3 site. The estimate of the possible power production from the extrapolated data obtained from the Log wind profile had the lowest deviation, it underestimated the possible power production by 1.09%. But it has been shown in section 4.2 that the Log wind profile is not a good representation of the atmospheric conditions at the FINO3 (far offshore site).

The extrapolated data from the extended and the Businger Dyer wind profile also underestimated the possible power production by 3.70% and 3.53% respectively. The underestimation of extrapolated data from the extended wind profile is higher than that of the Businger dyer wind profile because as shown in section 4.2, the Businger Dyer largely overestimates the wind speed at the hub height during stable conditions which will lead to a higher estimate in possible power production during stable conditions than the extended wind profile and hence, a lower underestimation of the overall possible power production as their performance during unstable and neutral conditions are similar. In general, the extended wind profile gives a good estimate of the possible power production.

6 Discussion

In this study we have suggested a new approach to wind profile modelling in wind farm installation campaign based on the use of the extended wind profile (Gryning's boundary layer shear profile). The approach was suggested and validated based on the analysis carried out with data from a far offshore site (FINO3). However, due to limitations in the available observation data the wind speed were extrapolated from 30 m elevation. As such, it would be useful to perform similar research with offshore observation extrapolating from a lower elevations (i.e. 10 m).

Due to the scope of this study, the suggested approach has only been tested for a site (FINO3) that is located far from shore (about 80 km) where it has been shown that very unstable conditions prevail. However, closer to shore it has also been shown that the atmospheric conditions become less unstable. It will be interesting to perform similar analysis with data from a site closer to shore to evaluate how well the suggested approach in this study will perform, especially compared to the widely used approach to wind profile modelling in wind farm installation campaign which is based on the power law wind profile.

Compared to the widely used approach based on the power law wind profile, we expect the suggested approach to perform even better for site close to shore. The atmospheric conditions becomes less unstable as we approach shore, and It has been shown that the power law wind profile (even with an exponent of 0.14) largely underestimates the wind speed at the required heights for wind farm installation campaign simulation during stable conditions. While, the extended wind profile which the suggested approach is based on performs reasonably well for stable conditions.

7 Conclusion

In this new era where intelligent simulation software tools which make use of wind profile models are being used to analyse and understand various stages of wind asset lifecycle, the extent to which the choice of adopted wind profile model used will impact simulation results is therefore questioned. Especially offshore, where the atmospheric boundary layer is typically much lower compared to onshore sites, the logarithmic shear profile are often not valid up to the hub height.

In this study, nine years of data from FINO3 offshore measurement platform was used to assess offshore atmospheric conditions. Different wind speed extrapolation models (A power law wind profile with an exponent of 0.12 and 0.14, the logarithmic wind profile with and without stability correction and the extended wind profile proposed by Gryning) were then evaluated and their impact on wind farm installation campaign simulation and possible power production estimation were assessed. Based on the findings, a new approach to wind profile modeling in wind farm installation campaign simulations using the extended wind profile is suggested.

The observations data from FINO3 used in this study shows that wind speed shear increases with increasing stability (A. A. M. Holtslag 1984; Van Ulden and Holtslag 1985). Very unstable (34%) and unstable(23%) conditions prevail at the FINO3 site which is similar to studies of the Ijmuiden (located similar distance from shore as FINO3 but located in the

Danish part of the North Sea) data by M. C. Holtslag, Bierbooms, and van Bussel (2017). In addition, it shows that there are more unstable conditions for the Dutch part of the North sea (FINO3) than the Danish part (ijmuiden) and less stable conditions for the Dutch part than the Danish part. This is similar to the observations made by Sathe, Gryning, and Peña (2011) for the Dutch part (more unstable conditions at OWEZ than at Horns Rev) and for the Danish part (less stable conditions at OWEZ as compared with that at Horns Rev). The data also shows that these very unstable conditions prevail at the site for lower wind speeds (i.e., between 2 m/s to 12 m/s), but their occurrence decreases with increasing wind speed (i.e., from 8 m/s to 24 m/s). Neutral conditions prevail above 22 m/s and stable conditions occurs between 2 m/s to 28 m/s.

The results from the evaluation of the wind profile model shows that for unstable conditions the power law wind profiles (both exponents) overestimates the wind speed, and the magnitude of the overestimation increases with increasing altitude. In fact, during very unstable conditions the average overestimation of the wind speed at 108 m elevation was a RMSE of approximately 1.6 m/s and 1.3 m/s for the power law wind profile with an exponent of 0.12 and 0.14 respectively. For stable conditions, the power law wind profiles (both exponents) significantly underestimate the wind speeds at hub height. The magnitude of the underestimation also increases with increasing altitude. During very stable conditions the average overestimation of the wind speed at 108 m elevation was a RMSE of approximately 2.0 m/s and 1.8 m/s for the power law wind profile with an exponent of 0.12 and 0.14 respectively. Hence, the wind shear during very stable condition is underestimated when using the power law wind profile with an exponent of 0.14.

The logarithmic wind profile without stability correction underestimates the wind speed even from near neutral unstable conditions. During very stable conditions the average overestimation of the wind speed at 108 m elevation indicated by the RMSE was approximately 2.5 m/s. While the logarithmic wind profile with the Businger Dyer stability correction function considered in this study seems to corresponds well with observations up to about 60 m elevation during unstable conditions, but above this altitude it underestimated the wind speed. During near neutral unstable condition, the average underestimation of the wind speed at 108 m elevation indicated by the RMSE was approximately 1.2 m/s. These logarithmic wind profile with the Businger Dyer stability correction function also largely overestimated the wind speed for very stable conditions, the average overestimation of the wind speed at 108 m elevation which was indicated by the RMSE was approximately 2.6 m/s.

The extended wind profile had a similar performance to the logarithmic wind profile with the Businger Dyer correction function for unstable conditions but the magnitude of the underestimation was lower. During near neutral unstable condition, the RMSE at 108m was approximately 1.1 m/s. However, for stable conditions the extended wind profile seems to fit well with the measured observations and had the lowest RMSE for all observation heights. Further analysis carried out based on friction velocity regime on the extended profile due to the results obtained for unstable conditions show that; the extended wind profile performs well for high wind speeds (i.e. above 14 m/s) but for low wind speeds (i.e. below 14 m/s) the wind shear is underestimated. In addition, it was found that the boundary layer height increases with increasing friction velocity and decreases with increasing stability.

Depending on the boundary layer height the performance of the different wind profiles considered in this study varied considerably. The extended wind profile performed the best for largest range of boundary layer heights. On a continuous scale of stability, the extended wind profile also performed the best.

In general, it is found that for all stability conditions considered in this assessment, the extended wind profile performs either as well as the other wind profiles considered in this study for unstable conditions. Except for near neutral unstable conditions where the power law wind profile with an exponent of 0.12 performs better. During stable conditions it performs significantly better. As such,incorporating the extended wind profile in wind turbine installation campaign simulations should result in a better representation of the atmospheric conditions for the far offshore site considered in this study.

To assess how the different wind profile model affect the installation simulation campaign, analyses were carried out based on the various wind weather windows required for offshore installation campaign defined in the base case (see section 5.1) in this study (section 5.1). It was found that the data from the power law wind profile (both) underestimated the number of available wind weather wind for the various installation operations. Compared to that of the measured data underestimation of up approximately 17% and 23% were obtained for the power law wind profile with an exponent of 0.12 and 0.14 respectively. Although the data from power law wind profile (both exponents) underestimates the number of available wind weather windows for the various installation operations, it not an indication that it is a good representation of the atmospheric conditions or that it provides a better safety margin. Because false wind weather window were predicted due to the large underestimations of the wind speed at the hub heights during stable conditions.

The data from the log wind profile both underestimated and overestimated the number of available wind weather windows for the various installation operations. The accuracy of the estimation of the number of wind weather windows when using the log wind profile model ranged between -2% and 5%. Though it seems to have the highest accuracy compared to the data from the other wind profile models, a lot of false weather windows were predicted when using the log wind profile model.

When using the data from extended wind profile and the logarithmic wind profile with the Businger Dyer stability correction function, the number of available windows for installation operations with a wind speed limit less than 14 m/s was overestimated. An overestimation of up to 8% and 7% was observed for the extended wind profile and logarithmic wind profile with the Businger Dyer stability correction function respectively. For the other required wind weather windows (i.e .installation operation with wind speed limit equals or greater than 14 m/s), the number of available wind weather windows using the two

profile models appeared to closely match that of the measured data. The accuracy in estimating the number of available wind weather windows range from - 0.5% to 1.22% and - 0.18 to 1.69% for the extended and the logarithmic wind profile with the Businger Dyer stability correction function respectively. Based on these findings, a new approach to wind profile modeling in wind farm installation campaign simulations using the extended wind profile is suggested (see section 5.3). The new approach with a compensation factor of 0.25 m/s had an accuracy within ±1% when estimating the number of available weather windows.

A sensitivity study of the accumulated waiting on weather (AWoW) to the installation campaign start month, the wind speed limit of the installation operations and the duration of the installation operation were carried out using the measured observed data. The results showed that there is room for optimization based on these parameters during offshore

installation projects. The variation in installation campaign start month from January (scenario SM1) to December (scenario SM12) with one month interval resulted in a variation in AWoW of up to 13% which also lead to a variation in the total installation time of about 6%. Hence, proper scheduling of the start of an installation campaign can help reduce the total installation time required to complete a wind farm installation campaign. Proper scheduling which can be achieved by using intelligent simulation software such as SIMSTALL of Shoreline to schedule the most weather sensitive operations for the optimum time when the weather conditions are most favorable.

A 10% increase in the wind speed limit of each installation operation lead to a decrease in AWoW of about 21% and a reduction of about 11% in the total installation duration. While a 10% decrease lead to an increase in AWoW of about 29% and an increase of about 15% in the total installation duration. This shows that technologies that can help increase the allowable wind speed limit that installation operation can be carried out will have a significant cost benefit to the installation campaign of an offshore wind farm. The benefits can also be weighed against the cost of such technologies using intelligent simulation tools to compare various alternative installation strategies. For instance, whether it will be beneficial to carry out the installation operations with a more expensive vessel with higher wind limit allowance (i.e. if the time gained from reduced AWoW by using such vessel does or does not outway the cost).

When the operation duration of each operation was reduced by 50% the AWoW is reduced by about 32% whereas for a 50% increase in operation duration the AWoW increased by about 39%. The results show that a reduction in operation duration required for installation operations can help reduce the increase in total installation time due to AWoW during an installation campaign. Hence, there is also room for optimization in the installation of a wind farm by evaluating the impact operation duration will have on waiting on weather using intelligent simulation tools such as SIMSTALL.

Finally, to evaluate the performance of the wind profile models and to validate the suggested approach given in this study (see section 5.3), a sensitivity study of the accumulated waiting on weather (AWoW) to the installation campaign start month (start month scenarios), the wind speed limit of the installation operations (wind speed limit scenarios) and the duration of the installation operation (installation duration scenarios) were carried out using the data from the wind profile models. The difference between observed and estimated AWoW was then studied.

The start month scenarios showed an overestimation of the AWoW of up to 17% and 22% by a power law with an exponent of 0.12 and 0.14 respectively. While using the suggested approach (based on the extended wind profile) with a compensation factor of 0.25 m/s (see section 5.3) overestimated the AWoW for the majority of the start month scenarios, the overestimations were less than 4.5%. For four of the start month scenarios (SM2, SM5, SM10 and SM11 scenarios) the AWoW were underestimated, the underestimations were less than 7%. However, an increase in the compensation factor from 0.25 m/s to 0.50 m/s eliminated the underestimations for these scenarios.

The wind speed limit scenarios showed an overestimation of the AWoW of up to 20% and 26% by a power law with an exponent of 0.12 and 0.14 respectively. While using the suggested approach (based on the extended wind profile) with a compensation factor of 0.25 m/s (see section 5.3) overestimated the AWoW for the majority of the wind speed limit

scenarios, the overestimations were less than 4%. For some of the wind speed limit scenarios the AWoW were underestimated, the underestimations were less than 3.5%. However, an increase in the compensation factor from 0.25 m/s to 0.50 m/s eliminated the underestimations for these scenarios.

The operation duration scenarios showed an overestimation of the AWoW of up to 20% and 35% by a power law with an exponent of 0.12 and 0.14 respectively. While using the suggested approach (based on the extended wind profile) with a compensation factor of 0.25 m/s (see section 5.3) overestimated the AWoW for the majority of the wind speed limit scenarios, the overestimations were less than 3.5%. For some of the operation duration scenarios the AWoW were underestimated, the underestimations were however less than 3%. An increase in the compensation factor from 0.25 m/s to 0.50 m/s eliminated the underestimations for these scenarios.

The estimation of the possible power production by the wind profile models was also assess, the power law wind profile with an exponent of 0.12 and an exponent of 0.14 overestimated the possible power production by 4.84% and 7.20% respectively. While, extrapolated data obtained using the extended wind profile underestimated the possible power production by 3.70%.

Atmospheric stability clearly affect the accumulated waiting on weather during offshore wind farm campaign simulation, and should be considered when simulations involving the installation phase of a wind farm project are involved. A better estimation of the possible power production is also achieved when atmospheric stability is accounted for.

References

Akylas, E., and M. Tombrou. 2005. “Interpolation between Businger–Dyer Formulae and Free Convection Forms: A Revised Approach.” *Boundary-Layer Meteorology* 115 (3): 381–98.

Argyle, P., and S. J. Watson. 2014. “Assessing the Dependence of Surface Layer Atmospheric Stability on Measurement Height at Offshore Locations.” *Journal of Wind Engineering and Industrial Aerodynamics* 131 (August): 88–99.

Asgarpour, M. 2016. “Assembly, Transportation, Installation and Commissioning of Offshore Wind Farms.” In *Offshore Wind Farms*, 527–41.

Badger, Merete, Alfredo Peña, Andrea N. Hahmann, Alexis A. Mouche, and Charlotte B. Hasager. 2016. “Extrapolating Satellite Winds to Turbine Operating Heights.” *Journal of Applied Meteorology and Climatology* 55 (4): 975–91.

Bak, Christian, Frederik Zahle, Robert Bitsche, Taeseong Kim, Anders Yde, Lars Christian Henriksen, Morten Hartvig Hansen, Jose Pedro Albergaria Amaral Blasques, Mac Gaunaa, and Anand Natarajan. 2013. “The DTU 10-MW Reference Wind Turbine.” In *Danish Wind Power Research 2013*. http://orbit.dtu.dk/files/55645274/The_DTU_10MW_Reference_Turbine_Christian_Bak.pdf.

Bak, Thomas, Angus Graham, Alla Sapronova, Zhen Chen, Torben Knudsen, John D. Sørensen, Mihai Florian, Peng Hou, and Masoud Asgarpour. 2015. “Norcowe Reference Wind Farm.” In *Annual Report Norcowe 2014*, 38–40.

Barlow, Euan, Diclehan Tezcaner Öztürk, Matthew Revie, Evangelos Boulougouris, Alexander H. Day, and Kerem Akartunalı. 2015. “Exploring the Impact of Innovative Developments to the Installation Process for an Offshore Wind Farm.” *Ocean Engineering* 109: 623–34.

Beinke, Thies, Abderrahim Ait Alla, and Michael Freitag. 2017. “Resource Sharing in the Logistics of the Offshore Wind Farm Installation Process Based on a Simulation Study.” *International Journal of E-Navigation and Maritime Economy* 7: 42–54.

Beljaars, A. C. M., and A. A. M. Holtslag. 1991. “Flux Parameterization over Land Surfaces for Atmospheric Models.” *Journal of Applied Meteorology* 30 (3): 327–41.

Besnard, F., and L. Bertling. 2010. “An Approach for Condition-Based Maintenance Optimization Applied to Wind Turbine Blades.” *IEEE Transactions on Sustainable Energy* 1 (2): 77–83.

Besnard, F., K. Fischer, and L. B. Tjernberg. 2013. “A Model for the Optimization of the Maintenance Support Organization for Offshore Wind Farms.” *IEEE Transactions on Sustainable Energy* 4 (2): 443–50.

Blackadar, A. K., and H. Tennekes. 1968. “Asymptotic Similarity in Neutral Barotropic Planetary Boundary Layers.” *Journal of the Atmospheric Sciences* 25 (6): 1015–20.

Bratton, Daniel C., and Carole A. Womeldorf. 2011. “The Wind Shear Exponent: Comparing Measured against Simulated Values and Analyzing the Phenomena That Affect the Wind Shear.” In *ASME 2011 5th International Conference on Energy Sustainability*, 2245–51. American Society of Mechanical Engineers.

Businger, J. A., J. C. Wyngaard, Y. Izumi, and E. F. Bradley. 1971. “Flux-Profile Relationships in the Atmospheric Surface Layer.” *Journal of the Atmospheric Sciences* 28 (2): 181–89.

Byun, Daewon W. 1991. “Determination of Similarity Functions of the Resistance Laws for the Planetary Boundary Layer Using Surface-Layer Similarity Functions.” *Boundary-Layer Meteorology* 57 (1): 17–48.

Charnock, H. 1955. “Wind Stress on a Water Surface.” *Quarterly Journal of the Royal Meteorological Society* 81 (350): 639–40.

Chenge, Yinguo, and Wilfried Brutsaert. 2005. “Flux-Profile Relationships for Wind Speed and Temperature in the Stable Atmospheric Boundary Layer.” *Boundary-Layer Meteorology* 114 (3): 519–38.
Consult, B. T. M. 2014. “World Market Update 2013 International Wind Energy Development Forecast 2014--2018.”
Dinwoodie, Iain, Ole-Erik V. Endrerud, Matthias Hofmann, Rebecca Martin, and Iver Bakken Sperstad. 2015. “Reference Cases for Verification of Operation and Maintenance Simulation Models for Offshore Wind Farms.” *Wind Engineering* 39 (1): 1–14.
DNV-OS-H101(2011) “Marine Operations, General” November.
DNV-OS-J101 (2011) “Design of Offshore Wind Turbine Structures” September.
DNV-RP-C205 (2010) “Environmental Conditions & Environmental Loads” October.
DNV-RP-J101 (2011) “Use of Remote Sensing for Wind Energy Assessments” April
Dyer, A. J. 1974. “A Review of Flux-Profile Relationships.” *Boundary-Layer Meteorology* 7 (3): 363–72.
Ederer, Nikolaus. 2015. “Evaluating Capital and Operating Cost Efficiency of Offshore Wind Farms: A DEA Approach.” *Renewable and Sustainable Energy Reviews* 42 (February): 1034–46.
Ekici, Deniz, Mike White, Michael Drunsic, and Others. 2016. “Offshore Wind Farm OWF Installation Best Practices Based on Field Experience.” In *Offshore Technology Conference*. Offshore Technology Conference. https://www.onepetro.org/conference-paper/OTC-26889-MS.
Eliassen, Lene, Jasna B. Jakobsen, Charlotte Obhrai, and Others. 2012. “The Effect of Atmospheric Stability on the Fatigue Life of Offshore Wind Turbines.” In *The Twenty-Second International Offshore and Polar Engineering Conference*. International Society of Offshore and Polar Engineers. https://www.onepetro.org/conference-paper/ISOPE-I-12-206.
Fairall, C. W., E. F. Bradley, and D. P. Rogers. 1996. “Bulk Parameterization of Air−sea Fluxes for Tropical Ocean−global Atmosphere Coupled−ocean Atmosphere Response Experiment.” *Journal of*. https://onlinelibrary.wiley.com/doi/pdf/10.1029/95JC03205.
“FINO3.” n.d. Accessed May 10, 2019. https://www.fino3.de/en/.
Grachev A A and Fairall C W 1997 Dependence of the monin-obukhov stability parameter on the bulk richardson number over the ocean Journal of applied meteorology 36 406-14.
Gryning, Sven-Erik, Ekaterina Batchvarova, Burghard Brümmer, Hans Jørgensen, and Søren Larsen. 2007. “On the Extension of the Wind Profile over Homogeneous Terrain beyond the Surface Boundary Layer.” *Boundary-Layer Meteorology* 124 (2): 251–68.
Haugen, D. A., J. C. Kaimal, and E. F. Bradley. 1971. “An Experimental Study of Reynolds Stress and Heat Flux in the Atmospheric Surface Layer.” *Quarterly Journal of the Royal Meteorological Society* 97 (412): 168–80.
Herman, S. A. 2002. *Offshore Wind Farms: Analysis of Transport and Installation Costs*. Energy Research Centre of the Netherlands.
Högström, U. L. F. 1988. “Non-Dimensional Wind and Temperature Profiles in the Atmospheric Surface Layer: A Re-Evaluation.” In *Topics in Micrometeorology. A Festschrift for Arch Dyer*, edited by Bruce B. Hicks, 55–78. Dordrecht: Springer Netherlands.
Holtslag, A. A. M. 1984. “Estimates of Diabatic Wind Speed Profiles from near-Surface Weather Observations.” *Boundary-Layer Meteorology* 29 (3): 225–50.
Holtslag, M. C., W. A. A. M. Bierbooms, and G. J. W. van Bussel. 2015. “Validation of Surface Layer Similarity Theory to Describe Far Offshore Marine Conditions in the Dutch North Sea in Scope of Wind Energy Research.” *Journal of Wind Engineering and Industrial Aerodynamics* 136 (January): 180–91.
———. 2017. “Extending the Diabatic Surface Layer Wind Shear Profile for Offshore Wind

Energy.” *Renewable Energy* 101 (February): 96–110.
Holtslag, M. C., W A A, and G. J. W. van Bussel. 2014. “Estimating Atmospheric Stability from Observations and Correcting Wind Shear Models Accordingly.” *Journal of Physics. Conference Series* 555 (1): 012052.
Irawan, Chandra Ade, Dylan Jones, and Djamila Ouelhadj. 2017. “Bi-Objective Optimisation Model for Installation Scheduling in Offshore Wind Farms.” *Computers & Operations Research* 78: 393–407.
Janajreh, Isam, Liu Su, and Fathi Alan. 2013. “Wind Energy Assessment: Masdar City Case Study.” *Renewable Energy* 52 (April): 8–15.
Kovács, András, Gábor Erdős, Zsolt János Viharos, and László Monostori. 2011. “A System for the Detailed Scheduling of Wind Farm Maintenance.” *CIRP Annals* 60 (1): 497–501.
Lange, Bernhard, Søren Larsen, Jørgen Højstrup, and Rebecca Barthelmie. 2004. “Importance of Thermal Effects and Sea Surface Roughness for Offshore Wind Resource Assessment.” *Journal of Wind Engineering and Industrial Aerodynamics* 92 (11): 959–88.
Ma, Xiaomei, Shuang Han, Jie Yan, and Yongqian Liu. 2015. “A Modified Method Based on Neutral Condition for Wind Profile Calculation under Different Atmospheric Stability.” *International Conference on Renewable Power Generation (RPG 2015)*. https://doi.org/10.1049/cp.2015.0411.
Monin, A. S., and A. M. Obukhov. 1954. “Basic Laws of Turbulent Mixing in the Atmosphere near the Ground.” *Trudy Geofizicheskogo Instituta, Akademiya Nauk SSSR* 24 (151): 163–87.
Motta, M., R. J. Barthelmie, and P. Vølund. 2005. “The Influence of Non-Logarithmic Wind Speed Profiles on Potential Power Output at Danish Offshore Sites.” *Wind Energy* 8 (2): 219–36.
MPI Offshore, MPI Resolution Operating Capabilities, 2016.[Online]. Available: “https://www.mpi-offshore.com/mpi-adventure/”
NEK IEC 61400-1 (2005) “Wind Turbines – Part 1: Design Requirements”.
NEK IEC 61400-3 (2009,) “Wind Turbines – Part 3: Design Requirements for Offshore Wind Turbines”.
Neumann, T., Stefan Emeis, and C. Illig. 2007. “Report on the Research Project OWID – Offshore Wind Design Parameter.” In *Wind Energy*, 81–85.
Obhrai, Charlotte, Siri Kalvig, Ove Tobias Gudmestad, and Others. 2012. “A Review of Current Guidelines and Research on Wind Modelling for the Design of Offshore Wind Turbines.” In *The Twenty-Second International Offshore and Polar Engineering Conference*. International Society of Offshore and Polar Engineers. https://www.onepetro.org/conference-paper/ISOPE-I-12-199.
Obukhov, A. M. 1971. “Turbulence in an Atmosphere with a Non-Uniform Temperature.” *Boundary-Layer Meteorology* 2 (1): 7–29.
Ortega-Izquierdo, Margarita, and Pablo del Río. 2016. “Benefits and Costs of Renewable Electricity in Europe.” *Renewable and Sustainable Energy Reviews* 61 (August): 372–83.
Panofsky, Hans A., and John A. Dutton. 1984. *Atmospheric Turbulence: Models and Methods for Engineering Applications*. Wiley-Interscience.
Paterson, J., F. D’Amico, P. R. Thies, R. E. Kurt, and G. Harrison. 2018. “Offshore Wind Installation Vessels – A Comparative Assessment for UK Offshore Rounds 1 and 2.” *Ocean Engineering* 148: 637–49.
Paulson, C. A. 1970. “The Mathematical Representation of Wind Speed and Temperature Profiles in the Unstable Atmospheric Surface Layer.” *Journal of Applied Meteorology* 9 (6): 857–61.
Peña, Alfredo, Sven-Erik Gryning, and Charlotte B. Hasager. 2008. “Measurements and

Modelling of the Wind Speed Profile in the Marine Atmospheric Boundary Layer." *Boundary-Layer Meteorology* 129 (3): 479–95.
Peña, Alfredo, Sven-Erik Gryning, and Charlotte Bay Hasager. 2010. "Comparing Mixing-Length Models of the Diabatic Wind Profile over Homogeneous Terrain." *Theoretical and Applied Climatology* 100 (3): 325–35.
Petersen, Erik L., Niels G. Mortensen, Lars Landberg, Jørgen Højstrup, and Helmut P. Frank. 1998. "Wind Power Meteorology. Part I: Climate and Turbulence." *Wind Energy: An International Journal for Progress and Applications in Wind Power Conversion Technology* 1 (S1): 25–45.
Robak, S., and R. M. Raczkowski. 2018. "Substations for Offshore Wind Farms: A Review from the Perspective of the Needs of the Polish Wind Energy Sector." *Bulletin of the Polish Academy of Sciences: Technical Sciences*. http://www.czasopisma.pan.pl/Content/108424/PDF/17-00902-kolor.pdf.
Sathe, A., S. E. Gryning, and A. Peña. 2011. "Comparison of the Atmospheric Stability and Wind Profiles at Two Wind Farm Sites over a Long Marine Fetch in the North Sea." *Wind Energy*. https://agupubs.onlinelibrary.wiley.com/doi/pdf/10.1002/we.456.
Shafiee, Mahmood. 2015. "Maintenance Logistics Organization for Offshore Wind Energy: Current Progress and Future Perspectives." *Renewable Energy* 77 (May): 182–93.
"Shoreline." n.d. Shoreline. Accessed November 17, 2018. https://www.shoreline.no/solutions/construction-design/.
Stull, Roland B. 1988a. *˜Anœ Introduction to Boundary Layer Meteorology*. Kluwer Academic Publ.
———. 1988b. "Similarity Theory." In *An Introduction to Boundary Layer Meteorology*, 347–404.
Sulawa, T., I. Jami, and R. Pound. 2009. "Balancing Availability, Reliability and Future Regulatory Impact against Overall Project Capex for Offshore Wind Farms." In *2009 CIGRE/IEEE PES Joint Symposium Integration of Wide-Scale Renewable Resources Into the Power Delivery System*, 1–7.
Sumner, Jonathon, and Christian Masson. 2006. "Influence of Atmospheric Stability on Wind Turbine Power Performance Curves." *Journal of Solar Energy Engineering* 128 (4): 531–38.
Tambke, Jens, Lorenzo Claveri, John A. T. Bye, Carsten Poppinga, Bernhard Lange, L. von Bremen, Francesco Durante, and Jörg-Olaf Wolff. 2006. "Offshore Meteorology for Multi-Mega-Watt Turbines." In *Proc. European Wind Energy Conference*. https://uol.de/fileadmin/user_upload/physik/ag/ehf/enmet/publications/wind/conference/2006/ewec_athen/Offshore_Meteorology_for_Multi_Mega_Watt_Turbines.pdf.
Tambke, Jens, Matthias Lange, Ulrich Focken, J�rg-Olaf Wolff, and John A. T. Bye. 2004. "Forecasting Offshore Wind Speeds above the North Sea." *Wind Energy* 8 (1): 3–16.
Topham, Eva, and David McMillan. 2017. "Sustainable Decommissioning of an Offshore Wind Farm." *Renewable Energy* 102 (March): 470–80.
Tsoutsos, T., I. Tsitoura, D. Kokologos, and K. Kalaitzakis. 2015. "Sustainable Siting Process in Large Wind Farms Case Study in Crete." *Renewable Energy* 75: 474–80.
Van Ulden, A. P., and A. A. M. Holtslag. 1985. "Estimation of Atmospheric Boundary Layer Parameters for Diffusion Applications." *Journal of Climate and Applied Meteorology* 24 (11): 1196–1207.
Vis, Iris F. A., and Evrim Ursavas. 2016. "Assessment Approaches to Logistics for Offshore Wind Energy Installation." *Sustainable Energy Technologies and Assessments* 14: 80–91.
Werkhoven, E. J., and J. P. Verhoef. 2012. "Offshore Meteorological Mast IJmuiden–Abstract of Instrumentation Report." *ECN-Wind Memo-12*.
WMO (World Meteorological Organization) (1983) "Guide to Meteorological Instruments and

Methods of Observation, Publication No. 8" World Meteorological Organisation,
York, Richard. 2007. "Demographic Trends and Energy Consumption in European Union Nations, 1960–2025." *Social Science Research* 36 (3): 855–72.
Zilitinkevich, S. S., and J. W. Deardorff. 1974. "Similarity Theory for the Planetary Boundary Layer of Time-Dependent Height." *Journal of the Atmospheric Sciences* 31 (5): 1449–52.

APPENDIX

Table 1. Wind Turbine Installation Vessel Input

Data	Value
Transit Speed (kn)	11
Dynamic positioning Speed (kn)	2
Dynamic Positioning Time (h)	0.5
Significant wave height jacking limit (m)	2.8
Wind speed crane operation limit (m/s)	20
Monopile Foundation capacity (pieces)	5
Transition piece capacity (pieces)	5
Wind turbine components (sets)	5

★ Wind turbine components set consist of one tower, nacelle (hub attached) and a set of three pieces of blades.

Table 2. Input for operation duration and limiting criteria.

Process	Time (h)	Weather Window (h)	Wind Speed Limit (m/s)	Wave Height Limit (m/s)	Reference
Transit to wind Farm					
Seafasten assets	3				
Jacking down	2				
Port manoeuvring	1				
Transit from wind farm					
Tansist			15.3	2.8	MPI Offshore (2016)
Port Manoeuvring	1				
Positioning/Field move	2	4	18		
Jacking at loading yard	2				
Mobilising	0				
Pile loadout					Beinke, Alla, and Freitag (2017)
Loading of each pile	2	4	18		
Transition piece					Beinke, Alla, and Freitag (2017)

loadout					
Loading of each transition piece	2	4	14		
Wind turbine loadout					Beinke, Alla, and Freitag (2017)
Preparing lifting	2				
backloading	3				
Loading of tower	1.5	3	14		
Loading of nacelle	2	4	14		
loading of blade set	2.5	5	12		
prepare vessel for transit	2				
Driving pile					Beinke, Alla, and Freitag (2017)
Upending MP from deck	2	4	18	3	
Stabbing MP	1	2	18	3	
Removing slings and place hammer	1				
Piling	3	6	18	3	
Remove hammer and place on deck	0.5				
Place temporary NAVaids	1				
Transition piece installation					Beinke, Alla, and Freitag (2017)
Transition piece installation	3	6	18	3	
Airtight Platform and bolting	6	12	18	3	
Finish work	1	2	18	3	
Wind turbine installation					Beinke, Alla, and Freitag (2017)
Prepare transition piece	1	2	12		
Prepare lifting	1	2	12		
Full tower	4	8	12		
Nacelle	3	6	10		
Blade (per blade)	2	4	8		*Paterson et al. (2018)
Secure WTG	4	8	12		
Jacking up					MPI Offshore (2016)
Positioning	1	2	12		
Preload	2				
Jackup	2	4	15	1.5	

Jacking Down

Prepare vessel for jacking down	1
Jacking down	2